MECHANISM OF PROJECTILE FRAGMENTATION IN ^{84}Kr-Em INTERACTIONS AT 0.95 GeV/A

A THESIS

SUBMITTED TO GAUHATI UNIVERSITY FOR THE

DEGREE OF DOCTOR OF PHILOSOPHY IN PHYSICS

IN THE FACULTY OF SCIENCE

SUBMITTED BY

BARNALI DEBNATH

DEPARTMENT OF PHYSICS

GAUHATI UNIVERSITY, GUWAHATI-781014

ASSAM : (INDIA)

2011

Dedicated to

My Father

Sri Heramba Ch. Debnath

My Mother

Smt. Nihar Debnath

&

My in-laws

Mr. Sandip Kr. Chanda

Ms. Manjula Chanda

Dr. Buddhadeb Bhattacharjee
Associate Professor of Physics
Phone: +91-361-2670968
09954499182 (M)
Fax : +91-361-2670968
e-mail : bb_22@rediffmail.com

Department of Physics
Gauhati University
Guwahati - 781014
Assam, India

CERTIFICATE

This is to certify with great pleasure that Ms. Barnali Debnath, M. Sc., B. Ed., has completed her works on this thesis entitled, "**Mechanism of projectile fragmentation in ^{84}Kr-Em interactions at 0.95 GeV/A**" under my supervision and guidance. The work is worthy of consideration for the award of Ph. D. degree of the Gauhati University. Ms. Debnath has fulfilled all the requirements prescribed under Ph. D. regulations of the Gauhati University. The thesis, she has submitted, is the result of her own investigations and to the best of my knowledge this work as a whole or part thereof has not been submitted to any other Universities / Institutions for any research degree.

18.11.11

(Buddhadeb Bhattacharjee)

Associate Professor
Department of Physics
Gauhati University

DECLARATION

I hereby declare that the thesis entitled "Mechanism of projectile fragmentation in ^{84}Kr-Em interactions at 0.95 GeV/A" is the result of investigations that have been carried out by me under the supervision of my research guide Dr. Buddhadeb Bhattacharjee, Associate Professor, Department of Physics, Gauhati University, Guwahati. I declare that this thesis as a whole or any part thereof had not been submitted by me for any research degree to this University or any other Universities / Institutions.

Barnali Debnath
18-11-11
(Barnali Debnath)

ACKNOWLEDGEMENT

It gives me immense pleasure to express with great reverence my deep sense of gratitude to my esteemed teacher and supervisor, Dr. Buddhadeb Bhattacharjee for his keen interest and constant support in the completion of this work. I must admit that without his able guidance and constructive comments, this thesis would not have been completed.

I am thankful to Prof. S. A. S. Ahmed, ex-Head of the Department of Physics, Prof. K. Barua, ex-Head of the Department of Physics and Prof. N. Singh, present Head of the Department of Physics, Gauhati University for providing facilities to carry out my work.

I express my deep gratitude to late Dr. S. K. Tuli, retired professor of Banaras Hindu University, Varanasi, India for providing the ^{84}Kr-expossed emulsion plates.

I acknowledge the suggestions and support bestowed upon me by all my teachers of the Physics Department, Gauhati University, Guwahati and my college teacher, Dr. Nirab Adhikari.

I would also like to thank the non-teaching staff of the department of Physics, Gauhati University, Guwahati for their kind help and cooperation.

I am thankful to Geology Department, Gauhati University, Guwahati for helping me to take the photograph of the nuclear emulsion interactions.

I take the privilege to extend my hearty thanks to Prof. Y. P. Viyogi, Director, Institute of Physics, Bhubeneswar, India, Dr. S. B. Santra, Indian Institute of Technology, Guwahati, India and Dr. A. Mukhopadhya, North Bengal University, Shiliguri, India for several fruitful discussion I had with them and to Dr. Arup Ratan Paul, IASST, Boragaon, Guwahati for valuable help.

I take this opportunity to thank the co-workers of my laboratory, Dr. S. Sengupta, Mr. R. Kakati, Mr. B. Sinha, Ms. R. Talukdar and Mr. K. Dey for their cooperation and various helps.

During my stay in Research Scholar Hostel, Gauhati University, Guwahati, several people have been of immense help to me. I wish I could extend my sincere thanks to all of them.

My friends have had a great role in making me comfortable in every way. I would like to express my thanks particularly to Ms. Nishigandha Talukdar, Ms. Ritumoni Nath, Ms. Purnima Konwor, Ms. Jolly Bhadra, Ms. Rupjyoti Gogoi, Mr. Shantunu Sinha, Mr. R. K. Chowdhury, Mr. S. Chowdhury.

Financial assistance in the form of salary of JRF and SRF from the Department of Atomic Energy, Board of Research in Nuclear Science (DAE-BRNS), Govt. of India, Mumbai is acknowledged with thanks.

My husband, Mr. Symon Chanda played an active role in the process of completion of this thesis. He always morally supported me and inculcated in me the great feelings of humanism and deserves a huge appreciation and special thanks.

I would record my gratitude to my family members for their sacrifice and moral support.

I would like to express my deepest sense of gratitude to my in-laws. Their constant support, love and blessings have made this work possible.

Last, but not the least, I convey a huge appreciation and heartiest thanks to my parents for their constant encouragement. It is their blessings and best wishes that led to the completion of this work. Perhaps, writing just a few lines would not express adequately my true feelings about their contributions during the entire period of my Ph.D. work. So, I prefer to keep these feelings close to my heart.

However, if I miss to mention any name that should have been properly thanked, he or she should consider it as a human error and pardon me for the same.

Barnali Debnath 18-11-11

(Barnali Debnath)

PREFACE

Heavy-ion collisions at intermediate and high-energies are of considerable interest, both in theoretical and experimental nuclear physics, because such collisions provide a unique opportunity to investigate nuclear matter away from normal nuclear matter density and temperature. Violent collisions between heavy nuclei of 0.1 – 2A GeV are often termed multifragmentation due to the large number and variety of ejectiles. In nuclear multifragmentation, excited nuclei break up into several pieces of smaller masses, each more massive than an alpha particle. Such collisions are complicated processes in which the roles of the mean-field and nucleon-nucleon interactions may both be important. It has been predicted that the study of nuclear multifragmentation reactions, as observed in intermediate energy heavy-ion collisions, can provide valuable information on the nuclear matter phase diagram and equation of state as well as assist to understand liquid-gas phase transitions in nuclei. The fragments produced in such reactions are believed to carry information about the decay process and hence the collision dynamics. Depending on its importance numerous works have been carried out by different workers but still there are some ambiguities that need to be addressed for complete understanding of the process.

Contrasting the fragments of the target spectator, different fragments of the projectile remnant are very straightforwardly and reliably distinguished from all other particles emitted from the collision vertex. This is because, the spectator fragments of the projectile nucleus have momentum per nucleon almost equal to that of the incident beam and hence they are emitted inside a narrow forward-angular cone centered on the direction of the incident beam, and remains relativistic.

Since in nuclear emulsion technique, the emulsion itself acts as the target as well as the detecting medium, one major advantage of working with nuclear emulsion is that, one can make observation on extreme forward angle. The

nuclear emulsion is a global 4π detector and has the best spatial resolution (0.1 mrad) among all detectors currently in use in high-energy physics. The capability of emulsion to record all the relativistic charged projectile fragments irrespective of their charge and emission angle makes emulsion experiments superior or at least competitive to other experimental technique for the study of projectile multifragmentation. Therefore, to study the multiply charged fragments of projectile this technique has been found to be an important tool.

In the present investigation, an attempt has therefore been made to study the inclusive charge yield distribution of projectile fragments in the light of cluster approximation technique to get evidences of critical behavior and liquid gas phase transition in the projectile fragmentation in ^{84}Kr-Em interactions at 0.95A GeV.

In the current study, an attempt has also been made to study the scaling behavior of the projectile fragments. Further, to characterize the fragments size distribution the gathered data on projectile fragments have been analyzed in the light of intermittency and generalized moments.

Chapter I is on general introduction where physics of heavy ion collision and collision dynamics have been described briefly. Different models of nuclear multifragmentation and various signatures of critical behavior of nuclear matter have also been discussed in this chapter.

Chapter II describe in details the experimental procedure followed in the present investigation. Brief ideas of nuclear emulsion, formation of latent image, processing of nuclear emulsion, its development, fixation, basic mechanism of track formation have been discussed here. Details of the exposure of emulsion stacks, scanning procedure, calibration of the stacks, classification of charged secondaries, selection criteria for various types of events, estimation of charge of projectile fragments have also been narrated in this chapter. Basic features of various charged secondaries are also discussed towards the end of this chapter.

Results on charge distribution and multiplicity distribution of different projectile fragments have been presented in chapter III. Scaling behavior of

projectile fragments is studied in the light of KNO scaling and the mass of the fragmenting system Z_b in this chapter.

Chapter IV deals with the study of critical behavior and possible liquid gas phase transition in the fragmentation of projectile nucleus. In this chapter an attempt has been made to examine the breakup of relativistic Kr nuclei when they interact with the different target nuclei of nuclear emulsion using cluster approximation technique. Experimental data is compared with a toy model generated data where the violation of mass conservation is considered due to the pre equilibrium emission and with the results reported by earlier workers. Sensitivity of various traditionally accepted signatures of critical behavior is examined. Different critical exponents are estimated and their scaling properties are examined.

As in multifragmentation, nuclei break up like percolation clusters, there might be some possibility of fractality in projectile fragments mass distribution also. The concept of fractality is also intimately connected with the intermittency. Thus, chapter V is on the studies of intermittency and fractal geometry in the projectile fragments. Experimental data is investigated in the light of scaled factorial moment (SFM) and generalized fractal moment G_q.

Chapter VI gives the summary of the present investigation and provides some concluding remarks on the results of present investigation.

CONTENTS

LIST OF FIGURES

LIST OF TABLES

Chapter I

General Introduction

1.1. Introduction

Ever since the pioneering work of H. G. Baumgardt et al. [1] and B. Jakobsson et al. [2] on experiments involving medium and heavy ions colliding at kinetic energies of hundreds of MeV per nucleon, it has become evident that nuclear matter behaves as a compressible liquid and can flow hydrodynamically. In principle, a heavy-ion collision (HIC) can form a compressed and heated system that might expand and undergo phase transition after the initial collision and enter into the coexistence or spinodals region breaking into droplets (fragments) and gaseous particles (light nuclei). Such type of collision is significant from the point of view –

(a) Length scale – Considering the nuclear radius as $r = r_0 A^{1/3}$, a medium to heavy ion would have a diameter ~ 5 - 7 fm. Since the saturation density is constant (~ 0.15 fm^{-3}) throughout the periodic table, the inter-nucleon distance is ~ 2.3 fm. Taking the nucleons' hard core radius as 0.5 fm [3], the 'packed spheres' density is ~ 2 fm^{-3}; this would be the maximum compression that will keep the nucleons not overlapping with one another.

(b) Energy scale – Since the binding energy of nuclei is ~ 8 MeV/A, the energy needed for the partial disassembly of two colliding medium size nuclei, say A = 100, is of the order of thousand MeV. As this energy comes from the kinetic energy of the projectile, beam energy of the order of a several tens of MeV is needed.

(c) Time scale – The time scale for the collision and possible thermalization of the participating nuclei is set by the kinetic energy of the projectile and the energy-transfer speed in nuclear matter. The energy-transfer time can be estimated using the high density value of the speed of sound, $c_s \sim 0.2$

c, taking the distance traveled as twice the nuclear radius, the resulting time is $t \approx 2r_0A^{1/3}/c_s \approx 55$ fm/c or 18×10^{-23} s for a A = 100 nucleus [4]. The duration of the collision can be estimated as the time needed for the projectile to traverse the target.

There are some caveats also, for example –

(a) Prompt emission – The detection of a possible phase transition must rely on the analysis of the final particles produced in the reaction. But since particles can be emitted at any time of the reaction, not all of them can be taken as a carrier of a possible signature of phase change. For instance, in an initial contact in HIC, single nucleons can be knocked out directly by the projectile. The nucleons do not participate in the energy sharing and are not emitted as a phase-change byproduct.

(b) Impact parameter – Non-central collisions will reduce the number of participants in the thermal soup. The non-participant nucleons, i.e. the 'spectators', will absorb varying amount of energies that can be used to evaporate particles blurring possible phase transition signatures.

(c) Particle production – At the above-mentioned energies, it is possible to produce pions and other elementary particles. This reduces the energy going into the heating of the system inhibiting, perhaps, the breakup of nuclei.

(d) Late emission – After the disassembly of the hot and dense nuclear blob into droplets, excited fragments might shake off a few nucleons to 'cool' down, again, contaminating the signature of those particles emitted during the phase change.

(e) Quantum effect – After bringing the temperature down by particle emission, the surviving nucleus will move toward isotopical stability by α and β decays. This process is certainly not directly related to the conditions that existed

during the phase transition and will modify the final mass and isotope distribution.

(f) Nuclear temperature – Since the temperature of the system varies during the reaction, different temperature measurement techniques yield different results. For instance, the slopes of the kinetic energy spectra can be used to estimate the temperature achieved by an evaporating hot source; this, presumably, would correspond to an early stage of the reaction. Isotope yield ratios, on the other hand, can also reflect the temperature of the system when chemical equilibrium is achieved. But due to the longer time needed in achieving isotope balance, the resulting temperatures would be from a later stage. Indeed, the temperatures measured from these methods vary distinctively [4]

Heavy ion collisions at intermediate and high energies are of considerable importance, both in theoretical and experimental nuclear physics, because of the facts that such collisions provide a unique opportunity to investigate the particle productions and interaction mechanisms, and other rare phenomena at high density and high temperature [5-12]. Intermediate energy heavy-ion collisions are complicated processes in which the roles of the mean-field and nucleon-nucleon interactions may both be important. Many reactions manifest the mixed features of both the low-energy deep-inelastic scattering mechanism and a high-energy participant-spectator mechanism [13]. Collisions of heavy ions at medium energy are interesting for the following reasons –

(a) Statistics or thermodynamics of nuclei: Nuclei are many-body systems that are large enough that a thermodynamic description is possible. On the other hand they are still small enough that the partition sum can be directly calculated and all thermodynamic quantities are deduced. In this respect nuclei

are singular because here thermodynamics can be formulated from first principle and yet it is by no means non-trivial [14].

(b) Equation of State: Heavy ion reactions at relativistic energies offer a wide range of possibilities to study the multi-fragment decay of highly excited nuclei [15-22]. The analysis of the kinetic energies of the decay products has not revealed significant flow effects [17, 23, 24]. Therefore, the spectator nuclei that are produced over wide ranges of excitation energy and mass in these reactions are well suited for the investigation of highly excited nuclear systems in thermodynamical equilibrium [25].

Violent collisions between heavy nuclei of 0.1 – 2A GeV are often termed multifragmentation due to the large number and variety of ejectiles. It has been predicted that the study of nuclear multifragmentation reactions as observed in intermediate energy heavy-ion collisions [15, 16, 26-28] can give valuable information on the nuclear matter phase diagram and equation of state [29-34], as well as for understanding liquid-gas phase transitions in nuclei [35-39]. Central to a description of the mechanism for multifragmentation are the questions of 'achievement of equilibration' and the associated role of collective nuclear expansion [27, 40-45]. There exists not a single one theoretical model that is capable of addressing the complete reaction time sequence or the whole range of experimental observables. Therefore one must use several models and/or assumptions in conjunction to piece together a reasonable scenario [46].

(c) Nuclei far from stability: Recently, high and intermediate energy projectile fragmentation has also proven to be a powerful tool for producing nuclei far from stability [47, 48]. The SIS/FRS facility at GSI allows one to use projectile fragmentation at incident energies around 1A GeV to produce the nuclei of interest [49].

(d) Resonance matter formation is expected to give an important contribution to the strangeness enhancement and the subthreshold antiproton production in relativistic heavy ion reactions at intermediate energies [50-56].

In nuclear collisions at projectile energies above 0.1 GeV/A, the concepts of participant-spectator model [57-59] are well applicable, where the de-Broglie wavelength of the incident projectile nucleons is shorter than the internucleon separation (d ~ 1.8 fm) inside the nucleus. Under this condition the projectile nucleons can recognize the individuality of nucleons inside the target nucleus. This implies that the individual interactions between the nucleons inside the projectile and target are likely to gain more importance than the interaction through the mean field. Thus, at these energies, a high-energy nucleus-nucleus collision can be considered as a superposition of nucleon-nucleon collisions. According to the participant-spectator model [57, 60-63], the overlapping region of nuclear volumes of two colliding nuclei is called the 'participant' part where multiple productions of new particles occur and the nuclear matter breaks up into nucleons. This process is the first stage of the collision, which is very rapid having a short time almost equivalent to the time taken by light to cross the target nucleus. The remaining parts of nuclei that do not participate in the disintegration process are called the 'spectator' regions of projectile and target nuclei. During the production process of new particles in the participant region, a fraction of available energy is transferred to the spectator parts of colliding nuclei, leaving those nuclear remnants in an excited state. Successively, the de-excitation of the nuclear remnants takes place and many fast and slow nucleons and nuclei are emitted from the projectile and target spectator parts [64].

In high-energy nucleus-nucleus collisions, the fragments from the projectile and the target nuclei can be well separated. The process, where a part of the nucleus is suddenly liberated, is called fragmentation [65] and if the second nucleus acts only as an energy injector, one denotes it limiting fragmentation [66]. In the laboratory frame, projectile spectator fragments are found to be high-energy particles emitted at small forward angles, whereas the target spectator fragments are low energy particles emitted over wide range of angles.

Based on this model, it is possible to distinguish between collisions at different impact parameters (peripheral, quasi-central, central collisions) between two nuclei of comparable masses. It is thus clear that collision geometry or otherwise the impact parameter plays a significant role in such participant-spectator model of nuclear collision, since the geometry of the collision determines the number of participant nucleons and hence the transfer of energy and momentum from projectile to target nucleus. For more central collision, greater is the number of participant nucleons resulting in a large transfer of energy and momentum from projectile to target [67].

1.2. A Simple Nuclear Equation of State

1.2.1. The Nuclear Equation of State

The equation of state (EOS) of a medium formally relates the pressure (p) with two independent variables, commonly taken as the density (n) and the temperature (T). This expression for p(n, T), can be obtained from the energy (ε) of the system through $p(n, T) = n^2(\delta\varepsilon(n, T)/\delta n)s$, where s is entropy. Adding an

interaction energy $\varepsilon_{int}(n)$ to the free nucleon gas, the energy per nucleon (measured with respect to the T = 0 value) is thus given by

$$\varepsilon(n, T) = \varepsilon_{int}(n) + [\varepsilon_F(n, T) - \varepsilon_F(n, 0)] = \varepsilon_0(n) + \varepsilon_T(n, T). \quad (1.1)$$

Here, the interaction energy per particle is assumed to be temperature independent and denoted by $\varepsilon_{int}(n) = \varepsilon_0(n)$. The thermal part of the energy per nucleon, ε_T, is given in terms of the free nucleon gas energy, $\varepsilon_F = E_F/N$, and its zero-temperature value, $\varepsilon_F(n, 0) = 3\mu_0(n)/5$. Here, E_F is the total energy on N number of particles; μ_0 is chemical potential at T = 0.

The parameterization introduced by Kapusta [68] sets the ground state energy as $\varepsilon_0(n) = \sum_{i=2}^{5} a_i (n/n_0)^{i/3}$, with the parameters $\{a_i\}$ adjusted to yield p = 0, ε_0 = - 8 MeV, K = 210 MeV (the isothermal compressibility is obtained from $K = n(\delta p/\delta n)_T$) and the correct zero-temperature value of the Fermi gas energy, all at saturation density. The corresponding equation of state is thus

$$p(n,T) = \frac{n_0}{3} \sum_{i=2}^{5} i a_i \left(\frac{n}{n_0} \right)^{i/3+1} + \varepsilon_T(n,T), \quad (1.2)$$

with a_2 = 21.1, a_3 = - 38.3, a_4 = - 26.7 and a_5 = 35.9 all in units of MeV. Fig. 1.1 shows the isothermal pressure curves obtained with Eq. (1.2) as a function of the number density. As seen in Fig. 1.1, the pressure isotherms have a behavior characteristic of classical media. Normally, a reduction in the volume occupied by a gas, i.e. an increase of the density, increases the pressure since $\delta p/\delta n > 0$. Fig. 1.1, however shows the existence of a region where $\delta p/\delta n < 0$. In this region the compressibility is negative, and the system responds to an increase of the density with a reduction of the pressure. This is not a stable region, as those density fluctuations that normally occur in any continuous media will break the system into pieces of low density (gaseous particles) and high density (liquid

particles). These regions are known as the isothermal (if $(\delta p/\delta n)_T < 0$) and adiabatic (for $(\delta p/\delta n)_s < 0$) spinodal regions.

But this is not the whole story, even before a nucleus enters the spinodals, there is a region where, although $\delta p/\delta n > 0$, no extra energy is needed to remove a nucleon from a nucleus, or to bind one more to a free nucleon. Inside this region, known as the coexistence region, uniform nuclear matter abandons the pressure isotherms and breaks into phases adopting a pressure determined by the temperature and the average density of the system.

1.2.2. Coexistence Curve

Inside the coexistence region the liquid and gaseous phases can be in equilibrium with one another. When this happens $T_{liquid} = T_{gas}$, $p_{liquid} = p_{gas}$ and $\mu_{liquid} = \mu_{gas}$, where μ is a chemical potential. Unfortunately these conditions show no special geometrical features in the pressure curves and the boundary of the coexistence region must be determined by a special technique known as the Maxwell construction. Fig. 1.2 shows the pressure isotherm for T = 13 MeV plotted sideways against the volume. The unstable region goes from point D to point F. To determine the boundary of the coexistence region it is necessary to look at the energy needed to add or subtract a nucleon from either phase, i.e. the Gibbs free energy, $g = \mu = \varepsilon - Ts + pV$, V is the volume.

Infinitesimal changes of the Gibbs free energy per particle are given by $dg = - sdT + Vdp$. In an isotherm, where $dT = 0$, the change in the Gibbs free energy per particle is the area below the curve V(p)dp. To determine the boundary of the coexistence region, this area must be equal to zero.

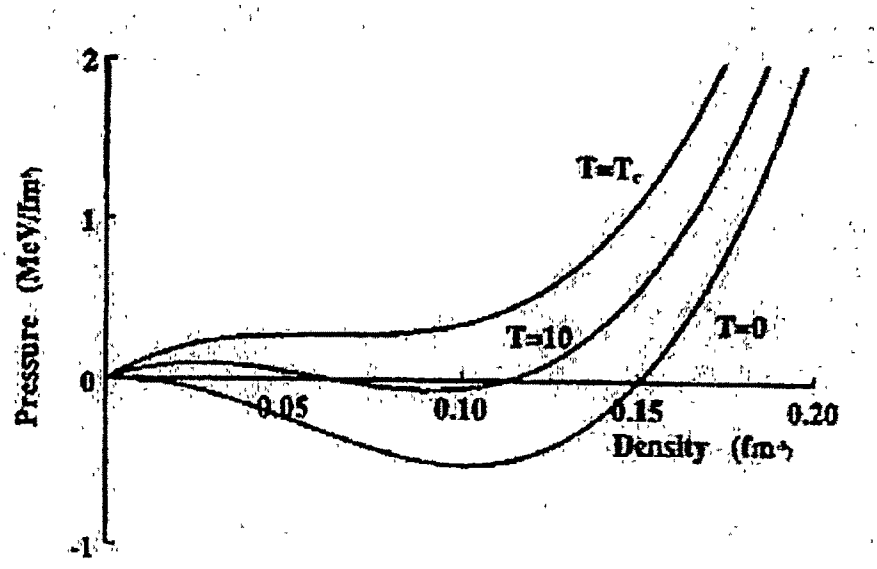

Fig. 1.1: Isothermal pressure curves as a function of the density for three temperatures, with T_c = 14.542 MeV [4]

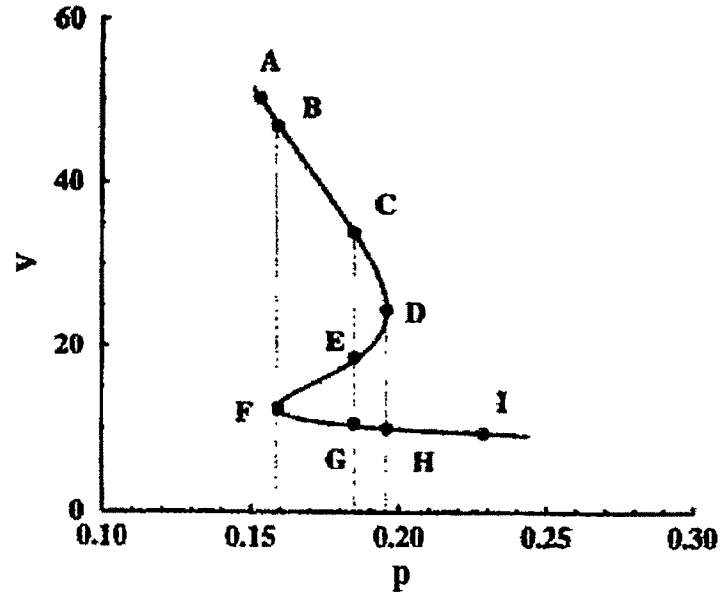

Fig. 1.2: Pressure Isotherm for T = 13 MeV plotted sideways versus the volume and showing the unstable region between points D and F [4].

Taking Fig. 1.2 as a reference, the area of interest is the one below the curve DEF. Due to the change in the sign of dp along the loop, (g_2 - g_1) is not a monotonous function of the limits. Then the corresponding expression for the EOS, in terms of the temperature and the volume, reads:

$$g_2 - g_1 = \int_{p_1}^{p_2} V(p)dp = \left[\left(\frac{5a_2}{3n_0^{2/3}} + \frac{8a_5}{3n_0^{5/3}V} \right) \frac{1}{V^{2/3}} + -\frac{2}{3}\left(\varepsilon_{01}^T + \varepsilon_{02}^T T\right) T \log(V) + \frac{7a_4}{3n_0^{4/3}} \frac{1}{V^{4/3}} + \frac{6a_3/n_0 + 4\varepsilon_{11}^T T + 4\varepsilon_{12}^T T^2}{3V} + \frac{\varepsilon_{21}^T T + \varepsilon_{22}^T T^2}{V^2} \right]_1^2 \tag{1.3}$$

Fig. 1.3 displays the behavior of g as a function of p for the EOS at a temperature of 13 MeV, i.e. below T_c. For a system to be in equilibrium g should be a minimum. So the allowed values of g are the ones lying on the curve ACGI. The points C and G are coincident, and can be determined by the condition $0 = \int_{p_c}^{p_g} V(p)dp$, which implies that

$$\int_{p_c}^{p_d} V(p)dp - \int_{p_e}^{p_d} V(p)dp = \int_{p_f}^{p_e} V(p)dp - \int_{p_f}^{p_g} V(p)dp . \tag{1.4}$$

This states that the areas determined by the curve of constant pressure p and the isotherm under study, to the left and the right of the intersect in the unstable region, must be equal. In this way the set of solutions of this 'equal areas' condition determine the so-called coexistence curve. The portions of the isotherms from the boundary of the coexistence curve to the limits of the unstable spinodal region are physically accessible, and are called the superheated vapor and supercooled liquid (Fig. 1.4).

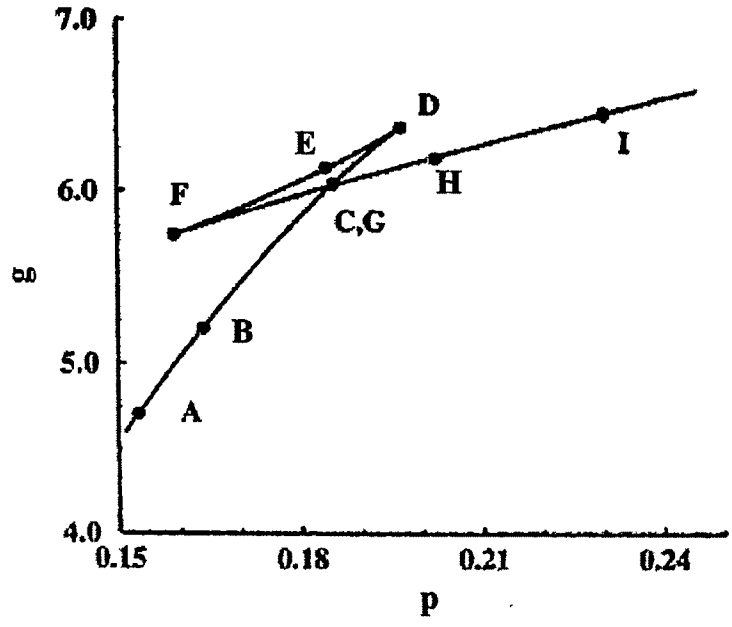

Fig. 1.3: g as a function of p for the EOS at T = 13 MeV, i.e. just below T_c [4].

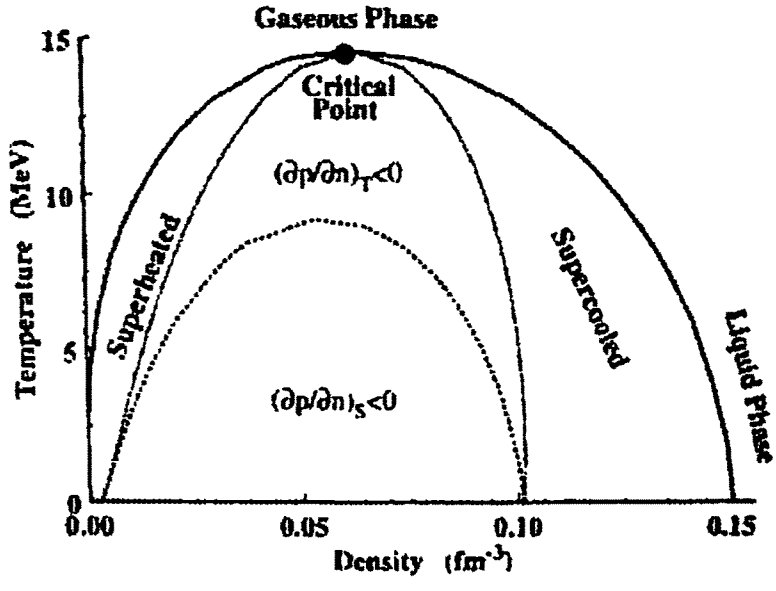

Fig. 1.4: Phase diagram of nuclear matter [4].

1.2.3. Spinodal Regions

The dotted line of Fig. 1.4 shows the boundary of the unstable region, this is known as the isothermal spinodal line. This curve was calculated solving $(\delta p(n, T)/\delta n)_T = 0$ for n for a number of temperatures. The right branch of the curve shows the points where a further increase of the liquid density results in no change of pressure. The left branch of the curve shows the corresponding points for the gaseous phase.

The left and right branches of the isothermal spinodal meet at the critical point (n_c, T_c).

For adiabatic processes, i.e., those conserve the total entropy of the system, the nuclear medium can be described by the entropy counterpart of Eq. (1.2). Again, the isentropic pressure p(n, s) has a zone of negative compressibility known as the mechanically unstable region. This boundary, known as the adiabatic spinodal line, is outlined in Fig. 1.4 with a dashed curve.

Nuclear physicists face major challenges in their efforts to explore the nuclear equation of state and the nuclear phase transitions. In nucleus-nucleus collision, one can establish the hot and dense conditions needed for this process but can't prepare the collision at a given pressure, temperature and density. To complicate things even more, such collisions do not stay at a given density and temperature, but expand and cool down within a very short interval of time ($\sim 10^{-21}$ sec.). There is also no direct way of measuring the state variables. Finally, there is the problem of finite particle number. Thus, one has to figure out what signatures of a phase transition remain when there are only so few elementary constituents present.

1.3. Phase Transition and Critical Phenomena

1.3.1. Critical Phenomena, Critical Exponents & its Scaling Properties

Critical phenomena [69-72] refers to the behavior of matter around the critical temperature (if in a second order phase transition) or the critical point (in a first order one). First order phase transitions are those that involve a latent heat. During such a transition, a system either absorbs or releases a fixed (and typically large) amount of energy. During this process, the temperature of the system will stay constant as heat is added. Because energy cannot be instantaneously transferred between the system and its environment, first order transitions are associated with "mixed-phase regimes" in which some parts of the system have completed the transition and others have not. Mixed phase systems are difficult to study, because their dynamics are violent and hard to control. However, many important phase transitions fall in this category, including the solid/liquid/gas transitions and Bose-Einstein condensation. Second-order phase transitions have no associated latent heat and are also called the continuous phase transitions. These are usually related to variations in the symmetry of the system under study, (i.e. when crossing the critical temperature a new symmetry appears in the system) although there are exceptions to this rule.

When symmetry is broken, one needs to introduce one or more extra variables to describe the state of the system. Such variables are called order parameters. It generally quantifies the different properties of a system above and below the critical temperature. The order parameter is normally a quantity which is 0 in one phase (usually above the critical point), and non-zero in the other. It characterises the onset of order at the phase transition. The order parameter susceptibility will usually diverge approaching the critical point.

A continuous phase transition in infinite system is generally characterized by the presence of some characteristic features. An interesting feature of the critical point is that in its vicinity various thermodynamic quantities of the system posses singularities. It is usual to express these singularities in terms of power laws. The powers of these relationships (six, traditionally denoted by α, β, γ, δ, η and ν) are called critical exponents, which determine the qualitative nature of the critical behavior of the system under study. It is an interasting fact that phase transitions arising in different physical systems often possess the same set of critical exponents. This phenomenon is known as universality. For example, the critical exponents at the liquid-gas critical point have been found to be independent of the chemical composition of the fluid. Further, they are an exact match for the critical exponents of the ferromagnetic phase transition in uniaxial magnets. Such systems are said to be in the same universality class. Several classes have been determined to exist (via the renormalization group [69-72]), as for example the so called three dimensional Ising model which comprises fluids, ferromagnetic materials, binary alloys, etc.. Universality is a prediction of the renormalization group theory of phase transitions, which states that the thermodynamic properties of a system near a phase transition depend only on a small number of features, such as dimensionality and symmetry, and are insensitive to the underlying microscopic properties of the system. Again, the divergency of the correlation length is the essential point. Thus, critical exponents are the fingerprints of a phase transition: to characterize a critical phenomenon of an unknown type, its related critical exponent must be compared with the corresponding ones of several universality classes.

The classification of critical phenomena can be further reduced by four relationships among the critical exponents resulting from the scaling hypothesis

of Widom [73] and Kadanoff [74]. Therefore, the main characteristic of the critical exponents is that they obey the scaling relation. Out of six critical exponents only two of them are independent and all the others can be evaluated from the knowledge of just two.

1.3.2. Percolation and Critical Behavior

Fig. 1.5 shows an example how a 20x20 square lattice is slowly filled up from probability p = 0.1 to p = 0.9. In this problem the occupied sites are either isolated from each other or they form small groups of neighbors. These groups are called clusters. In the figure the largest cluster at p = 0.6 is symbolized by overlapping crosses +, which distinguish it clearly from the smaller clusters also present there. Isolated sites are regarded as clusters of size unity; and generally any cluster consisting of s occupied connected sites is called s-cluster.

In a large lattice there will be more clusters than in a small lattice; thus it is convenient to divide the number of clusters by the number of lattice sites in the whole lattice. This ratio is called the number n_s, of s-clusters if it is an average over many different distributions of occupied sites among the lattice sites.

If p is close to zero, most occupied sites will be isolated, with only a few pairs and triplets present (Fig. 1.5 with p = 10%). If, on the other hand, p is close to unity then nearly all occupied sites are connected to each other and form one large cluster extending from one end of the lattice to the other (p = 90%). Generally, in a sufficiently large lattice there is either one or none, but never two or more such 'infinite' clusters or 'networks' [75]. This infinite cluster percolates through the lattice just as water is percolating through wet sand along the network of wet pores. At p = 70% and 80% figure shows that besides this percolating network many finite clusters exist, too. A clear distinction thus exists

for large lattices: either an 'infinite' cluster exists, or it does not. Therefore it is possible that for an infinite lattice a sharply defined percolation threshold p_c exists, i.e., a critical point, where for the first time an infinite network percolates through the lattice with finite probability. Thus p_c indicates a phase transition such that: for p above p_c one percolating network exists; for p below p_c no percolating network exists.

In this sense percolation is a phase transition [69], which generally can be defined as the phenomenon that a system exhibits a qualitative change at one sharply defined parameter value, if that parameter is changed continuously. Only in an infinite system (thermodynamic limit) one observe a true phase transition in this sense. For example, in the finite system of Fig. 1.5, one can't say precisely whether $p = 0.6$ is above or below the percolation threshold p_c; for the large cluster percolates horizontally but not vertically. Such accidental difference between horizontal and vertical directions becomes less and less probable if the lattice size increases. Thus p_c is defined uniquely in an infinite system.

More quantitatively, the percolation probability P_∞ can be called as the fraction of occupied sites belonging to the infinite percolation network. Then P_∞ vanished below p_c and is nonzero above p_c; closed to p_c one can define a 'critical exponent' β by postulating $P_\infty \propto (p - p_c)^\beta$ for p slightly above p_c. The behavior of the infinite network and of large finite clusters for p very close to p_c, is called the critical behavior of percolation theory; the region of parameters where it applies is called the scaling region.

In general, every lattice site has three choices: it can be empty, with probability $(1 - p)$; it can be part of the infinite network of occupied sites, with probability $p \cdot P_\infty$; or it can be part of one of the many finite clusters including single sites, with probability $p(1 - P_\infty)$. Since each s-cluster contains exactly s

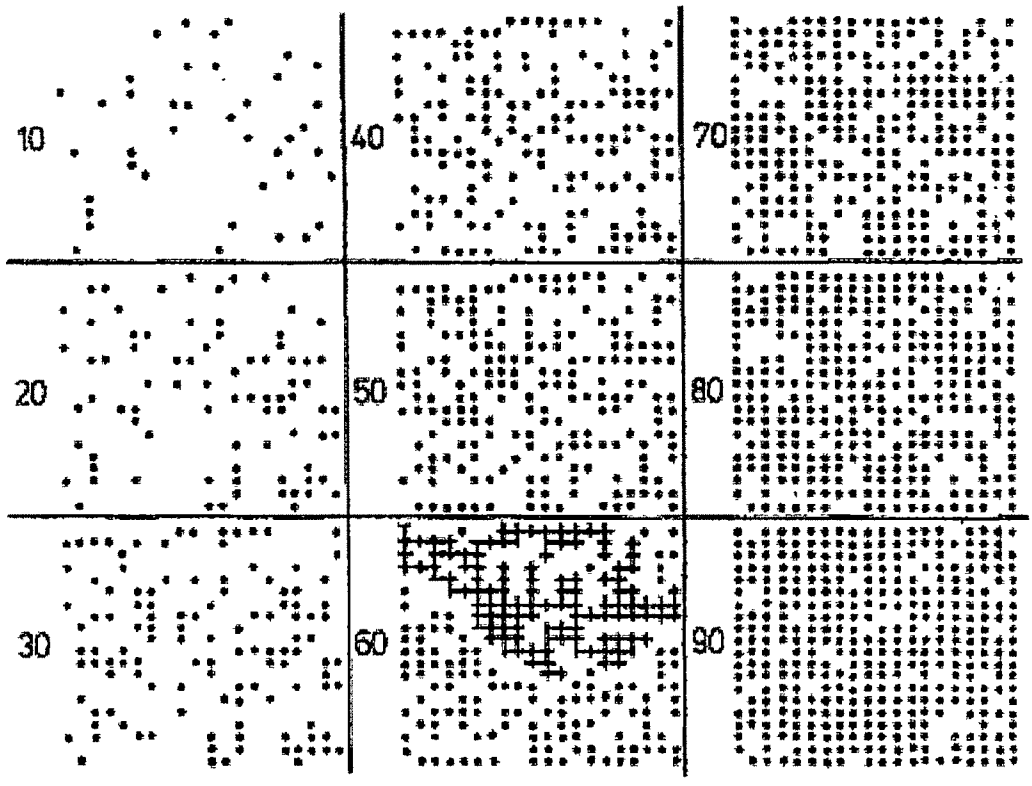

Fig. 1.5: Examples for percolation on a 20x20 square lattice, for p = 0.1, 0.2,...0.9. Occupied sites are shown as dots; empty sites are not shown. The overlapping process at 60% probability gives the largest 'percolating' cluster [76].

sites, the probability of any lattice site to belong to an s-cluster is $P_s = s \cdot n_s$. The sum of all these probabilities equals unity:

$$1 - p + pP_\infty + \sum_s s \cdot n_s = 1 \qquad (1.5)$$

where the summation runs over all finite cluster sizes, s = 1, 2.... Thus, knowing all the cluster numbers n_s, one can calculate from the above equation the strength P_∞ of the infinite network [76].

1.3.3. Critical Phenomena in Finite System

The finding of experimental nuclear fragments mass spectra that could be fitted by a power law in proton-induced fragmentation of Krypton and Xenon targets [77] triggered the interest on the study of critical phenomena in nuclei. The two main lines of research are the calculation of critical exponents of nuclear matter and the determination of the caloric curve of nuclei.

A number of complications, absent in infinite systems, appear in the nuclear case. One such complication is finite size effect. Finite size effects are introduced by the fact that nuclei are composed by just a few tens of particles. Likewise, since excited nuclear systems are produced by means of nuclear reactions, these are formed out of equilibrium. Moreover Coulomb instabilities come into play and modify possible critical behavior.

The effect of the system size on a liquid-to-gas transition is very pronounced and difficult to quantify. For instance, when enough energy is added to a cold liquid drop, it begins to evaporate particles. At high energies, however, the drop undergoes a fragmentation process, breaking into many pieces & start expanding. This collective radial motion is characteristic of finite system and has

no counterpart in the infinite case. The connection between this breakup of an excited drop and a phase transition is not well understood yet.

1.3.3.1. Finite Size Scaling

For an infinite system there exists a critical singularity at a particular pressure (p_c) and temperature (T_c). In finite systems all divergences are replaced by maxima in positions shifted with respect to the infinite case. Now problem is : how to describe the behavior of finite systems in the neighborhood of the critical temperature? In this case, the scaling form of the singular part of the free energy density takes the form [70]:

$$f_s(\varepsilon, L^{-1}) = \varepsilon^{2-\alpha} f_s(\varepsilon^{-1/y_\varepsilon}, L^{-1}), \tag{1.6}$$

Here L represents the size of the system, ε is the difference between T and T_c, y_ε is a parameter related to the critical exponents.

Eq. (1.6) can be written in term of $\xi_\infty(\varepsilon)$, i.e. the bulk correlation length corresponding to the infinite system ($L = \infty$),

$$f_s(\varepsilon, L^{-1}) = \varepsilon^{2-\alpha} f_s(\xi_\infty L^{-1}). \tag{1.7}$$

When $L >> \xi_\infty(\varepsilon)$, the correlation length of the system is not affected by the boundaries of the system, and the thermodynamic properties are those of the infinite system. On the other hand, when the system approaches the critical point, the correlation length goes to infinity and the boundaries of the system play a noticeable role. For example, from Eq. (1.6), the specific heat has the form:

$$c(\varepsilon, L^{-1}) = L^{\alpha/\nu} D(\varepsilon L^{1/\nu}), \tag{1.8}$$

where α and υ are critical exponents and D(x) is a scaling function with a maximum at x_0. Thus, the specific heat will have a peak at a temperature shifted

from the one corresponding to the infinite system: $\varepsilon_L = x_0 / L^{1/\nu} \propto L^{-1/\nu}$ or $T = T_c + x_0 / L^{1/\nu}$.

1.4. Some Models to Describe Projectile Fragmentation in A+A Collision

Competing models suggest different decay mechanisms and experiments have yet to discriminate between several theoretical scenarios [64, 78] that ranged from the sequential decay of the compound nucleus [38, 79] to statistical nuclear models [14, 80, 81], percolation models [76, 82-88] and Ising models [89-94]. The liquid-gas phase transition in nuclear matter has well been described using cluster approximation technique by a phenomenological model [95, 96] what is known as Fisher droplet model and will be described in details in Sec. 1.4.2 to establish the relationship between the various parameters of equation of state and the observables of multifragmentation experiments. Both the simple and sophisticated models are frequently used in an attempt to understand how real nuclei breakup when subjected to large excitation energies, a process known as nuclear multifragmentation. Many of these models assume equilibrium thermodynamics and produce results often interpreted as evidence of a phase transition.

In the following sections, some of the models widely used to describe nuclear multifragmentation are briefly discussed.

1.4.1. Statistical Multifragmentation Model (SMM)

There are several statistical models that have been used to study multifragmentation [14, 38, 81, 97-105] but the most widely used is the statistical multifragmentation model put forwarded by J. Bondorf et al. [81, 97, 99].

In the most general consideration, the process of nuclear fragment production may be subdivided into several stages: (a) the formation of an intermediate highly excited nuclear system, (b) the expansion of the system and its disassembly into individual fragments, (c) the de-excitation of hot primary fragments. Schematically this process is shown in Fig. 1.6.

SMM is a statistical description of the simultaneous breakup of an expanded excited nucleus into nucleons and hot fragments [81, 97, 99, 106]. The statistical multifragmentation model is based on the assumption of statistical equilibrium at a low-density freezeout stage of the nuclear system formed during the collision. At this stage, primary fragments are formed according to their equilibrium partitions. Equilibrium partitions are calculated according to the microcanonical ensemble of all breakup channels composed of nucleons and excited fragments of different masses. The model conserves total excitation energy, momentum, mass, and charge numbers. The statistical weight of decay channel j is given by $W_j \propto \exp[S_j(E_0, V, A_0, Z_0)]$, S_j is the entropy of the system in channel j and E_0, V, A_0 and Z_0 are the excitation energy, volume, mass, and charge numbers of the fragmenting source. Different breakup configurations are initialized according to their statistical weights. The fragments are then propagated in their mutual Coulomb field and allowed to undergo secondary decay [107]. In the model, successive particle emission from hot fragments with $A > 16$ is the assumed de-excitation mechanism. The de-excitation of these

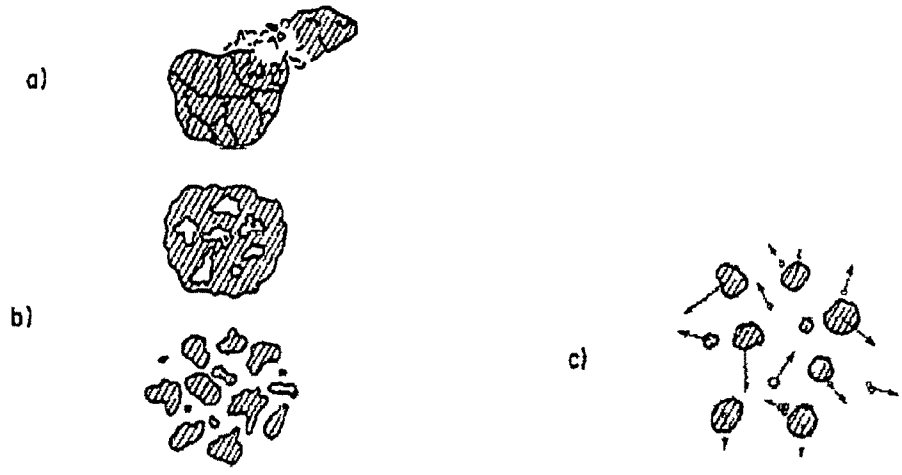

Fig. 1.6: Schematic view of the fragmentation process: (a) formation of highly-excited system with initial fluctuations (cracks); (b) formation of fragments during the expansion stage; (c) propagation and de-excitation of fragments after the break-up of the composite system [97].

fragments is treated by means of the standard Weisskopf evaporation model. Light fragments (A < 16) de-excite via Fermi breakup. The lightest particles (A < 4) can be formed only in their ground states and undergo no secondary decay [108].

If the free energy F_f of a partition f is known, the entropy and the energy may be calculated using the conventional thermodynamical formulae. The free energy $F_f(T, V)$ of the system consisting of fragments of different kinds and being in thermal equilibrium with a common temperature, T may be conveniently expressed as [97]

$$F_f = -T \ln Z_f \tag{1.9}$$

where the statistical sum for a given partition f is written as:

$$Z_f(T,V) = \sum_{\{r,p,\varepsilon\}} \exp(-E_F / T). \tag{1.10}$$

The sum runs over all the coordinates, momenta and excitation energies of the fragments forming the partition f. Here E_F is the total energy of the configuration F in the quasiclassical approximation and given by

$$E_F = \sum_{i=1}^{M} \left(E_i^{g\,s} + \frac{p_i^2}{2m_i} + \frac{s_i^2}{2I_i} + \varepsilon_i \right) + U_F, \tag{1.11}$$

Here, M is the total number of fragments including nucleons. The terms in round brackets stand respectively for the ground state energy, translational, rotational and internal excitation energies of the i^{th} fragment. p_i, s_i are momenta and angular momenta and m_i is the effective mass of the i^{th} fragment with respect to translational motion. The last term is the fragment interaction energy. After calculating the statistical sum the free energy of the system may be written in the form:

$$F_f(T,V) = F_f^{tr}(T,V) + \sum_{A,Z} F_{AZ}(T,V) N_{AZ} + E_0^C(V). \tag{1.12}$$

The first term corresponds to the translational motion of fragments. The second term contains the contributions from internal excitation energy and Coulomb energy of individual fragments. This additive representation becomes possible in the Wigner-Seitz approximation after subtracting the Coulomb energy of a total charge homogeneously distributed over the whole volume V (the last term in Eq. (1.12)).

The direct calculation of F_{AZ} for composite nuclear fragments in a hot nuclear medium is a very complicated task. They assume that all the fragments except the lightest one may be treated as drops of nuclear matter. Unlike nuclei in their ground states, these drops have nonzero temperature and are surrounded by nucleons and other clusters. It was also assumed that these drops have a spherical shape with radius $R_{AZ} = r_0 A^{1/3}$ corresponding to the normal nuclear density (r_0 = 1.2 fm).

The free energy F_{AZ} of an individual fragment of (A, Z) kind, ($Z \geq 3$) is parameterized as follows:

$$F_{AZ} = F_{trans} + F_{vol} + F_{surf} + F_{sym} + F_{coul} \tag{1.13}$$

The terms in the right hand side are, respectively, the translational, volume, surface, symmetry and Coulomb contributions. This free energy is used to determine the fragment formation probability.

This solution explicitly assumes the inhomogeneous nature of the hot MF final state. Light fragments $Z < 3$ may also be present in the hot MF final state. For the $Z \geq 3$ fragments, a quantum mechanical description is used for the temperature dependent volume, surface, and translational free energy of the fragments. The temperature independent parameters are based on the coefficients of the semiempirical mass formula. The critical temperature, at which the surface

tension of neutral nuclear matter droplets would go to zero, is in the range suggested by infinite neutral nuclear matter calculations [109].

In SMM the translational free energy depends on the free volume. The free volume, V_f, can be expressed in terms of the volume of the multifragmenting system at normal nuclear density, V_{rem},

$$V_f = \chi V_{rem}, \tag{1.14}$$

where the free volume parameter χ depends on the SMM fragment multiplicity according to the relation

$$\chi = \left[1 + \frac{d}{R_0}(M^{1/3} - 1)\right]^3 - 1, \tag{1.15}$$

where $R_0 = 1.17A_0^{1/3}$ fm and M is the charged plus neutral hot fragment multiplicity. The crack width parameter, *d*, scales the magnitude of the multiplicity dependent free volume. The breakup volume V_b, which includes the volume of the fragments, is $V_b = (1 + \kappa)V_{rem}$, where κ is the Coulomb reduction parameter.

Here the version of the model that incorporates only thermal degrees of freedom is given. Consequently, radial expansion or angular momentum is not included here.

1.4.2. Fisher Droplet Model (FDM)

The focal point of most of the phase transitions studies is to find out standard thermodynamical variables such as a system's temperature, density, compressibility, etc. But in present day nuclear multifragmentation (MF) experiment, these quantities are difficult or impossible to measure directly. Therefore a theory is considered necessary which deal with the accessible

quantities of MF experiments. To that end Fisher's gas-to-liquid phase transition model that is called Fisher droplet model, based on Mayer's condensation theory, is followed [96, 110, 111]. According to FDM, the free energy for the formation of clusters of size A_f can be given by

$$\Delta G_{A_f} = -k_b T A_f \ln[g(\mu,T)] - k_b T \ln[f(A_f,T)] + k_b T \tau \ln(A_f) + \cdots \quad (1.16)$$

where k_b is the Boltzmann constant and g is the bulk formation energy, or volume and can be written as

$$g(\mu,T) = \exp[(\mu - \mu_{coex})/k_b T], \quad (1.17)$$

here μ is the chemical potential and μ_{coex} is the chemical potential along the coexistence curve.

The surface free energy of cluster formation is represented by the f term where

$$f(A_f,T) = \exp[a_0 \omega A_f^{\sigma} \varepsilon T_c / k_b T] \quad (1.18)$$

In the above equation,

$\sigma \rightarrow$ is a critical exponent and is related to the ratio of the dimensionality of the surface to the dimensionality of the volume

$a_0 \rightarrow$ is a constant of proportionality relating the average surface area of a droplet to its number of constituents and

$\omega \rightarrow$ is the surface entropy density

$\varepsilon \rightarrow$ is a measure of the distance from the critical point.

Generally for usual thermodynamic systems $\varepsilon = (T_c - T)/T_c$, in the percolation treatment $\varepsilon = (p_l - p_c)/p_c$ and for multifragmentation $\varepsilon = (m_c - m)/m_c$ is to be used. All formulations of ε are such that $\varepsilon > 0$ corresponds to the liquid region whereas $\varepsilon < 0$ is for gas region. This form of the surface free energy is applicable on only one side of the critical point, the single phase side. A more general form suggested by efforts from percolation theory [76, 112-114] that can

be applied on both sides of the critical point and leads to a power law that describes the behavior of the order parameter is

$$f(z) = A\exp[-(z-B)^2/C], \tag{1.19}$$

where the scaling variable z is

$$z = A_f^{\sigma}\varepsilon\,. \tag{1.20}$$

The physical interpretation of the parameters A, B, and C is an open question.

Finally τ is another critical exponent depending principally on the dimensionality of the system and has its origins in considerations of a three dimensional random walk of a surface closing on itself, thus for three dimensions $2 \le \tau \le 3$ [115].

From the free energy of cluster formation the average cluster distribution normalized to the size of the system is

$$n_{A_f}(\varepsilon) = \exp(-\Delta G_{A_f}/k_bT) = q_0 A_f^{-\tau} f(z) g(\mu,T)^{A_f}\,. \tag{1.21}$$

Here q_0 is normalization constant and dependent solely on the value of τ [116]. At the critical point $\varepsilon = 0$ both f and g are unity and the cluster distribution is given by a pure power law

$$n_{A_f}(\varepsilon) = q_0 A_f^{-\tau}\,. \tag{1.22}$$

If the first moment of the normalized cluster distribution is considered at the critical point then [116]

$$M_1(\varepsilon = 0) = \sum_{A_f} n_{A_f}(\varepsilon) A_f = q_0 \sum_{A_f} A_f^{1-\tau} = 1.0 \tag{1.23}$$

where the sum runs over all clusters. From Eq. (1.23) it is obvious that the value of the overall cluster distribution normalization constant, q_0, is dependent on τ via a Riemann ζ function

$$q_0 = 1.0/\sum_{A_f} A_f^{1-\tau} \tag{1.24}$$

The above is true only if the scaling assumptions in the FDM apply to all clusters. For finite size systems even at the critical point this is only approximately true. However, it will be seen that Eq. (1.24) holds reasonably well at the critical point for systems with a continuous phase transition over some range in cluster size.

In the FDM it is assumed that all clusters of size A_f can be treated as an ideal gas, so that the total pressure of the entire cluster distribution can be determined by summing all of the partial pressures:

$$P/(k_bT) = \sum_{A_f} n_{A_f}(\varepsilon) = q_0 \sum_{A_f} A_f^{-\tau} f(z) g(\mu,T)^{A_f}$$

$$= M_0(\varepsilon). \qquad (1.25)$$

It is clear from Eq. (1.25) that the pressure of the system is related to the zeroth moment of the cluster distribution.

The density is then

$$\rho = \frac{\delta P}{\delta \mu} = q_0 \sum_{A_f} A_f^{1-\tau} f(z) g(\mu,T)^{A_f}$$

$$= \sum_{A_f} n_{A_f}(\varepsilon) A_f = M_1(\varepsilon) \qquad (1.26)$$

The density is given by the first moment of the cluster distribution.

It is now a simple matter to derive the power law that describes the divergence of the isothermal compressibility κ_T. By definition:

$$\kappa_T = -\frac{1}{V}\left(\frac{\delta V}{\delta P}\right)_T = \frac{1}{\rho}\left(\frac{\delta \rho}{\delta P}\right)_T \qquad (1.27)$$

Noting that $k_bT\rho = g(\mu, T)[\delta P/\delta g(\mu, T)]$, Eq. (1.27) can be rewritten as

$$\kappa_T = \frac{-1}{\rho^2}\left(g(\mu,T)\frac{\delta P}{\delta g(\mu,T)} + g(\mu,T)^2 \frac{\delta^2 P}{\delta g(\mu,T)^2} \right)_T \qquad (1.28)$$

that leads to

$$\kappa_T = (\rho k_b T)^{-1} + (\rho^2 k_b T)^{-1} \sum_{A_f} n_{A_f}(\varepsilon) A_f^2$$

$$= (\rho k_b T)^{-1} + (\rho^2 k_b T)^{-1} M_2(\varepsilon). \qquad (1.29)$$

The sum in the second term illustrates the relation of the second moment of the cluster distribution $M_2(\varepsilon)$ to the isothermal compressibility. The sums in Eqs. (1.25), (1.26) and (1.29) run over all clusters in the gas and excludes the bulk liquid drop. In percolation and multifragmentation the largest cluster on the liquid side of the critical point will be considered as the liquid drop and will thus be excluded from the sum. On the gas side of the critical point, the sum runs over all clusters, as there is no longer a liquid drop.

In the thermodynamic limit, large A_f dominate the sum so that it may be treated as an integral giving

$$\kappa_T = (\rho k_b T)^{-1} + (\rho^2 k_b T)^{-1} \int_0^\infty n_{A_f}(\varepsilon) A_f^2 dA_f . \qquad (1.30)$$

Working along the liquid-gas coexistence curve so that $g(\mu, T) = 1$ Eq. (1.30) reduces to

$$\kappa_T = (\rho k_b T)^{-1} + (\rho^2 k_b T)^{-1} \int_0^\infty A_f^{2-\tau} f(z) dA_f \qquad (1.31)$$

A change of variables from A_f to z shows that near the critical point

$$\kappa_T \sim (\rho^2 k_b T)^{-1} \left| \frac{q_0}{\sigma} \int_0^{\pm\infty} dz f(z) |z|^{(3-\tau-\sigma)/\sigma} \right| |\varepsilon|^{(\tau-3)/\sigma}$$

$$= (\rho^2 k_b T)^{-1} \Gamma_\pm |\varepsilon|^{-\gamma} \qquad (1.32)$$

This is the so-called γ-power law that describes the divergence of the isothermal compressibility and the second moment of the cluster distribution near the critical point. The scaling relation between the exponents γ, σ and τ is

$$\gamma = \frac{3-\tau}{\sigma}. \qquad (1.33)$$

The absolute normalization constants of the $M_2(\varepsilon)$ power law depend on the scaling function f(z) the exponent σ and the overall normalization of the cluster distribution q_0 which in turn depends on the exponent τ

$$\Gamma_{\pm} = \left| \frac{q_0}{\sigma} \int_0^{\pm\infty} dz f(z) |z|^{(3-\tau-\sigma)/\sigma} \right|. \tag{1.34}$$

The second moment is related to the isothermal compressibility by the temperature and density of the system.

The derivation of the γ-power law demonstrates one way to arrive at the scaling relations between the critical exponents. In addition it illustrates the existence of only two independent exponents and shows the relation of the moments of the cluster distribution to familiar thermodynamic quantities.

1.4.3. Cascade Evaporation Model (CEM)

The first such model was originally developed by Chen et al., [117] for nucleon-nucleus collisions and later generalized to high-energy heavy ion interactions [118-124].

In cascade evaporation model [125] each of the colliding nuclei in its coordinate system is considered as a Fermi gas of nucleons in a Wood-Saxon potential well, V(r) that may be written as

$$V(r) = B + (P_F^2/2m) \tag{1.35}$$

Where m is the mass of free nucleon, B is the average binding energy of a nucleon inside the nucleus and P_F is the local Fermi momentum. The momentum distribution inside the nucleus may approximately be given by the relation, $W(P)dP \sim P^2dP$ with $0 \leq P \leq P_F(r)$, that is isotropic in the momentum space. The maximum value of local Fermi momentum $P_F(r)$ may be expressed in terms of nuclear density $\rho(r)$ as

$$P_F(r) = h[3\pi^2 \rho(r)]^{1/3} \quad (1.36)$$

This is an approximation of two-parameter Fermi distribution; values of these parameters can be found from the electron elastic scattering experiments. Practically, this distribution is cut off at a distance R where $\rho(R)/\rho(0) = 0.01$.

The form of nuclear density is an oscillatory one for nuclei having mass number $A \leq 16$ and a Wood-Saxon one for $A > 16$. The distance between any two of the nucleons inside a nucleus is taken to be not less than $2r_c$ (~ 0.4 fm) where, r_c is the radius of the nucleon core.

It was assumed that a nucleon of the incident nucleus in the laboratory frame can be considered [132] as independent particle and characterized by a four vector, space-time (**r**, t) and four vector momentum-energy (**p**, E) having an effective mass 'm_{eff}' as

$$m_{eff} = \sqrt{(E^2 - \mathbf{p}^2)}$$
$$= m - V(r) \quad (1.37)$$

This consideration is also applicable for the nucleons of the target nucleus in the coordinate system connected with the projectile. The effect of the nuclear potential on a particle entering the nucleus may be increasing the particle kinetic energy by the quantity, V(r).

The approximation of independent particle with effective mass allows one to use the relativistic kinematics, taking into consideration in particular the effect of relativistic compression and the symmetry, of the problem with respect to the colliding nuclei. In this model, the collision is assumed to be made up of a superposition of individual binary collisions.

The dynamics of the interaction are followed in time by using Monte-Carlo method with the probability of scattering on another particle given by free particle cross-section. The incident particle can interact with any target nucleon

lying in the path with a cylindrical cut of cross-section area $\pi(r_{int} + \lambda_D)^2$, where λ_D is the de-broglie wavelength and r_{int} is nothing but the quantity which is nearly double the value of the strong interactions range and taken to be 1.3 fm [126].

Thus the probability of scattering of n^{th} nucleon after traversing without any interaction with (n^{th} - 1) nucleons is given by the binomial distribution

$$W_n = \sum_{i=1}^{n-1}(1-q_i)q_n \tag{1.38}$$

where q_i, i = 1, 2, 3....(n - 1) is the partial probability. This partial probability may be expressed in the terms of interaction cross-section for the i^{th} nucleon, σ_i as

$$q_i = [\ \sigma_i/(r_{int}+\lambda_D)^2] \tag{1.39}$$

Tracing the time evolution of the interacting system, at a fixed time t, all possible collisions are considered and the one which is realized before the others is chosen, i.e. $D_t = \min(t_i)$. Thus for two particle collisions chosen in this way, the reaction characteristics are selected at random, demanding that the Pauli principle holds.

The cascading stage ends when the colliding projectile and target nuclei are separated at such a distance where the potential wells of these nuclei do not overlap further and all cascading particles are emitted from nuclei. In this model, the Coulomb force acting between the projectile and the target is taken into account. Effectively this corresponds to an increase in the impact parameter and a rotation of all the coordinate system by a particular angle [127].

1.5. Signature of Phase Transition

For infinite nuclear matter, the existence of different phases is predicted by theoretical calculations since the early 80s [29, 97, 128, 129]. Then, the

possibility of observing a nuclear liquid–gas phase transition in the laboratory has been inferred from several experimental observations associated to the multi-fragmentation of finite nuclei. These observations indicate the occurrence of a change of state in finite nuclei, which is interpreted to be the finite system counterpart of a phase transition [130]. Several experimental features have been proposed as signatures of phase transition. Among these features are: abnormal partial energy fluctuations [131, 132], charge correlations [133], a double peaked distribution of an order parameter (bimodality) [134-136], fluctuation properties of the heaviest fragment size [137, 138], Fisher scaling [139], vaporisation [140], flattening of the caloric curve [141, 142]. Due to the various experimental conditions, each of these signals presents some weaknesses. Thus the occurrence of a phase transition would be strongly reinforced by a simultaneous observation of several signatures [143, 144]. A few of the possible phase transition signals are -

1.5.1. Mass Yield

The mass distribution of the droplets can be related to the process of nucleation. Depending on whether the phase transition takes place on the supersaturated region, coexistence region or at the critical point, the mass yield will have a characteristic dependence on the droplet size. To use this as a signature of the phase change, a careful analysis of the experimental mass distribution is necessary. Characteristic mass yield distribution which can be well represented by a power-law fit as observed by earlier workers [145, 146] were initially interpreted as indications of a critical phenomenon. In principle, a pure power law should exist only in processes taking place at the critical point, and with a unique exponent τ independent of the system size, etc., on the other hand a

set of τ value underlines the fact that not all reactions correspond to disassemblies at the critical point and these experimental data rather can be used as an indication of critical phenomena.

1.5.2. Caloric Curve

Another possible experimental signature of a phase transition might appear in the caloric curve of nuclear matter. Energy added during a phase transition is used to break inter-particle bonds and produces, not an increase of the temperature, but a plateau. Obtaining the caloric curve from a disassembling nucleus, however, is a demanding task, as it requires the simultaneous extraction of the temperature achieved in the reaction as well as the excitation energy deposited in the nuclear system. To extract a phase transition signature from the caloric curve, the temperature used would have to be that of the nuclear system while the presumed transition takes place. Experimentally, however, this is hard to do as it is only the final products of the reaction that are detected. Pochodzalla and colleagues [36] among others [147-149] have used experimental data to construct such a caloric curve.

1.5.3. Bimodality

Bimodality is a property of finite systems undergoing a first-order phase transition [150-152]. The discontinuity of the order parameter at a first order phase transition is expected to be replaced, in a finite system, by a bimodal distribution of the order parameter close to the transition point [153]. Thus, it is a generic feature that concerns not only nuclear physics but also a broad domain of physics such as astrophysics, or soft-matter physics. Bimodality means that the

probability distribution of an order parameter of the considered system at phase transition exhibits two peaks separated by a minimum [134-136, 144]. Indeed, if the system is in a pure phase, the order parameter distribution consists in one peak and can be characterized by its mean value and its variance. By contrast, if the system is in the coexistence region, the distribution presents two peaks, well separated, whose properties are related to the two different phases of the system [151]. It provides a definition of an order parameter as the best variable to separate the two maxima of the distribution [13]. The bimodality signal is robust in the sense that it is observed even if a sizable amount of the total available momentum is still aligned along the beam direction, with only a slight change of the deduced transition temperature [144]. Recently Chomaz and Gulminelli [154] demonstrated that bimodality of the probability distribution of the order parameter is equivalent to the other definitions of phase transition proposed up to now [155].

1.5.4. Δ-scaling

Δ-scaling is a signal proposed in the framework of the universal fluctuation theory [156]. It may be used to distinguish between different phases and to identify critical points. Δ-scaling is observed when two or more probability distribution $P_N(m)$ of the observable m for a system of size 'N' collapse onto a single scaling curve f(z(Δ)) independent of system size when plotted in terms of the scaling variables:

$$< m >^{\Delta} P_N(m) = f(z(\Delta)) = f\left(\frac{(m - < m >)}{< m >^{\Delta}}\right) \qquad (1.40)$$

where <m> is the mean value of the distribution $P_N(m)$ and ½ ≤ Δ ≤ 1. Here <m> plays the role of a scale parameter and can replace N as a measure of the size of

the system. A weaker (necessary but not sufficient) condition for Δ-scaling is that the variance of the distribution should scale with its mean value as $\sigma^2 \sim \langle m \rangle^{2\Delta}$ so that in a log-log plot of σ^2 versus $\langle m \rangle^2$ data should fall on a straight line of slope Δ.

The scaling law (1.40) with $\Delta = 1/2$ is associated with low temperature ('ordered' system), or with observables that are not related to an order parameter. Scaling with $\Delta = 1$ is seen at high temperature ('disordered' system) and also for critical systems. For m to be an order parameter it must exhibit a corresponding change of Δ-scaling regime when some suitable control parameter (e.g., available energy, temperature, or bond breaking probability) is varied [137, 138].

1.5.5. Negative Heat Capacity

Another signal of phase transition is negative heat capacity. This phenomenon is univocally associated to first order phase transitions with a finite latent heat in isolated systems with a size comparable to the range of the forces governing its equation of state [128]. A negative heat capacity occurs whenever the entropy presents an anomalous curvature as a function of the available energy. It has been shown in Ref. [157] that heat capacity may be deduced from the measurement of the fluctuations in the sharing of the available energy between independent degrees of freedom. Since the heat capacity can be negative only in the microcanonical ensemble, from an experimental point of view events with defined excitation energy have to be selected. For such a sorting, the total heat capacity may be approximately written as

$$C \approx \frac{C_1^2}{C_1 - \frac{\sigma^2}{T^2}} \tag{1.41}$$

Where C_1 is the partial heat capacity for a subset of degrees of freedom (for instance momentum space), T is the temperature and σ^2 is the variance associated with the sharing of the total available energy between the degrees of freedom subset and the other ones. The total heat capacity becomes negative when these fluctuations become larger than the fluctuations associated to the canonical ensemble. To study different systems, this formalism has been used by different workers [131, 132].

1.5.6. Fluctuations

One of the most striking characteristics of systems undergoing continuous phase transitions is the occurrence of fluctuations that exist on all length scales in a small range of the control parameter. Fluctuations in cluster size and the density of the system arise because of the disappearance of the latent heat at the critical point. In a cluster distribution the most readily observed fluctuations are those in the size of the largest cluster. For the studied system the root mean square (rms) fluctuations in the size of the largest cluster normalized to the size of the system $\Delta(A_{max}/A_0)$, has been calculated as a function of the system's control parameter. Campi first studied this measure of the fluctuation in the cluster distribution for gold multifragmentation and percolation [86]. The observation of a maximum in the fluctuations of the size of the largest cluster is a hint of the presence of criticality but not sufficient to distinguish systems with and without critical behavior. On the other hand, the absence of a peak in the fluctuations would indicate that the clusters of the system were not produced near a critical point [115].

1.6. Motivation

Depending upon the target-projectile combination and the incoming projectile energy, the excited nucleus decays predominantly by the emission of nucleons, deuterons, tritons, helium nuclei, intermediate mass fragments (IMFs) and very heavy fragments. To understand the dynamics involving the formation of various fragments in the final state of both p-nucleus and nucleus-nucleus reactions, numerous experiments have been performed at low, intermediate and high energies [15, 23, 25, 26, 35, 41, 78, 145, 158-184].

Since in nuclear emulsion technique, the emulsion itself acts as the target as well as the detecting medium, one major advantage of working with nuclear emulsion is that, one can make observation on extreme forward angle. The nuclear emulsion is a global 4π detector and has the best spatial resolution (0.1m rad) among all detectors currently in use in high-energy physics [185-188]. At relativistic energies, various projectile fragments (PFs) essentially travel with the same speed of the beam and are highly directional. These energetic PFs are recorded in emulsion with 100% detection efficiency and such intrinsic feature of emulsion makes it a unique detector among all the particle detectors currently in use in high-energy collision studies [172]. In the study of A+A collisions using this technique, it has been realized that observations on PFs have considerable advantages over the conventional measurements on target fragments (TFs). This is essentially due to the facts that, in emulsion, the charge of various PFs can be determined with much more accuracy than that of TFs and the fragments can be easily distinguished from the rest of the charged secondaries due to their confinement into narrow forward angle.

For a reasonable comparison of the fragments coming out of the different systems at different energies, the corresponding multiplicity should be scaled in mass as well as in energy domain. One such scaling, used by different workers to check their experimental data, is KNO scaling [189]. In case of projectile fragmentation studies it is found that the main emphasis has been laid on the studies of alpha particles. However, the study of KNO scaling for projectile fragments having charge $Z_{PF} = 1$ and $Z_{PF} \geq 3$ has not been carried out with the same vigor and enthusiasm. Though a few results have been appeared on the scaling properties of $Z_{PF} = 1$ and $Z_{PF} \geq 3$ [190, 191], no serious effort has been made to study the KNO scaling of all the projectile fragments emitted from Kr-beam particularly at the SIS energies. The present investigation therefore attempts to study the KNO scaling for all the projectile fragments coming out of the ^{84}Kr-Em interaction at 0.95A GeV.

In the study of projectile fragmentation, Z_b, the mass of the fragmenting system is found to play an important role. It gives the idea about the centrality of the collision and hence the energy-momentum transferred to the participant part of the colliding nuclei [166]. The correlation between mean number of intermediate mass fragments (IMFs) with Z_b is studied by different workers for various systems at different energies. From such studies it was opined that this correlation is target invariance [15,166, 168, 169]. ALADIN collaboration reported that when both the parameters are normalized with the charge of the projectile beam, it follows a universal pattern. Therefore, in the present investigation an attempt has also been made to check whether the intermediate mass fragments produced in the Kr-Em interactions follow the same universal pattern or not.

The objective of heavy-ion physics at the Fermi energy scale is to explore the phase diagram of nuclear matter and establish the properties of the phase transition from the liquid self-bound ground state to a gas of free nucleons [192]. Present experimental knowledge of the finite temperature nuclear equation of state is limited. This is mainly due to the incompleteness of the measurements and the difficulty to connect the ephemeral finite excited systems produced by collision processes with the equilibrium properties of the bulk [193]. Intense theoretical and experimental investigations have been carried out during the last two decades on relativistic heavy ion collisions to gather information about liquid gas phase transition of low density nuclear matter in hot nuclei and hence the fragmentation mechanism [194-198].

Several techniques have been applied to analyze the experimental data to find out the evidences of phase transition. EOS collaboration, on the basis of their study on Au-C collisions at 1A GeV [115] and its comparison with two theoretical models, such as one that undergoes phase transition and the other that does not, opined that not all but only a few of the traditionally accepted signatures of critical behavior could serve as sensitive tools to study criticality. In the present investigation, by generating a nuclear multifragmentation 'toy model' different from that of EOS one in the sense that the principle of mass conservation has been violated to account for the pre-equilibrium emission, an attempt has been made to re-examine whether the list of sensitive and insensitive tools put forwarded by EOS collaboration is final and complete. Evidence of critical behavior and phase transition, if any, has been examined in the projectile fragmentation of Kr-Em interactions at 0.95A GeV using cluster approximation technique considering total multiplicity as the order parameter.

Further, in their attempt to get the signatures of critical behavior in the case of break up of nuclei, several workers have evaluated the values of the exponents σ, β, τ and γ from experimental data and then compared these values with the values obtained for different three-dimensional known systems exhibiting critical behavior. As mentioned earlier, one important feature of these exponents is that they are universal and depend neither on the structural details of the lattice nor on the type of percolation, but only on the dimension of the lattice. They obey certain scaling relations and all of them can be evaluated from the knowledge of just two.

However, though there is a broad agreement between the values of different exponents as estimated by various groups [35, 78], in a number of cases, a careful cross check reveals that the cited values of the exponents suffer from internal inconsistencies and do not follow the corresponding scaling relation [173, 199]. There are also reports that the value obtained for an exponent is sensitive to the range of values chosen for the control parameter and to the system under investigation [78, 173]. It may therefore be inferred that the values of the critical exponents, considered as the representative of critical phenomenon, as cited by various groups are not unambiguous. Therefore, an attempt has been made, by evaluating a higher order moment that is related to skewness, to find the complete set of values of exponents γ, β and τ that follow the corresponding scaling relation.

In multifragmentation, nuclei break up like percolation clusters and the structure of the cluster can well be described by the fractal concept. Thus, there might be some possibility of fractality in projectile fragments mass distribution also. Further, the concept of fractality and intermittency are closely related to each other. Therefore in the present investigation an attempt has also been made

to look for intermittency in the fragmentation mechanism of the projectile in the light of scaled factorial moment [200, 201] and subsequently the fractal behavior of the projectile fragments.

References

[1] H. G. Baumgardt *et al.*, Z. Phys. A **273**, 359 (1975).

[2] B. Jakobsson *et al.*, Nucl. Phys. A **276**, 523 (1977).

[3] J. D. Walecka, *Theoretical Nuclear and subnuclear Physics* (Oxford University Press, New York, 1995).

[4] J. A. Lopez and C. O. Dorso, *Phase transformation in nuclear matter* (World Scientific, Singapore, 2000).

[5] K. Werner, Phys. Rep. **232**, 87 (1993).

[6] M. Murray, J. Phys. G **31**, S1137 (2005).

[7] B. B. Back *et al.* (E917 Collaboration), Phys. Rev. Lett. **86**, 1970 (2001).

[8] B. B. Back *et al.* (E917 Collaboration), Phys. Rev. C **66**, 054901 (2002).

[9] I. G. Bearden *et al.* (BRAHMS Collaboration), Phys. Lett. B **523**, 227 (2001).

[10] I. G. Bearden *et al.* (BRAHMS Collaboration), Phys. Rev. Lett. **88**, 202301 (2002).

[11] B. B. Back *et al.* (PHOBOS Collaboration), Phys. Rev. Lett. **87**, 102303 (2001).

[12] H. F. Liu *et al.*, Phys. Rev. C **75**, 054613 (2007).

[13] Y. G. Ma *et al.*, Phys. Rev. C **71**, 054606 (2005).

[14] D. H. E. Gross, Rep. Prog. Phys. **53**, 605 (1990).

[15] C. A. Ogilvie *et al.*, Phys. Rev. Lett. **67**, 1214 (1991).

[16] M. B. Tsang *et al.*, Phys. Rev. Lett. **71**, 1502 (1993).

[17] W. Trautmann *et al.*, Acta Phys. Pol. B **25**, 425 (1994).

[18] W. Reisdorf *et al.*, Nucl. Phys. A **612**, 493 (1997).

[19] V. Lips *et al.*, Phys. Rev. Lett. **72**, 1604 (1994).

[20] K. Kwiatkowski *et al.*, Phys. Rev. Lett. **74**, 3756 (1995).

[21] J. A. Hauger *et al.*, Phys. Rev. Lett. **77**, 235 (1996).

[22] L. G. Moretto and G. J. Wozniak, Ann. Rev. Nucl. Part. Science **43**, 379 (1993).

[23] A. Schuttauf *et al.*, Nucl. Phys. A **607**, 457 (1996).

[24] V. Lindenstruth, PhD Thesis, Universitat Frankfurt (1993), report GSI-93-18.

[25] H. Xi *et al.*, Z. Phys. A **359**, 397 (1997).

[26] R. T. de Souza *et al.*, Phys. Lett. B **268**, 6 (1991).

[27] D. R. Bowman *et al.*, Phys. Rev. Lett. **67**, 1527 (1991).

[28] G. F. Peaslee *et al.*, Phys. Rev. C **49**, R2271 (1994).

[29] G. Bertsch and P. J. Siemens, Phys. Lett. B **126**, 9 (1983).

[30] G. Fai *et al.*, Phys. Lett. B **164**, 265 (1985).

[31] G. Peilert *et al.*, Phys. Rev. C **39**, 1402 (1989).

[32] J. D. Frankland *et al.*, Phys. Rev. C **71**, 034607 (2005).

[33] H. Stocker and W. Greiner, Phys. Rep. **137**, 277 (1986).

[34] Q. Pan and P. Danielewicz, Phys. Rev. Lett. **70**, 2062 (1993).

[35] M. Gilkes *et al.*, Phys. Rev. Lett. **73**, 1590 (1994).

[36] J. Pochodzalla *et al.*, Phys. Rev. Lett. **75**, 1040 (1995).

[37] D. H. E. Gross *et al.*, Nucl. Phys. A **488**, 217c (1988).

[38] W. A. Friedman, Phys. Rev. C **42**, 667 (1990).

[39] W. A. Friedman, *Proceedings of the 1st Catania Relativistic Ion Studies, eds. S. Costa et al.,* (World Scientific, Singapore, 1996).

[40] S. J. Yennello *et al.*, Phys. Rev. Lett. **67**, 671 (1991).

[41] K. Hagel *et al.*, Phys. Rev. Lett. **68**, 2141 (1992).

[42] W. C. Hsi *et al.*, Phys. Rev. Lett. **73**, 3367 (1994).

[43] S. C. Jeong *et al.*, Phys. Rev. Lett. **72**, 3468 (1993).

[44] D. Heuer *et al.*, Phys. Rev. C **50**, 1943 (1994).

[45] M. Lisa *et al.*, Phys. Rev. Lett. **75**, 2662 (1995).

[46] J. Lauret *et al.*, Phys. Rev. C **57(3)**, R1051 (1998).

[47] C. Longour *et al.*, Phys. Rev. Lett. **81**, 3337 (1998).

[48] T. Faestermann *et al.*, Eur. Phys. J. A **15**, 185 (2002); Y. P. Viyogi *et al.*, Phys. Rev. Lett. **42**, 33 (1979); T. J. M. Symons *et al.*, Phys. Rev. Lett. **42**, 40 (1997).

[49] T. Yamaguchi *et al.*, Phys. Rev. C **74**, 044608 (2006).

[50] C. Spieles *et al.*, Mod. Phys. Lett. A **8**, 2547 (1993).

[51] R. Mattielo *et al.*, Phys. Rev. Lett. **63**, 1459 (1989).

[52] G. F. Chapline *et al.*, Phys. Rev. D **8**, 4302 (1973).

[53] M. Hofmann *et al.*, Phys. Rev. C **51**, 2095 (1995).

[54] K. Sneppen and C. Gaarde, Phys. Rev. C **50**, 338 (1994).

[55] M. Gazdzicki *et al.*, nuclth/9701013 (1997).

[56] M. Goncalves *et al.*, Eur. Phys. J. A **7**, 435 (2000).

[57] J. D. Bowman *et al.*, Lawrence Barkely Laboratory Report LBL – 2908 (T.I.D. – 4500) R61 (1973).

[58] S. Nagamiya *et al.*, Phys. Rev. C **24**, 971 (1981).

[59] S. Nagamiya *et al.*, *Proceedings of the Bielefeld Workshop, May, 1982, eds. M. Jacob and H. Satz,* p. 28 (1982).

[60] R. J. Glauber, *Lectures of Theoretical Physics, eds. W. E. Brittin and L. G. Dungman*, Vol. **1**, p. 315 (Interscience, New York, 1959).

[61] J. Hufner, Report No. GSI 80-1 (1980).

[62] H. R. Schmidt and J. Schukraft, Report No. CERN-PPE/92-42 (1992).

[63] B. K. Singh and S. K. Tuli, Nuovo Cimento Soc. Ital. Fis., A **112**, 1093 (1999).

[64] M. A. Jilany, Phys. Rev. C **70**, 014901 (2004).

[65] A. S. Goldhaber, Phys. Lett. B **47**, 306 (1974).

[66] H. H. Heckman *et al.*, Phys. Rev. Lett. **28**, 236 (1972).

[67] S. Sengupta, PhD Thesis, Gauhati University, Guwahati (2009).

[68] J. Kapusta, Phys. Rev. C **29**, 1735 (1984).

[69] H. E. Stanley, *Introduction to Phase Transition and Critical Phenomena* (Oxford University Press, Oxford, 1971).

[70] N. Goldenfeld, *Lectures on Phase Transitions and the Renormalization Group* (Massachusetts, 1992).

[71] J. M. Yeomans, *Statistical Physics of Phase Transitions* (Clarendon Press, Oxford, 1994).

[72] J. J. Binney *et al.*, *The Theory of Critical Phenomena, an introduction to renormalization group* (Oxford Science Publications, Oxford, 1995).

[73] B. Widom and J. Chem., Phys. **43**, 3892 (1965).

[74] L. Kadanoff, Physics **2**, 263 (1966).

[75] V. K. S. Shante and S. Kirkpatrick, Adv. Phys. **20**, 325 (1971).

[76] D. Stauffer, Phys. Rep. **54**, 1 (1979).

[77] A. S. Hirsch *et al.*, Phys. Rev. C **29**, 508 (1984).

[78] M. I. Adamovich, Eur. Phys. J. A **5**, 429 (1999).

[79] R. J. Charity *et al.*, Nucl. Phys. A **483**, 371 (1988).

[80] H. R. Jaqaman and D. H. E. Gross, Nucl. Phys. A **524**, 321 (1991).

[81] J. Bondorf *et al.*, Nucl. Phys. A **444**, 460 (1985).

[82] W. Bauer, Phys. Rev. C **38(3)**, 1297 (1988).

[83] W. Bauer *et al.*, Annu. Rev. Nucl. Sci. **42**, 77 (1992).

[84] W. Bauer *et al.*, Nucl. Phys. A **152**, 600 (1986).

[85] J. D. Desbois, Nucl. Phys. A **466**, 724 (1987).

[86] X. Campi, Phys. Lett. B **208**, 351 (1988).

[87] X. Campi, J. Phys. A: Math. Gen. **19**, L917 (1986).

[88] X. Campi and H. Krivine, Z. Phys. A **344**, 81 (1992).

[89] S. Das Gupta *et al*, Nucl. Phys. A **621**, 897 (1997).

[90] J. M. Carmona *et al.*, Nucl. Phys. A **643**, 115 (1998).

[91] J. Pan and S. Das Gupta, Phys. Rev. C **51**, 1384 (1995).

[92] J. Pan and S. Das Gupta, Phys. Rev. Lett. **80**, 1182 (1998).

[93] X. Campi and H. Krivine, Nucl. Phys. A **620**, 46 (1997).

[94] F. Gulminelli and Ph. Chomaz, Phys. Rev. Lett. **82**, 1402 (1999).

[95] A. L. Goodman *et al.*, Phys. Rev. C **30**, 851 (1984).

[96] M. E. Fisher, Physics (N.Y.) **3**, 255 (1967).

[97] J. Bondorf *et al.*, Phys. Rep. **257**, 133 (1995).

[98] D. H. E. Gross, Phys. Rep. **279**, 119 (1997).

[99] J. Bondorf *et al.*, Nucl. Phys. A **443**, 321 (1985).

[100] A. S. Botvina *et al.*, Nucl. Phys. A **475**, 663 (1987).

[101] D. Durand, Nucl. Phys. A **541**, 266 (1992).

[102] K. C. Chase and A. Z. Mekjian, Phys. Rev. C **49**, 2164 (1994).

[103] K. C. Chase *et al.*, Phys. Rev. C **55**, 1410 (1997).

[104] S. J. Lee and A. Z. Mekjian, Phys. Rev. C **56**, 2621 (1997).

[105] S. Das Gupta and A. Z. Mekjian, Phys. Rev. C **57**, 1361 (1998).

[106] J. Bondorf *et al.*, Phys. Lett. B **150**, 57 (1985).

[107] P. F. Mastinu *et al.*, Phys. Rev. C **57(2)**, 831 (1998).

[108] R. P. Scharenberg *et al.*, Phys. Rev. C **64**, 054602 (2001).

[109] D. G. Ravenhall *et al.*, Nucl. Phys. A **407**, 572 (1983).

[110] D. Stauffer and C. S. Kiang, Adv. Colloid Interface Sci. **7**, 103 (1977).

[111] D. Stauffer and A. Aharony, *Introduction to Percolation Theory*, 2nd ed. (Taylor and Francis, London, 1992).

[112] J. Hoshen *et al.*, J. Phys. A **12**, 1285 (1979).

[113] P. L. Leath, Phys. Rev. Lett. **36**, 921 (1976).

[114] P. L. Leath, Phys. Rev. B **14**, 5046 (1976).

[115] J. B. Elliott *et al.*, Phys. Rev. C **62**, 064603 (2000).

[116] H. Nakanishi and H. E. Stanley, Phys. Rev. B **22**, 2466 (1980).

[117] K. Chen *et al.*, Phys. Rev. **166**, 949 (1968).

[118] Y. Yarik and Z. Fraenkel, Phys. Rev. C **20**, 2227 (1979).

[119] A. Capella *et al.*, Nucl. Phys. B **241**, 75 (1984).

[120] A. Capella *et al.*, Z Phys. C **10**, 249 (1981).

[121] I. Otterlund *et al.*, Z phys. C **20**, 281 (1983).

[122] Y. Yariv and Z. Fraenkel, Weizmann Institute Preprint WIS-18/80 (1980).

[123] K. K. Gudima and V. D. Toneev, Yad. Fiz. **27**, 658 (1978).

[124] K. K. Gudima and V. D. Toneev, Yad. Fiz. **31**, 1455 (1980).

[125] K. K. Gudima and V. D. Toneev, Preprint R2-10431 JINR, Dubna (1977).

[126] V. S. Barashenkov *et al.*, Ups. Fiz. Nauk. **103**, 93 (1973).

[127] V. Singh, PhD Thesis, Banaras Hindu University, Varanasi (1998).

[128] D. H. E. Gross, *Microcanonical Thermodynamics: Phase Transitions in Small Systems, Lecture Notes in Physics*, Vol. **66** (World Scientific, Singapore, 2001).

[129] A. Bonasera *et al.*, Riv. Nuovo Cimento **23(2)**, 1 (2000).

[130] Ph. Chomaz, *International Nucl. Phys. Conference INPC* (2001); *AIP Proceedings*, Vol. **610**, p. 663 (2002).

[131] M. D'Agostino *et al.*, Nucl. Phys. A **650**, 329 (1999).

[132] N. Le Neindre *et al.*, *Proceedings of the XXXVIII International Winter Meeting on Nuclear Physics*, p. 404 (Bormio, 2000).

[133] G. Tabacaru *et al.*, Eur. Phys. J. A **18**, 103 (2003).

[134] B. Tamain *et al.* (INDRA, ALADIN Collaborations), *Proceedings of the IWM Meeting*, p. 83 (Caen, 2003).

[135] M. Pichon *et al.* (INDRA, ALADIN Collaborations), *Proceedings of the XLIst Winter Meeting on Nuclear Physics, eds. I. Iori, A. Moroni and Bormio*, 26 January–1 February, (Italy, 2003).

[136] M. Pichon *et al.* (INDRA, ALADIN Collaborations), *Ricerca Scientifica ed Educatione Permanente, Suppl.*, Vol. **120**, p. 149 (2003).

[137] R. Botet *et al.*, Phys. Rev. Lett. **86**, 3514 (2001).

[138] J. Frankland *et al.* (INDRA, ALADIN Collaborations), Phys. Rev. C **71**, 34607 (2005).

[139] J. B. Elliott *et al.*, Phys. Rev. Lett. **88**, 042701 (2002).

[140] B. Borderie *et al.* (INDRA Collaboration), Eur. Phys. J. A **6** 197 (1999).

[141] J. Pochodzalla *et al.* (ALADIN Collaboration), Phys. Rev. Lett. **75**, 1040 (1995).

[142] J. Natowitz *et al.*, Phys. Rev. C **65**, 034618 (2002).

[143] M. F. Rivet *et al.* (INDRA, ALADIN Collaborations), Nucl. Phys. A **749**, 73 (2005).

[144] M. Pichon *et al.* (INDRA, ALADIN Collaboration), Nucl. Phys. A **779**, 267 (2006).

[145] J. E. Finn *et al.*, Phys. Rev. Lett. **49**, 1321 (1982).

[146] A. I. Warwick *et al.*, Phys. Rev. C **27**, 1083 (1983).

[147] D. Fabris *et al.*, Phys. Lett B **196**, 429 (1987).

[148] K. Kwiatkowski *et al.*, Phys. Lett. B **423**, 21 (1998).

[149] S. Samaddar *et al.*, Phys. Rev. Lett. **79** 4962 (1997).

[150] T. L. Hill, *Thermodynamics of Small Systems* (Benjamin, New York, 1963).

[151] Ph. Chomaz *et al.*, Phys. Rev. E **64**, 046114 (2001).

[152] K. C. Lee, Phys. Rev. E **53**, 6558 (1996).

[153] K. Binder and D. P. Landau, Phys. Rev. B **30**, 1477 (1984).

[154] Ph. Chomaz and F. Gulminelli, Physica A **330**, 451 (2003).

[155] O. Lopez and M. F. Rivet, Eur. Phys. J. A **30**, 263 (2006).

[156] R. Botet and M. Ploszajczak, Phys. Rev. E **62**, 1825 (2000).

[157] Ph. Chomaz and F. Gulminelli, Nucl. Phys. A **647**, 153 (1999).

[158] P. A. Gorichev *et al.*, Sov. Phys. JETP **41**, 327 (1961).

[159] R. W. Minich *et al.*, Phys. Lett. B **118**, 458 (1982).

[160] B. Jakobsson *et al.*, Z. Physik A **307**, 293 (1982).

[161] J. W. Harris *et al.*, Nucl. Phys. A **471**, 241 (1987).

[162] B. Jakobsson *et al.*, Nucl. Phys. A **509**, 195 (1990).

[163] Y. D. Kim *et al.* Phys. Rev. Lett. **63**, 494 (1989).

[164] E. Piasecki *et al.*, Phys. Rev. Lett. **66**, 1291 (1991).

[165] D. R. Browman *et al.*, Phys. Rev. Lett. **67**, 1527 (1991).

[166] J. Hubele *et al.*, Z. Phys. A **340**, 263 (1991).

[167] J. Hubele *et al.*, Phys. Rev. C **46**, R1577 (1992).

[168] P. Kreutz *et al.*, Nucl. Phys. A **556**, 672 (1993).

[169] P. L. Jain *et al.*, Phys. Rev. C **50**, 1085 (1994).

[170] G. Singh and P. L. Jain, Phys. Rev. C **49**, 3320 (1994).

[171] G. Rusch *et al.*, Phys. Rev. C **49**, 901 (1994).

[172] G. Singh and P. L. Jain, Phys. Rev. C **54**, 3185 (1996).

[173] M. L. Cherry *et al.*, Phys. Rev. C **52**, 2652 (1995).

[174] C. F. Powell *et al.*, *The Study of Elementary Particles by the Photographic Method* (Pergamon Press, London, 1958).

[175] W. H. Barkas, *Nuclear research Emulsions*, Vol. I (Technique and Theory Academic Press Inc., 1963).

[176] C. J. Waddington, Int. J. Phys. E **2**, 739 (1993).

[177] D. G. Enteria *et al.*, Phys. Rev. C **52**, 3179 (1995).

[178] C. J. Waddington and P. S. Freier, Phys. Rev. C **31**, 388 (1985).

[179] N. T. Porile (EOS Collaboration), *Proceedings of the 7th Int. Conf. on Nuclear Reaction Mechanisms, June 6-11, ed. E. Gadioli*, p. 555 (Varena, 1994).

[180] J. B. Elliott *et al.*, Phys. Rev. C **49**, 3185 (1994).

[181] J. Pocodzalla *et al.*, Prog. Part. Nucl. Phys. **39**, 443 (1997).

[182] W. Trautmann, *Multifragmentation in relativistic heavyion reactions, in Correlations and Clustering Phenomena in Subatomic Physics* (Plenum Press, New York, 1997).

[183] W. Trautmann (ALADIN collaboration), nuclex/9803011, presented at *14th Winter Workshop on Nuclear Dynamics, Snowbird, 31 Jan - 7 Feb* (Utah, 1998).

[184] H. G. Ritter *et al.*, *Proceedings of the 5th Interactions Conferences on Nucleon - Nucleon Collisions* (1994), LBL Report No 36105 (1994).

[185] M. M. Aggarwal, *Proceedings on 3rd International Conference on Physics and Astrophysics of Quark Gluon Plasma, eds B. C. Sinha, D. K. Srivastava and Y. P. Vyogi* (Narosa Publishing House, New Delhi, India, 1998).

[186] B. Bhattacharjee and S. Sengupta, Int. J. Mod. Phys. E **14**, 1223 (2005).

[187] S. Aoki *et al.*, CERN-EP / 2001-074; V. Bradnova *et al.*, JINR-LHE-0983-2.

[188] M. I. Adamovich *et al.*, Phys. Lett. B **262**, 369 (1991).

[189] Z. Koba *et al.*, Nucl. Phys. B **40**, 317 (1972).

[190] F. H. Liu, Phys. Rev. C **62**, 024613 (2000).

[191] F. H. Liu, Chin. J. Phys. **41(5)**, 486 (2003).

[192] P. Chomaz, Nucl. Phys. A **685**, 274 (2001).

[193] M. D'Agostino *et al.*, Nucl. Phys. A **749**, 55c (2005).

[194] J. Hufner, Phys. Rep. **125**, 129 (1985).

[195] M. A. Jilany, J. Phys. G: Nucl. Part. Phys. **29**, 2263 (2003).

[196] B. K. Srivastava *et al.*, Phys. Rev. C **65**, 054617 (2002).

[197] B. K. Srivastava *et al.*, Phys. Rev. C **64**, R041605 (2001).

[198] B. K. Srivastava (EOS Collaboration), Pramana J. Phys. **57**, 301 (2001).

[199] D. Kudzia *et al.*, Phys. Rev. C **68**, 054903 (2003).

[200] A. Bialas and R. Peschanski, Nucl. Phys. B **273**, 703 (1986).

[201] A. Bialas and R. Peschanski, Nucl. Phys. B **308**, 857 (1988).

Chapter II

Experimental Techniques

&

Some Features of the Emitted Charged Secondaries

2.1. Introduction

Nuclear radiations or various types of subatomic particles (both charged and uncharged) as well as different charged fragments coming out as a result of nuclear reactions are the signals which carry with them information about the properties of the nuclear matter away from normal nuclear temperature and density. Hence their detection and characterization are of prime importance in understanding the dynamics of nuclear reactions. The sensitive devices that have been developed for this purpose over the years can be classified into different categories depending on the principles of detection of nuclear radiation. Detectors are basically similar devices working under different operating parameters, exploiting different phenomenon. A schematic representation of classification of various detectors is given in Fig. 2.1.

For the present investigation the photo nuclear emulsion technique has been employed which rely on visualization and characterization of trajectories of the charged particles coming out of the interaction vertex.

Nuclear emulsion is the tool that led Becquerel in 1896 to discover radioactivity and since has played an important role in the development of nuclear physics [1]. Among the important discoveries made with this quasi-solid state detector was the production of secondary stars as a result of the interaction of primary cosmic radiation with the nuclei of atmospheric constituents [2]. The explanation of the properties of the π-meson [3] showing it to be the long sought for bonding particle which stabilizes complex nuclei from disintegration by their internal electrostatic repulsive force, as first predicted by YUKAWA [4], stimulated the further use of emulsions by physicists throughout the world. Among their findings, first by exposure to cosmic radiation on mountain tops and subsequently in experiments utilizing high energy accelerators, was the discovery

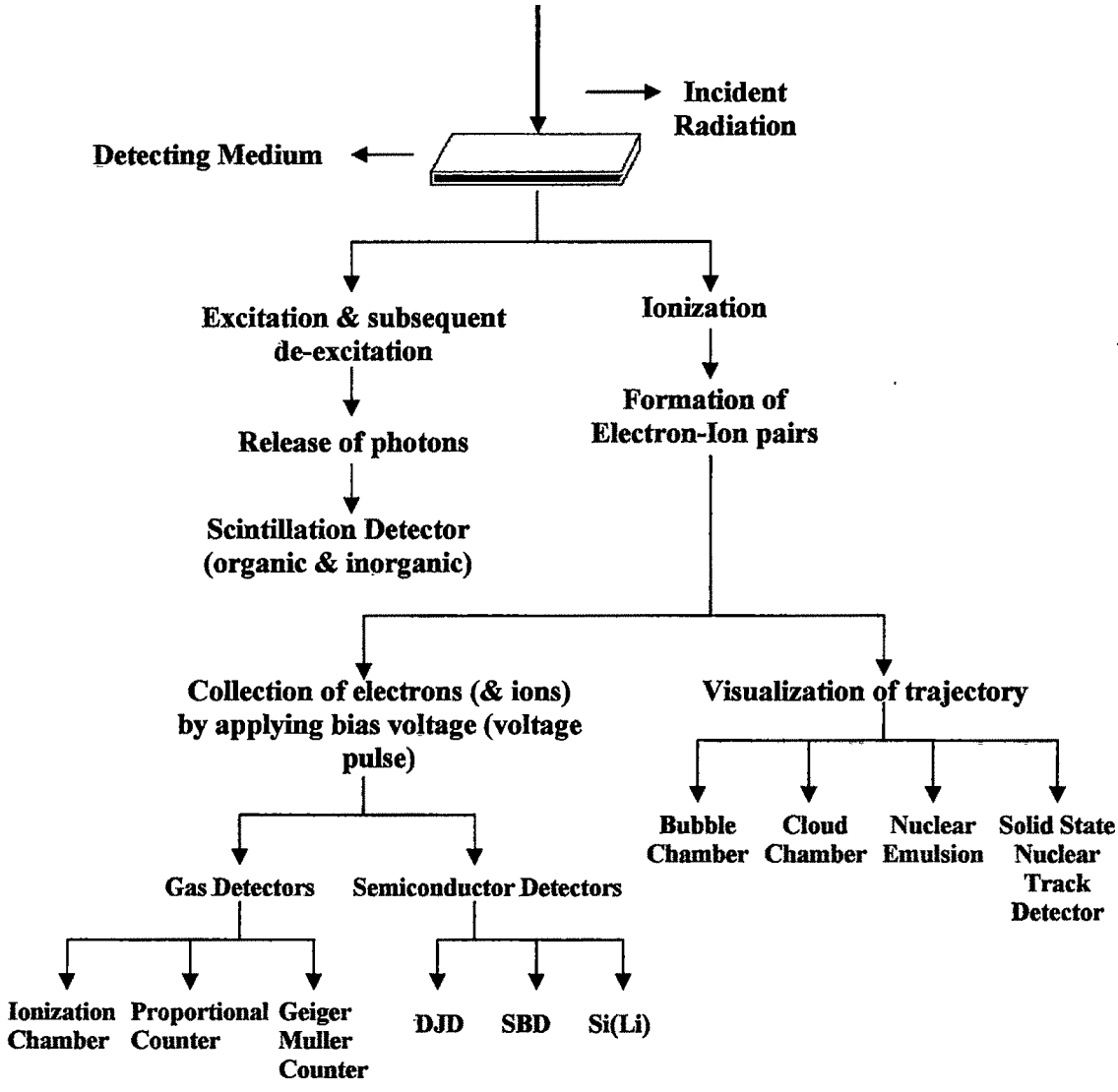

Fig. 2.1: Classification of detectors.

of the existence of a host of fundamental particles which the perplexed theoreticians dubbed as the strange particles. Another group of investigators flying small blocks of emulsions in Skyhook balloons near the top of the atmosphere observed the tracks produced by multiple-charged particles of $Z \geq 2$, the heavy primaries.

The utilization of the emulsion as an ionizing particle detector had been significantly increased with the discovery of the anti-proton [1]. Throughout the following decade the range of materials was improved and extended until the versatility of nuclear emulsions in the recording of charged particles and ionizing radiation was recognized by workers in many other fields such as in autoradiography in medical & biological research, in metallurgy and in the study of chemically reactive surfaces.

The photographic emulsion is a well-known device for the study of ionizing radiations having a rather venerable antiquity. An advantage of studying high-energy nucleus-nucleus collisions with nuclear emulsion is that the technique provides an opportunity to study nuclear reactions with variable targets (such as H, CNO and AgBr). Another advantage is that it can record all types of charged particles having energies up to the relativistic regime. Due to the higher density of the medium, the elapsing time of charged particles is higher in comparison to other detectors. As a result the probability of interactions between the projectile particle and the target increases. The high stopping power of the emulsion makes it useful for studying even the unstable particles. Since in this technique, the emulsion itself acts as the target as well as the detecting medium, another major advantage of working with nuclear emulsion is that one can make observation on extreme forward angle. The nuclear emulsion is a global 4π detector and has the best spatial resolution (0.1 mrad) among all detectors

currently in use in high-energy physics [5-8]. The capability of emulsion to record all the PFs irrespective of their charge and emission angle makes emulsion experiments superior or at least competitive to other experimental technique for the study of projectile multifragmentation [9-11].

In emulsion the trajectory of the charged particle can be recorded permanently and may be analyzed later according to the convenience of the experimenter [12]. Due to its size, weight & compactness, it can be easily handled.

In particle physics, depending on the energy of the emitted particles & the discrimination required, selection of type of emulsion is made. To meet the needs of physicists engaged in various researches, different types of emulsion, e.g., Ilford G5, Ilford C2, NIKFI BR2 etc., have been produced by different manufacturers. A major disadvantage of using nuclear emulsion is that only the interactions with nuclei normally present in the emulsion or with which the emulsion can be loaded can only be studied, as it's composition cannot be changed arbitrarily. Because of the manual scanning, in general the statistics of emulsion data remains to be less. Further, nuclear emulsion is insensitive to neutral particles and gamma radiations.

2.2. Mechanism of Visualization of Particle Trajectories in Nuclear Emulsion Detector and Visualization of Particle Trajectories

2.2.1. Composition of Nuclear Emulsion

A photographic emulsion basically consists of (a) small crystals of silver

halide, (mostly the bromide of density 6.47 g/cc, but with a small admixture of iodide); (b) gelatine and a plasticizer, such as glycerine; and (c) water [13].

According to the method of manufacture and depending upon the type of emulsion, the silver halide is in the form of microcrystals, or 'grains', cubic or nearly spherical in form with linear dimensions between ~ 0.1 μ and ~ 1 μ. The sensitivity of the emulsion depends on the size of the silver halide crystals: large grains are more sensitive to ionizing radiation than small ones. Generally a low sensitivity emulsion is used to detect high-energy radiation or particles, as there is plenty of energy available to liberate electrons and form electron deficient bromine atoms. However, to detect very high-energy particles a more sensitive emulsion is required as they deposit very little energy along their tracks & travel too fast to be trapped by the halide crystals.

The elements present in the gelatine and plasticiser are carbon, nitrogen, oxygen, hydrogen and sulphur. Gelatine is not a pure substance and chemical composition may vary depending on the different sources of supply.

The primary function of the gelatine of an emulsion is to provide a three dimensional network which serves to locate the small crystals of the halide and to prevent them migrating during development and fixation. Gelatine is a complex organic substance that is able to absorb large quantities of water. In doing so, the volume may increase tenfold. In the expanded condition, diffusion of water and salts can take place through the interstices between the chains of atoms of the expanded molecular network of the gelatine; but the silver bromide crystals, and the silver grains which replace some of them after development, remain fixed in position. These features are of fundamental importance in recording tracks by emulsions. The details of the tracks revealed that any movement of the grains in an emulsion relative to the gelatine is extremely small; for when produced by a

particle of great energy, the grains in a track lie on a straight line to within a fraction of a micron. The gelatine molecules are absorbed to the ions in the surface of the halide, so that the grains are held fixed, like flies on a spider's web. That there is sometimes small relative movement of the grains is indicated by the existence of 'spurious scattering'.

The glycerin is incorporated in the emulsion as a 'plasticiser'. It reduces the brittleness of the emulsion. For convenience gelatine, plasticizer and water altogether are termed as 'gel-phase'.

2.2.2. Formation of the Latent Image

A photographic emulsion is essentially a dispersion of silver halide crystals in a gelatin matrix. This quasi-solid state detector is fundamentally the same as general purpose photographic emulsion, but has several distinguishing features:

(i) The silver halide crystals are very uniform in size and sensitivity

(ii) There are very few crystals that may be developed without exposure to a charged particle.

(iii) The silver to gelatin ratio is much higher (about eight times) than in a conventional emulsion.

(iv) The nuclear emulsion layer is commonly ten to hundred times thicker.

When such an emulsion is exposed to ionizing radiation or light, some of the halide 'grains' are modified. The modifications in the grains brought about by the action of light or radiations are commonly invisible, and the effect is described as the formation of a 'latent image'.

When a silver halide crystal absorbs energy from the incident radiation, it has the effect of liberating mobile electrons leaving electron deficient bromine

atoms. Transfer of an electron from an adjacent bromine ion can overcome the electron deficiency of the first bromine ion, which in turn creates an electron deficiency in the later. In this way, a positive hole can move through the crystal lattice. It is important for latent image formation that a significant proportion of electrons and positive holes are trapped separately, otherwise they could recombine and regenerate halide ions.

2.2.3. Processing of Nuclear Emulsion

For experiments on nuclear physics and cosmic radiation, plates coated with emulsions of thickness up to 600 or 1000 μ have been commonly employed. The processing of such emulsions presents serious problems because of their great thickness and the high concentration of halide. The amount of silver to be removed from the emulsion during fixation is sometimes a hundred times greater than that involved in work with conventional photographic plates of the same surface area. The removal of large quantities of silver halide has the effect that the final processed emulsion has a thickness of about one half that of the original.

The most important requirements in processing the emulsion are to ensure that there is a nearly constant degree of development with depth, and that the final emulsion is free from significant distortion. These conditions are necessary for the successful application of the various methods of determining the mass and energy of charged particles by measuring the grain-density and scattering of their tracks.

The great thickness of the emulsion prevents the successful application of conventional methods of development.

2.2.4. Development

The development is the process by which the latent image contained in an emulsion is made visible by the reduction of silver ions in the silver halide crystal to metallic silver.

The difficulties faced with the processing of thick emulsion with high silver halide concentration can be overcome by the method of development by temperature cycle [13].

The plates are soaked in the developer at low temperature, so that although the chemicals can penetrate into the emulsion, development proceeds very slowly. This process goes on until the diffusion is complete. The plates are then taken to a 'hot-bath', maintained at such a temperature that the development takes place at a faster rate.

2.2.5. Fixation

After development, the plates are immersed in a 'stop-bath' consisting of a 0.5% aqueous solution of acetic acid at 5°C, which arrests development. The purpose of fixation is to remove all the residual silver halide, leaving the metallic silver to form the image. If the silver halide were left in the emulsion, it would slowly go brown and degrade the image. In the process of fixation, a slow flow of fixing solution is maintained over the horizontally placed plates in a fixing bath maintained at a temperature below 10°C. It is an advantage to maintain the fixing bath at a low temperature, < 10°C, for although this reduces the rate of fixing by limiting the degree of swelling of the gelatine, it reduces the distortion in the final plate [13].

2.2.6. Basic Mechanism of Track Formation in Emulsion

When an energetic heavy charged particle travels through a photographic emulsion, there is momentary electrostatic interaction between the charged particle and the atomic electrons of the emulsion along its path. As a result the particle loses its energy and gradually slows down by giving momentum and kinetic energy to all the electrons surrounding the path of travel of the particle. When its energy is less than a few KeV, it ceases to ionize, and its track terminates. The distance from its point of origin to the last developed grain, along the trajectory, is known as track length, R, of the charged particle. The rate of energy loss of the charged particle having charge Ze and moving with a velocity β is given by [12]

$$-\frac{dE}{dR}=\frac{2\pi nZ2r_0^2}{\beta^2}\left(\ln\frac{2m_ec^2\beta^2W_{\max}}{I_0^2(1-\beta^2)}-2\beta^2-2C\right) \tag{2.1}$$

Here, $r_0=\frac{e^2}{m_ec^2}$, the classical radius of electron

m_e = mass of electron

I_0 = mean ionization potential

β = relative particle velocity

W_{max} = maximum energy imparted to the electron.

C = correction term to be applied at high velocity of the projectile.

Each charged particle exhibits a *dE/dR* curve that is distinct from other particle. This characteristic is often exploited in particle physics to identify various particles.

In emulsions, formation of δ-rays (knocked out electrons of high energy) plays a decisively important role in the production of tracks by charged particles.

It ensures that there may be liberated within a grain an amount of energy much greater than the maximum value which would be possible if the parent particle lost energy at a uniform rate along the track. Thus, at minimum ionization, the specific ionization of a particle of charge |e| is ~ 700 KeV/mm. For a uniform rate of loss of energy, the maximum amount which could be absorbed in a grain of diameter 0.3 μ would be ~ 300 eV, for traversal of a grain along a diameter. On the other hand, the range of a δ-ray of energy less than 5 KeV is so short, and its path is so contorted by scattering, that when produced in a particular grain, it must frequently be brought to rest within it. The δ-rays of energy less than ~ 5 KeV are particularly effective in the formation of latent images in the grains along a track as they are frequently arrested within the grain in which they originate. Above this energy, the effective range rapidly increases, and the electrons escape from the grains actually affected by the charged particles. They may then make the neighboring grains develop in the form of spurs to the parent track, or give recognizable δ-ray track. For very energetic particles, a large part of the rate of loss of energy is due to energetic delta rays, relatively few in number. The increasing rate of loss of energy in the extreme relativistic region does not contribute to an increase in the grain-density (the mean number of fully developed grains per unit length of a track) in the tracks. In emulsion, experimentally it is found that when the velocity of a charged particle approaches c, the grain-density or blob-density in its track reaches a minimum value for $\beta = 0.95$ and then gradually rises to a nearly constant value for $\beta > 0.995$. If the grain density at the minimum and at the constant value are represented by g_o and g_p respectively, then it can be said that g_o is generally about 11% less than g_p.

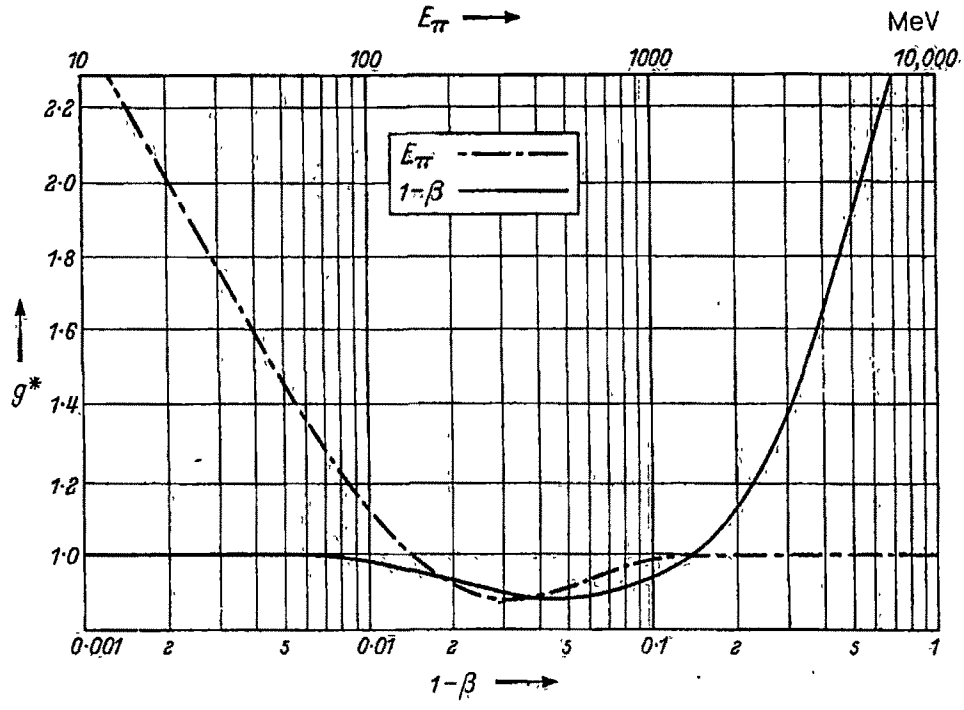

Fig. 2.2: Characteristic example of the variation of normalized grain density g^* (defined latter on) (a) with 1 - β for particles with charge e (solid line) and (b) with energy of π-meson having mass $273m_e$ (dash dotted line) [13].

2.2.7. The Stacks and their Exposure

For the present investigation, stacks of highly sensitive NIKFI BR-2 emulsion plates of dimension 16.9 × 9.6 × 0.06 cm^3 were used. The composition of NIKFI BR2 emulsion has been given in table 2.1 [14, 15].

Table 2.1: The chemical composition of NIKFI BR2 emulsion.

Element	^{1}H	^{12}C	^{14}N	^{16}O	^{80}Br	^{108}Ag
No. of atoms/cc x 10^{22}	3.150	1.410	0.395	0.956	1.028	1.028

The plates were horizontally exposed to ^{84}Kr beams of energy 0.95 GeV/A at SIS of the GSI, Dramstadt, Germany.

2.2.8. Scanning Procedure

Interactions with minimum detection bias were found by double line scanning along the track, fast in the forward direction and slow in the backward direction under 800X magnification with a Carl Zeiss Optical microscope. Care was taken to reject those incident tracks that had ambiguity in ionization and were inclined to the general beam direction. Any event lying within 25 μm from either surfaces of each emulsion plate and occurring within a 20 μm thickness from both the surfaces of the pellicle was not taken into current sample of events, as for such an event there is a greater chance of making errors in counting the number, and measuring the angle of tracks. It has been ensured that all the selected events lie within the first one third of the plate to minimize the variation in the incident beam energy. Proper care has also been taken against under/over counting the number of tracks and inclusion of elastic collision and

electromagnetic dissociated events. Disintegration centers were then scrutinized and different parameters of various tracks were recorded under a magnification of 1875X using oil immersion objective with the same microscope. All total 542 minimum biased Kr–Em interactions are considered for the present work.

2.2.9. Calibration of the Stacks

Tracks produced in wet emulsions have a pronounced tendency to appear with small angles of 'dip', reduced length and width in the processed emulsion. This results from the 'shrinkage' of the emulsion in passing from its wet state to that when it is dry and fixed. During the procession of nuclear emulsion its volume reduces as fixer dissolves the silver halide crystals. The factor by which the volume decreases is known as shrinkage factor (S) [13] and can be defined as–

S = original thickness of emulsion layer / final thickness of emulsion layer

Thus, for any quantitative measurement of track parameters, it is essential to calibrate the emulsion plate with the shrinkage factor that is generally supplied by the manufacturer of the emulsion plates.

2.3. Classification of Secondaries

The events produced by particles of the incident beam are called primary interaction and the particles being emitted from the vertex of the primary interaction are called secondary particles. The tracks of different secondary charged particles emitted from the interactions in nuclear emulsion can be classified according to the standard emulsion terminology on the basis of their ionization (I) and grain density (g). The grain-density, 'g', in a track,

corresponding to a particular value of the specific ionization, depends on the degree of development of the emulsion and also on the type of the emulsion used. For accurate results, it is therefore necessary to determine a new quantity, called normalized grain density and is defined as $g^* = g/g_o$; where g_o, as mentioned earlier, is the minimum grain density of the track of an electron or any other particle of charge 'e' moving in the same emulsion at a velocity in the extreme relativistic region [13].

According to the emulsion terminology the tracks coming out of an interaction fall into four different categories [13, 16]. They are given below-

2.3.1. Shower Tracks

These are the trajectories made mainly by singly charged pions with an admixture (to the extent of ~ 10 to 15 percent) of other strange mesons. The total number of relativistic single final state charged particles in an event is called the multiplicity of the shower particles and is denoted by n_s. As they are generally produced in the first stage of nuclear collision ($t \sim 10^{-22}$ sec), they move with very high velocity ($\beta \sim 0.7$) carrying energy greater than 400 MeV. Their normalized grain density, g^* is less than equal to 1.4. According to the definition of the track grain density of the shower particles, the singly charged projectile fragments are also shower particles. As the singly charged projectile fragments are produced by the projectile spectator, not by the participant part, a careful distinction of the shower tracks is necessary in the angle given by the Fermi momentum at each interaction vertex [17]. Therefore, tracks of such type in the forward PF angle were further subject to rigorous scanning for separating the produced pions and singly charged projectile fragments (protons, deuterons, tritons) looking at the multiple scattering of produced particle [18].

2.3.2. Gray Tracks

These tracks are caused by target associated fast particles, most of which are knocked out protons in the energy range of 30 to 400 MeV and in the velocity range $0.3 \leq \beta \leq 0.7$ with a very small contribution from relatively slow pions and projectile associated fast protons [19-22]. These particles have normalized grain density $1.4 < g^* \leq 6.8$ and their residual range (R) in emulsion is greater than 3 mm [23]. These particles are believed to be emitted during or shortly after the passage of the incoming particle. In nucleus-nucleus interactions, the number of such particles is a parameter of the cascading effect inside the target nucleus [8, 22, 24]. The total number of gray tracks in an event is denoted by n_g.

2.3.3. Black Tracks

Slow protons and fragments of the residual target nucleus in the final non-violent stage of nuclear collision cause these tracks. These particles, with energy < 30 MeV move with velocity less than 0.3c, produce normalized grain density greater than 6.8 in emulsion. The maximum range of the black track is not more than 3 mm in emulsion. The total number of black tracks in an event is denoted by n_b.

Both gray and black fragments are called target fragments as they are parts of target nucleus. In an interaction the total number of gray and black tracks represents the total number of heavily ionizing charged fragments in that event which is symbolically represented by n_h ($= n_g + n_b$). The number of heavy tracks in an event (n_h) is of special significance from the point of view that this number can be used to decide the nature of the target nucleus.

2.3.4. Projectile Fragments (PFs)

The particles, which are emitted from the spectator part of the projectile nucleus, are called projectile fragments. The projectile fragments move with almost same momentum as that of beam. They are generally confined in an extreme forward angle, θ_f, relative to the beam direction, which can be defined as, $\theta_f = \frac{P_f}{P_L}$, where P_f is Fermi momentum of nucleon and P_L is the beam momentum [19]. Considering $P_f = 0.2$ GeV, the projectile fragmentation angle θ_f is found to be 0.12 radian or 7.03 degree for the energy of the present work. They have charge $Z_{PF} \geq 1$ and their ionization remains nearly constant over a few mm. The total number of projectile fragments in an event is denoted by n_{PF}.

The final states of an emulsion event characterized by different multiplicities of the secondary charged particles (n_{ch}) is considered to be the sum of all charged particles that are emitted in the interaction, $n_{ch} = n_s + n_g + n_b + n_{PF}$.

2.4. Selection Criteria for the Type of Events

For the present study, the following selection criteria for determining the type of events [10, 18, 25, 26] is used.

a) $N_h \leq 1$: Kr- H interaction

b) $2 \leq N_h \leq 8$: Kr-CNO interaction (having no short track)

Kr-AgBr interaction (at least one short track)

c) $N_h > 8$: Kr-AgBr interaction

The event statistics for different targets of emulsion is shown in table 2.2. A few photographs of Kr interactions with different nuclei of emulsion targets are shown in Fig. 2.3.

Table 2.2: The statistics for various categories of ^{84}Kr–Em interactions for different targets of nuclear emulsion.

Interaction	Number
^{84}Kr–H	105
^{84}Kr–CNO	215
^{84}Kr–AgBr	222

2.5. Charge Estimation of Projectile Fragments

The charge of the projectile fragments can be estimated by measuring different track parameters. The basic principle behind the measurement of all these parameters is ionization made by the moving charged particle. In emulsion, tracks due to relativistic charged particle show a narrow central core around the trajectory of the particle, and a number of associated delta rays. In the tracks of Z = 1 projectile fragments, grains are well separated and can be considered individually. But with the increase of the charge of the fragments, density of the developed grains increases and at certain level it is not possible to resolve the adjacent grains. In the tracks of heavily charged fragments, the grains get clogged to each other to form blobs and thus the counting of individual grains become impossible. One then counts per unit length the number of developed blobs and the gaps between them as the measure of PF charge. For further increase of the charge, significant numbers of delta rays are formed. At certain limit of the charge of the particle it again becomes difficult to treat the delta rays individually and as a whole a significant width of the track of an emitted secondary is found.

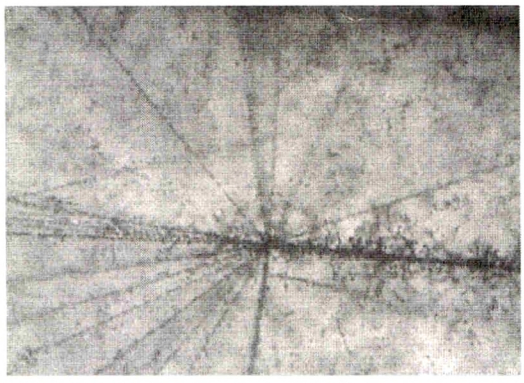

(a) Kr-AgBr (Peripheral)

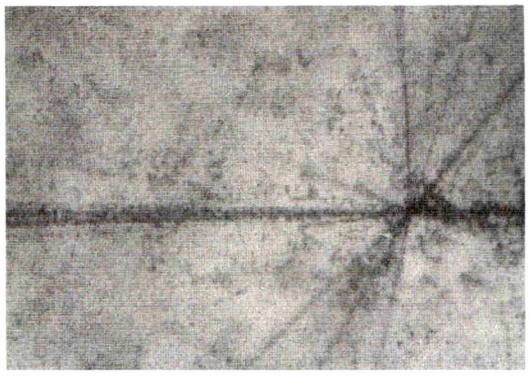

(b) Kr-AgBr (Peripheral)

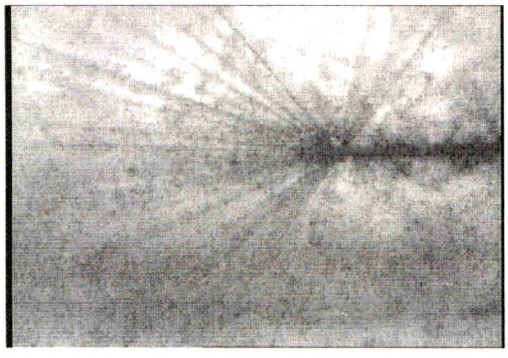

(c) Kr-AgBr (Central)

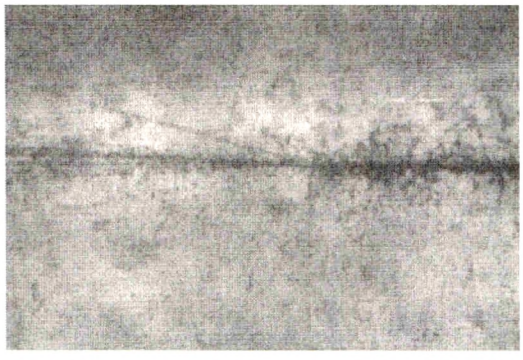

(d)Kr-CNO

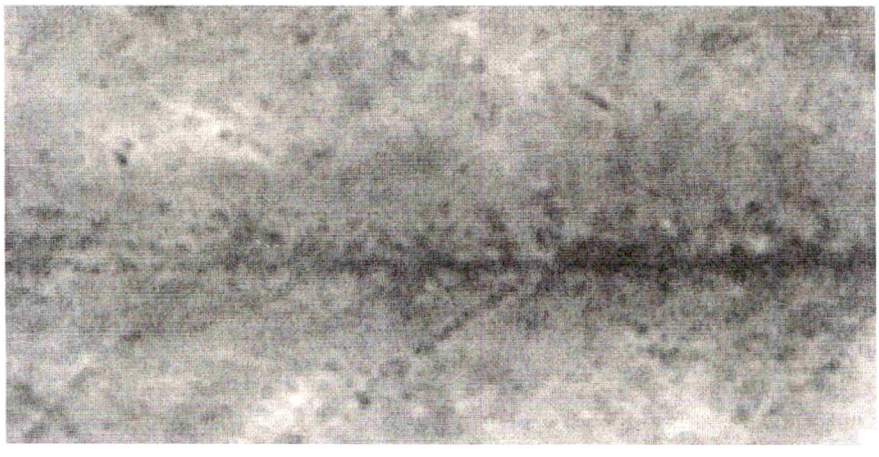

(e) Kr- H

Fig. 2.3: Photograph of ^{84}Kr-AgBr non central (a and b); ^{84}Kr-AgBr central (c); ^{84}Kr-CNO (d) and ^{84}Kr-H (e) interactions.

As all the above mentioned track parameters possess some limitations towards the measurement of charge of various charged particles and therefore it is not very worthy to apply a single method to determine the charge of the various PFs with different Z_{PF} values. The different methods which are used to measure the charge of various PFs in this work are listed below:-

Z_{PF} value	Techniques adopted
1	Grain density, Hole density
2-5	Grain/Blob density, Hole density, Gap length coefficient and δ-ray density
6-12	Blob density, δ-ray density
≥13	δ-ray density and/or Relative track width measurement

2.5.1. Blob & Hole Density Measurement

As mentioned above, in a track two or more developed grains clogged to each other to form what is called a 'blob' and the number of blob per unit length (say, 100 μm) is called blob density. It is symbolically represented by 'B'. The space between two consecutive grains or blobs is called a 'hole'. The number of holes per 100 μm is called hole density and is denoted by 'H'. For this work only those holes are considered whose length are greater than or equal to a certain minimum length [13]. This method is well applicable only when the ionization is low i.e., for lighter fragments. For heavier fragments, ionization increases with nuclear charge resulting a less number of blob densities, because the small blobs continue to coalesce into a larger one. Thus, this technique is relatively insensitive to further increase in ionization.

Following earlier works [27, 28], the frequency of grain and/or blob density for all PFs of the entire data sample is arbitrarily plotted in Fig. 2.4(a). It shows that some distinct peaks are there against some particular grain and/or blob density. As PFs with $Z_{PF} = 1$ will not be able to produce enough ionization in emulsion to produce too many grains/blobs per unit length along its trajectory resulting in maximum number in case of hole density. On the other hand, for PF's with $Z_{PF} \geq 3$, the small blobs coalesce into larger blobs resulting in a net decrease in the number (an increase in blob length) of blobs per unit length. The peak at maximum blob density is assigned to $Z_{PF} = 2$. The subsequent peaks are assigned to the corresponding higher Z_{PF} values of the projectile fragments. In Fig. 2.4(b) the variation of grain/blob density against the square of the charges of various PF's is plotted. The frequency distribution of hole density is shown in Fig. 2.5(a) and Fig. 2.5(b) represents the variation of hole density against Z_{PF}^2.

2.5.2. Gap Length Coefficient

It is defined as the ratio of the total number of observable gaps to the number of gaps greater than l [28]. The gap length coefficient (G) can be estimated using the following relation [29]

$$G = - (1/l)\ln(B/H) \qquad (2.2)$$

It is nearly proportional to the rate of the energy loss of the ionizing particle and does not depend on the mean developed grain size.

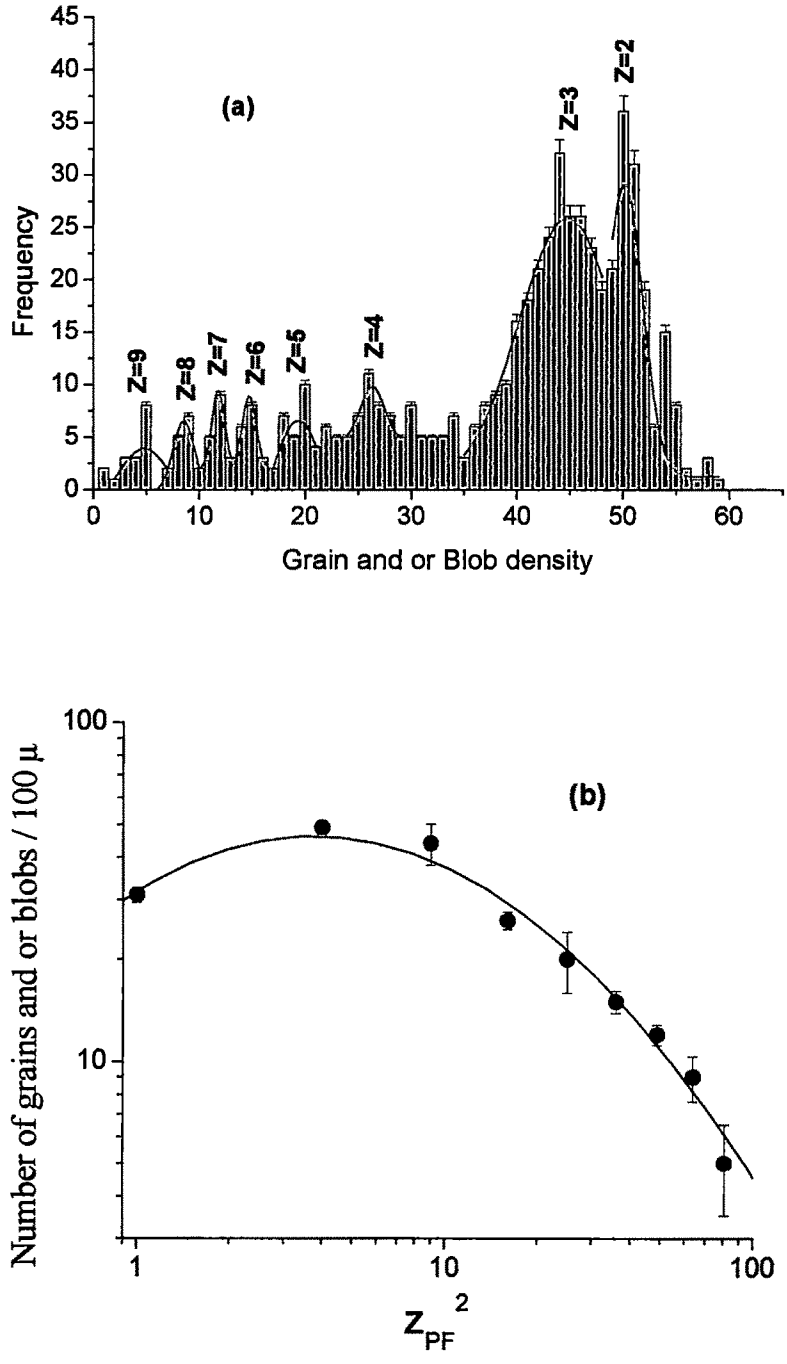

Fig. 2.4: (a) Frequency distribution of grain and or blob density. (b) Calibration of grain and or blob density as a function of Z_{PF}^2.

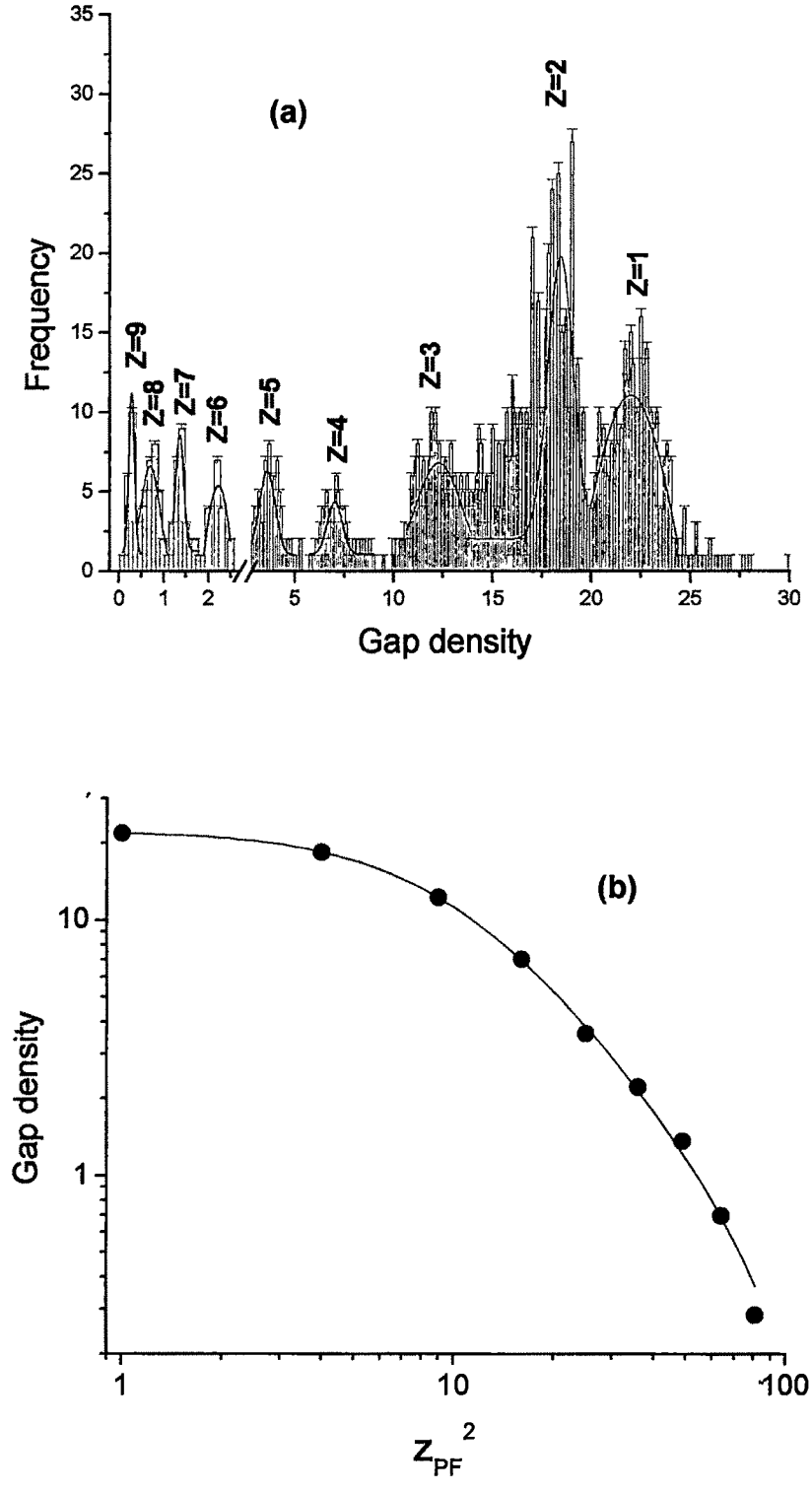

Fig. 2.5: (a) Frequency distribution of hole density. (b) Calibration graph for hole density density

2.5.3. Delta Ray Density Measurement

At higher values of Z_{PF}, delta rays possessing energy > 5 KeV escape from the parent grain with considerable kinetic energy and produce recognizable delta (δ) shaped tracks or small spurs made up of one or two grains contiguous to the tracks. To measure the delta ray density, different workers have adopted various conventions [18, 25, 26, 30, 31]. For the present work, to determine the delta ray density, only those delta tracks are considered which are continuous, clearly originating from the parent particle and have three or more grains remaining inclined against the direction of propagation of the parent particle. The number of such tracks per 100 μm is taken as a δ-ray density (N_δ). The frequency distribution of δ-ray density and its variation with the corresponding $Z_{PF}^{\ 2}$ values of different PFs are shown in Figs. 2.6(a) and 2.6(b) respectively. Obviously, the peak corresponding to the minimum δ-ray density represents the average number of δ-ray density for $Z_{PF} = 2$.

2.5.4. Relative Track Width Measurements

For relativistic nuclei with $Z_{PF} = 13$ and for higher values, the increased value of N_δ makes it difficult to count correctly the individual δ-ray track. At this stage one can obtain the measure of ionization from the width of the particle's track. With the greater nuclear charge, the maximum energy of the δ-rays varies more rapidly along the track. Further, the number of δ-rays of a given energy, per unit length of track varies as Z_{PF}^2. As these features together determine the width of the solid core of the track, with the increase of the Z_{PF} value, there is an increase in the maximum width of the core [13]. Also, Nakagawa et al. [32], from

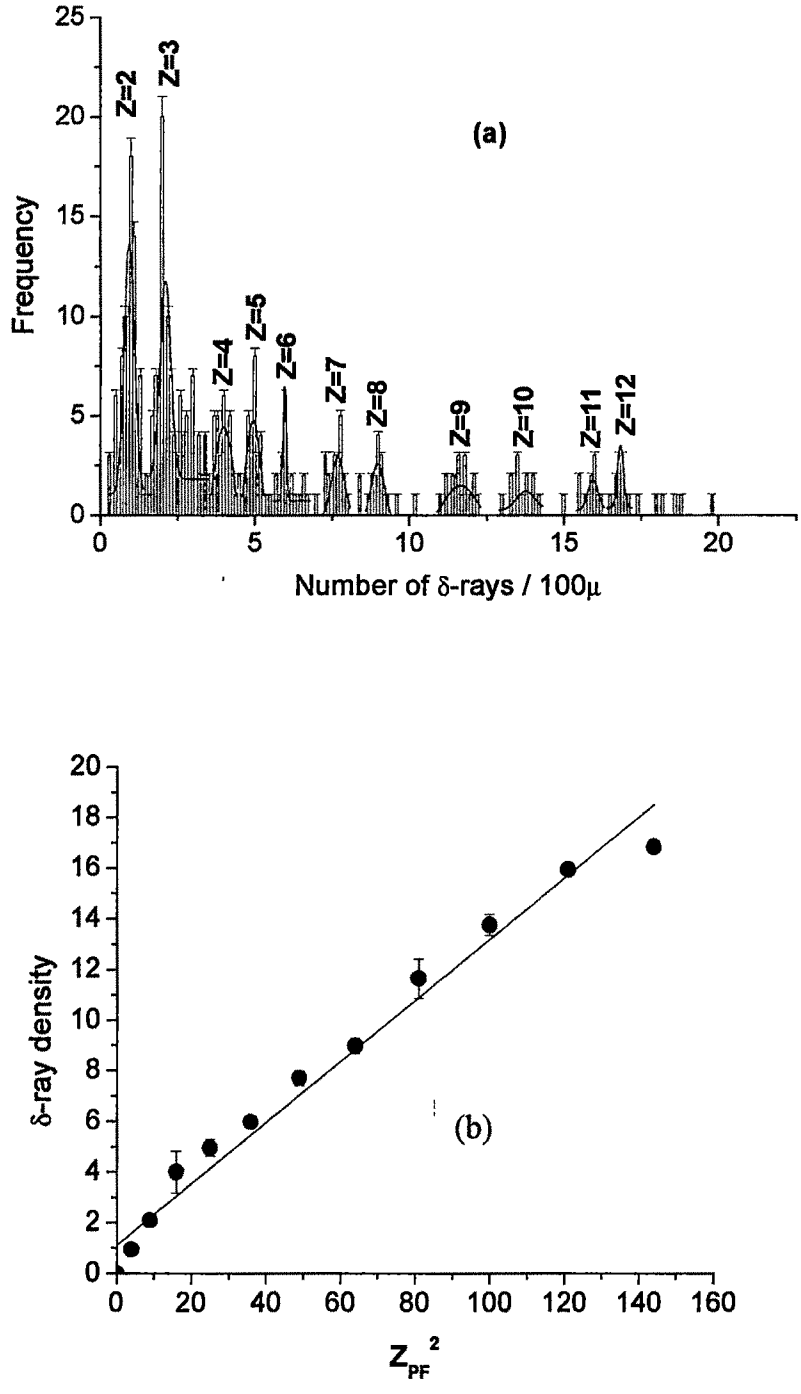

Fig. 2.6: (a) Frequency distribution of δ-ray density. (b) Calibration curve of δ-ray density as a function of Z_{PF}^{2}.

the measurements in G-5 emulsion, have shown that the average width W of a track is approximately proportional to Z. In relative track width measurement method, the unknown charge of the ionizing particle can be determined using the relation [33]

$$Z_{PF} = \frac{W_{PF}}{W_{Proj}} \times Z_{Proj} \tag{2.3}$$

where, Z_{Proj} is the charge of the projectile and W_{PF} & W_{Proj} represent the width of the projectile fragment and projectile respectively. The method seems to be applicable for tracks near the maximum of their widths. W_{Proj} and W_{PF} were measured at a number of different points just before and after the interaction vertex with the help of a filar micrometer. Only the core part of the track was measured for estimating the width of the track.

While assigning charge to the heaviest PF, the requirement of charge conservation is taken into account.

2.6. Determination of Space Angle of Various Charged Secondaries

The space angle of each charged secondary particle was determined with the help of a goniometer that can measure up to $1/6^{th}$ of a degree. The goniometer is attached in one of the eyepieces of microscope and the vertex of interaction is focused at the center of the goniometer. One of the reference lines of goniometer is then aligned with the direction of beam and the direction of incident projectile is recorded from the circular and vernier scales attached to the goniometer. The projection angle (θ_p) of each secondary track in the plane of focus is then directly read from the goniometer scale with the help of same reference line aligning with various secondaries one by one. The true dip angle (δ) i.e. the angular depression

of the track from the horizontal plane of the emulsion can be calculated using the relation,

$$\delta = \tan^{-1}\left(\frac{S.\Delta Z}{L}\right) \tag{2.4}$$

where, ΔZ = the true difference of depth between vertex and any other point of the track at a distance L from the vertex.

The space angle (θ) of the track (having projected angle θ_p and dip angle δ) with respect to beam, is given by

$$\cos\theta = \cos\theta_p \cos\delta_1 \cos\delta_2 + \sin\delta_1 \sin\delta_2 \tag{2.5}$$

where δ_1 & δ_2 respectively are the dip angles of the track and the beam respectively with respect to the interaction vertex.

2.7. Some Features of Various Charged Secondaries of Present Investigation

2.7.1. Mean Multiplicity of Charged Secondaries

Mean multiplicity of produced particles and target associated charged secondaries emitted from Kr-Em interaction are tabulated in table 2.3. For comparison, the results reported by other groups for different systems at few GeV/A are also listed in the table.

From the above table it is seen that the obtained results agree well with the result reported by Krasnov et al. [45]. Excluding Ar [44], it is seen that for projectile energies 0.6 - 4.5 AGeV, average multiplicity of produced particle increases with the increase of projectile mass up to $A_p = 32$ and then for higher projectile it seems to be saturated. Variation of $\langle n_g \rangle$ with the projectile mass also shows the same pattern. Up to $A_p = 32$, $\langle n_g \rangle$ linearly increases with the increase of the size of the projectile and then it gives the impression of saturation. This

may be due to the fact that at certain energy range, with the increase of projectile mass, nucleon-nucleon interaction increases. But once the projectile procures the target mass, there is no such further increase in nucleon-nucleon encounters which makes $<n_s>$ and $<n_g>$ independent of A_p. For target associated slow particle, except the proton beam, the mean value is almost independent of projectile mass. Earlier workers like A. Dabrowska et al. [47], M. I. Adamovich et al., [8], P.L. Jain et al., [48] and Krasnov et al. [45] also reported similar result. Such a constant number of evaporated black particles suggest that approximately same excitation energy has been deposited to the target residue, irrespective of the size of the projectile nucleus [45]. This also shows that the excitation of the target nucleus together with the subsequent evaporation of particles and fragments seem to be independent of the first stage of the collision.

Table 2.3: Average multiplicity of different charged secondaries

Projectile	Energy (A GeV)	$<n_s>$	$<n_g>$	$<n_b>$	Ref.
^{1}H	0.95	0.54±0.04	1.11±0.07	2.61±0.11	34
^{1}H	4.5	1.63±0.02	2.81±0.06	3.77±0.08	35
^{12}C	4.5	7.67±0.19	5.93±0.34	4.49±0.24	36
^{14}N	2.1	8.85±0.28	5.29±0.31	4.57±0.22	37
^{16}O	3.7	-	6.4±0.5	5.1±0.3	38
^{16}O	4.5	10.5±0.60	7.60±0.60	4.88±0.29	39
^{22}Ne	4.1	9.9±0.39	5.52±0.26	4.01±0.15	40
^{22}Ne	4.1	8.38±0.22	7.58±0.23	7.63±0.17	41

(Cont...)

^{24}Mg	4.5	11.1±0.3	7.9±0.3	5.3±0.2	42
^{28}Si	4.5	11.26±0.33	8.59±0.26	4.69±0.23	36
^{28}Si	4.5	11.8±0.3	6.4±0.2	4.8±0.1	42
^{28}Si	4.5	11.98±0.67	7.28±0.55	5.69±0.35	43
^{32}S	4.5	12.46±0.74	7.9±0.56	5.91±0.39	40
^{40}Ar	1.0-1.2	5.3±0.3	6.5±0.3	5.3±0.2	44
^{84}Kr	0.95	10.73± 0.69	8.18±0.52	4.65±0.29	P. W.
^{84}Kr	0.8-0.95	10.6±0.4	7.8±0.4	4.1±0.2	45
^{139}La	0.6-1.2	11.5±0.6	6.0±0.3	4.4±0.2	46

2.7.2. Multiplicity Distribution of Produced Particles and Target Fragments

In Fig. 2.7(a, b, c), we have plotted multiplicity distribution of produced particles, fast and slow target fragments respectively emitted from Kr-Em interactions. The experimental data is compared with that of the FRITIOF generated data. Average frequency of n_s is in good agreement with the FRITIOF estimated values. In case of grey particle, except for higher multiplicity region, experimental data is more or less in agreement with that of FRITIOF data but for black particle, experimental value of average frequency is systematically high due to non-consideration of slow particle cascading into the nuclei in the FRITIOF.

2.7.3. Multiplicity Distribution of Projectile Fragments

The multiplicity distribution of all the charged projectile fragments with Z_{PF} = 1-35 emitted from Kr-Em interactions is shown in Fig. 2.8. The distribution

is fitted with a Gaussian function. The width of the distribution at half maximum is found to be 10.95 with a maximum at 5. On comparison with Kr-AgBr data at the same energy [27], it is observed that the width of the distribution is broader in case of Kr-Em interactions. This is probably due to the fact that in emulsion, target varies from H to AgBr ensuing more different channels to break the projectile. On the other hand, if the result is compared with that of ^{238}U-Em interactions at 0.96A GeV [49], it is found that the distribution of ^{238}U-Em interactions is more widely dispersed which could be due to the reason that a heavier beam splits up into variety of ejectiles resulting in increased multiplicity. Further details on multiplicity distribution of PFs will be discussed in next chapter.

2.8. Multiplicity correlation

The number of charged secondaries produced in an interaction depends mostly on the amount of energy and momentum transferred in a collision, which in turn, depends on the number of nucleon-nucleon collisions. The number of such nucleon-nucleon collisions on the other hand depends on the collision geometry or otherwise the impact parameter of the collision. In simple geometrical picture, nucleus-nucleus collisions may broadly be divided into following three categories:-

Peripheral: $b \sim R_T + R_P$

Quasi central: $|R_T + R_P| > b \geq |R_T - R_P|$

Central: $0 \leq b \leq |R_T - R_P|$

where b is the impact parameter and R_T and R_P are the radii of the target and the projectile nuclei respectively.

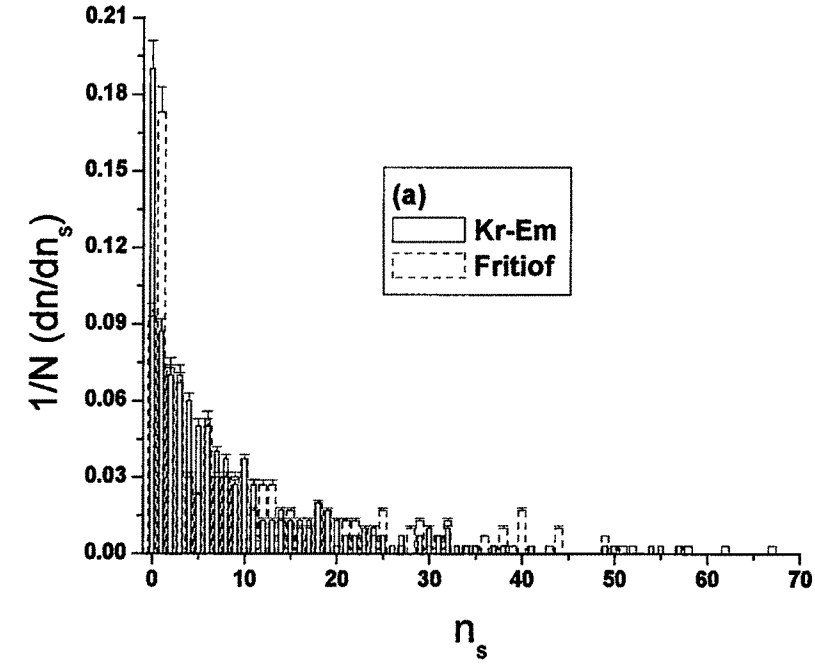
0.21
0.18
0.15
0.12
0.09
0.06
0.03
0.00
1/N (dn/dn$_s$)
(a)
Kr-Em
Fritiof
0
10
20
30
40
50
60
70
n$_s$

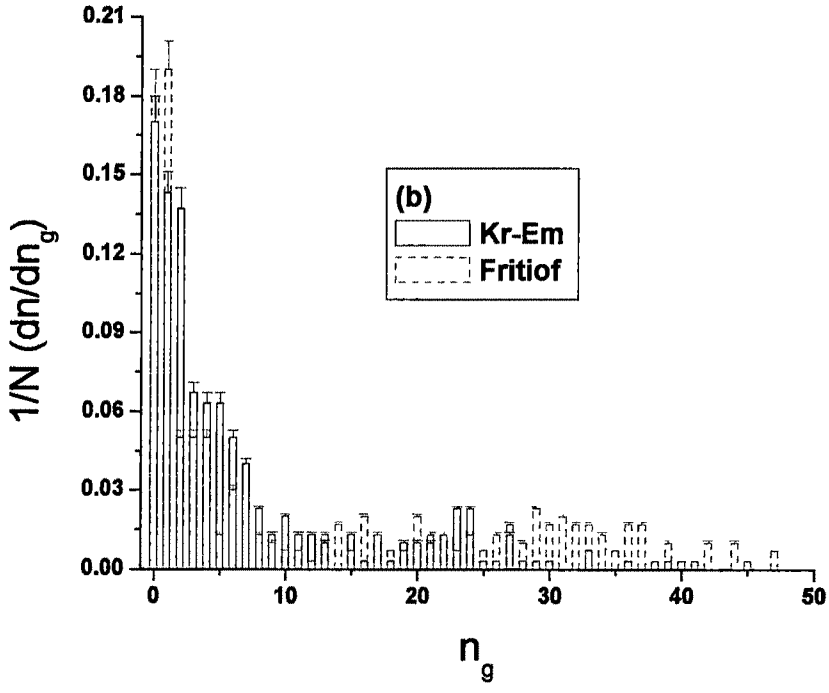
0.21
0.18
0.15
0.12
0.09
0.06
0.03
0.00
1/N (dn/dn$_g$)
(b)
Kr-Em
Fritiof
0
10
20
30
40
50
n$_g$

(Fig. 2.7: Cont...)

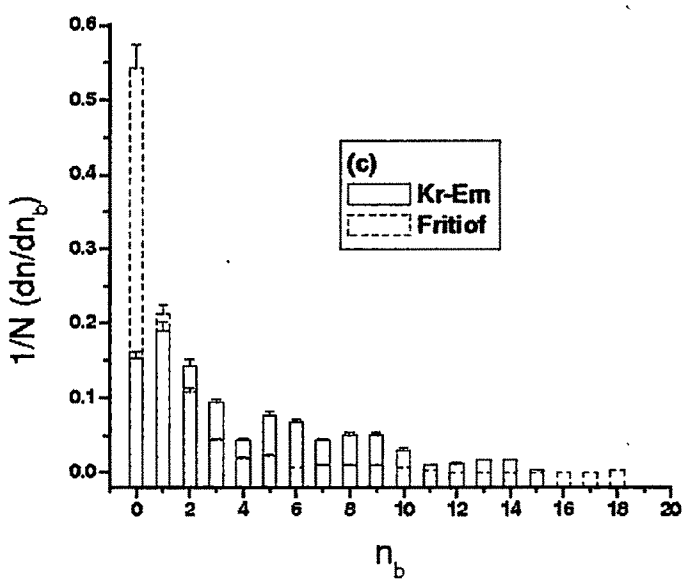

Fig. 2.7: Frequency distribution of normalized (a) shower particles, (b) grey particles, and (c) black particles for Kr-Em ineractions.

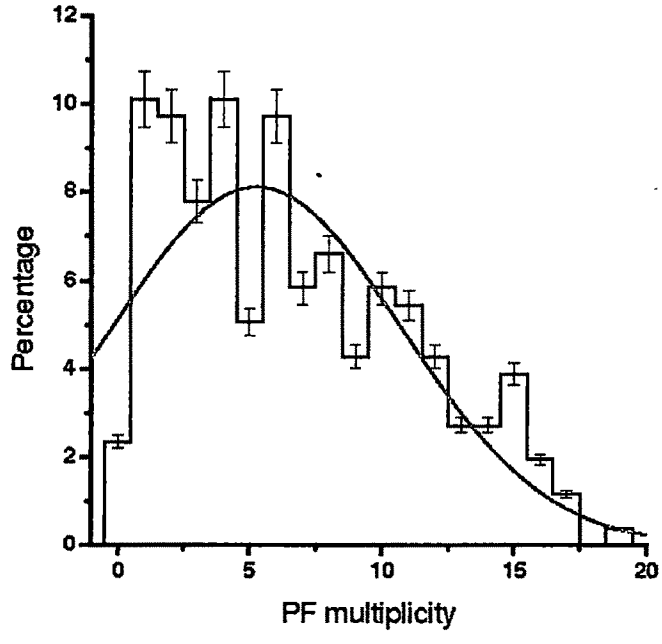

Fig. 2.8: Multiplicity distribution of projectile fragments emitted from Kr-Em interactions.

But impact parameter is not a directly measurable quantity. Some experimentally observable quantities that are often used by emulsion workers as the measure of impact parameter are:

(i) average number of produced particles in an event, $\langle n_s \rangle$ [17, 50, 51]

(ii) average number of heavily ionizing particles, $\langle n_h \rangle$ [14, 52-54, 58]

(iii) total charge of the projectile fragments, Q_{PF} [18, 45, 53, 55-61].

In heavy ion collisions, the total charge Q_{PF} of the projectile fragments is often considered to be a reliable parameter to determine the collision geometry. Depending upon the colliding system, it is believed that for central collisions the overlapping of projectile and target nuclei is maximum and there is no or little portion of incident projectile nucleus left as spectator to produce any PFs. Hence for central collision, Q_{PF} is expected to be very small ($Q_{PF} \leq 2$). On the other hand, events with large Q_{PF} (i.e., $Q_{PF} \sim Q_{beam}$) are categorized as peripheral collisions. Here the participant part is very small. Collisions lying in between central & peripheral collisions are often termed as quasi-central collision [62]. Considering Q_{PF} as a measure of the degree of centrality of the collision, an attempt has been made to find the correlation between Q_{PF} and the parameters such as n_s, n_h that are also considered as the measure of centrality of collision.

2.8.1. Correlation between $\langle n_s \rangle$ and Q_{PF}

Variation of $\langle n_s \rangle$ with Q_{PF} is shown in Fig. 2.9. From the figure it can be seen that average number of produced particle decreases linearly with the increase of Q_{PF} i.e. from central to peripheral interactions. This result well agreed with the result reported by Krasnov et al. [45] and Adamovich et al. [63] for ^{84}Kr-Em interactions at 0.95 GeV/A and ^{28}Si-Em interactions at 3.7 GeV/A respectively.

2.8.2. Correlation between $<n_h>$ and Q_{PF}

Fig. 2.10 shows the variation of average number of heavily ionizing tracks with Q_{PF}. As expected, the plot shows that the mean number of heavily ionizing particle gradually increases with the increase in centrality of the collision. Similar result is also reported by other workers like Fu-Hu Liu [38] for ^{16}O-Em interactions at 3.7A GeV and 200A GeV, S.A. Krasnov et al. [45] for ^{84}Kr-Em interactions at 950 MeV/A and A. Abd El-Daiem [64] for ^{24}Mg and ^{28}Si interactions with AgBr emulsion nuclei at 4.5 A GeV.

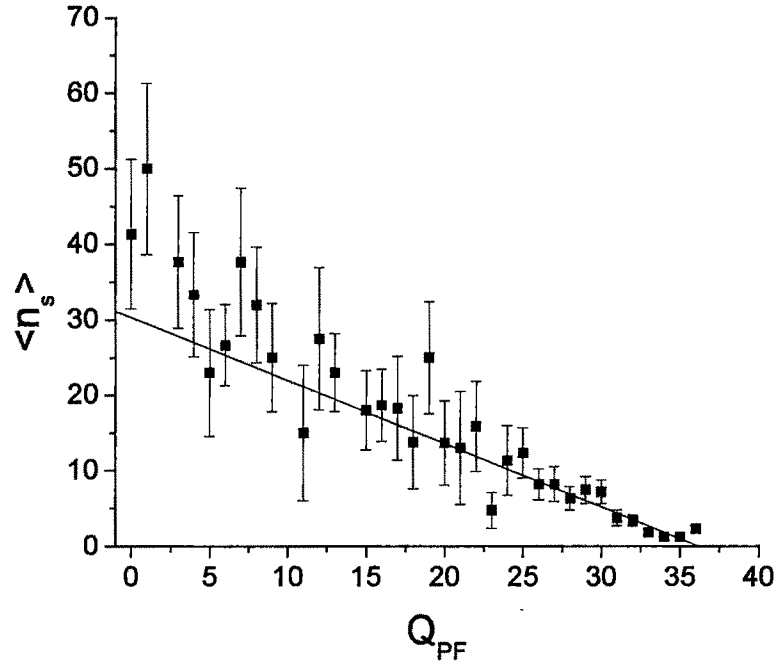

Fig. 2.9: Variation of average relativistic produced particle with Q_{PF}. Solid line is the best fitted line with R = 0.905.

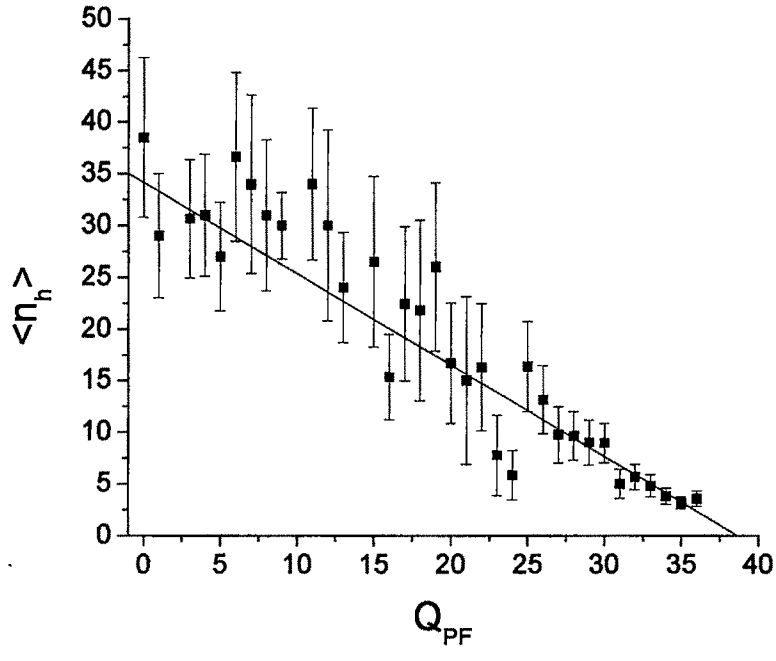

Fig. 2.10: $\langle n_h \rangle$ vs. Q_{PF}. Solid line represents the best fitted line with R = 0.954.

References

[1] H. Yagoda, Space Science Reviews, **1(2)**, 224 (1962).

[2] M. Blau and H. Wambacher, Sitzber. Akad. Wiss. Wien. Abt. 2a **146**, 623 (1937).

[3] C. M. G. Lattes *et al.,* Nature **160**, 453 (1947).

[4] H. Yukawa, Proc. Phys. Math. Soc. Jap. **17**, 48 (1935).

[5] S. Aoki et al., CERN-EP/2001-074.

[6] V. Bradnova *et al.*, JINR-LHE-0983-2.

[7] M.Aggarwal, *III International Conference of the Physics and Astrophysics of Quark Gluon Plasma (QGP Conf. Proc.), eds. B. C. Sinha, D. K. Srivastava and Y. P. Viyogi* , p. 189 (Narosa Publishing House, New Delhi, India, 1998).

[8] M. I. Adomovich *et al.*, Phys. Lett. B **262**, 369 (1991).

[9] A. Dabrowska *et al.*, Acta Physica Polonica B **31(3)**, 725 (2000).

[10] B. Bhattacharjee, Nucl. Phys. A **748**, 641 (2005).

[11] B. Bhattacharjee and S. Sengupta Int. J. Mod. Phys. E **14(8)**, 1223 (2005).

[12] W. H. Barkas, *Nuclear research emulsion*, Vol. **1** (Academic press, NY & London, 1963).

[13] C. F. Powell *et al.*, *The study of elementary particles by the photographic method* (Pergamon Press, London, 1959).

[14] A. Abdelsalam *et al.*, J. Phys. G: Nucl. Part. Phys. **28**, 1375 (2002).

[15] V. Singh *et al.*, arXiv:nucl-ex/0412051 v1 22 Dec (2004).

[16] B. Bhattacharjee *et al.*, Ind. J. Phys. **81(7)**, 717 (2007).

[17] F. H. Liu, Chinese J. of Phys **41(5)**, 486 (2003).

[18] N. N. Abd-Allah, J. of the Phys. Soc. of Japan **69(4)**, 1068 (2000).

[19] D. H. Zhang *et al.*, Chinese Phys. Soc. and IOP Publishing Ltd. **13(8)**, 1239 (2004).

[20] T. Ahmed *et al.*, Phys. Rev. C **47(6)**, 2974 (1993).

[21] M. I. Adamovich *et al.* (EMU01 Collaboration), Cosmic and Subatomic Phys. Report LUIP 8907 (1989).

[22] N. N. Abd-Allah and M. Mohery, Turk J. Phys. **25**, 109 (2001).

[23] F. H. Liu *et al.*, Phys. Rev. C **69**, 057601 (2004).

[24] T. Ahmed and M. Irfan, Phys. Rev. C **44**, 1555 (1991).

[25] R. K. Shivpuri and V. K. Verma, Phys. Rev. D **47(1)**, 123 (1993).

[26] M. El-Nadi *et al*, Nouvo Cimento A **107**, 1 (1994).

[27] S. Sengupta, PhD Thesis, Gauhati University, Guwahati (2009).

[28] V. Singh, PhD Thesis, Banaras Hindu University, Varanasi (1998).

[29] P. H. Fowler and D. H. Perkins, Phil. Mag. **46**, 587 (1955).

[30] H. L. Bradt and Peters, Phys. Rev. **74**, 1828 (1948).

[31] D. A. Tidman *et al.* Proc. Roy. Soc. A **66**, 1019 (1953).

[32] S. Nakagawa *et al.*, J. Phys. Soc. **11**, 191 (1956).

[33] R. Katz and E. J. Kobetich, Phys. Rev. **186(2)**, 344 (1969).

[34] W. O. Lock *et al.*, Proc. Roy. Soc. A **231**, 368 (1990).

[35] A-ABDDKLMTU-B Collaboration, Z. Phys. A **302**, 133 (1981).

[36] T. Ahmad and M. Irfan, Nuovo Cimento A **106(2)**, 171 (1993).

[37] G. M. Chernov *et al.*, Nucl. Phys. A **280**, 478 (1977).

[38] F. H. Liu, Chinese J. Phys. **40(2)**, 159 (2002).

[39] V. A. Antonchik *et al.*, Sov. J. Nucl. Phys. **39**, 774 (1984).

[40] N. N. Abd-Allah and M. Mohery, Czechoslovak J. Phys. **51(11)**, 1189 (2001).

[41] B. P. Bannik *et al.*, Z. Phys. A **329**, 341 (1988).

[42] A. El-Naghy *et al.*, Tr. J. Phys. **19(9)**, 1170 (1995).

[43] F. H. Liu *et. al.*, Phys. Rev. C **67**, 047603 (2003).

[44] V. A. Antonchik *et al.*, Yad. Fiz. **51**, 765 (1990).

[45] S. A. Krasnov *et al.*, Czechoslovak J. Phys. **46(6)**, 531 (1996).

[46] A. Gill *et al.*, Int. J. Mod. Phys. A **5**, 755 (1990).

[47] A. Dabrowska *et al.*, INP Krakow Report No. 1617/PH (1993).

[48] P. L. Jain *et al.*, Phys. Rev. C **44**, 844 (1991).

[49] P. L. Jain *et al.*, Phys. Rev. Lett. **68(11)**, 1656 (1992).

[50] M. S. El-Nagdy, Phys. Rev. C **47(4)**, 346 (1993).

[51] M. I. Adamovich *et al.*, J. Phys. G: Nucl. Part. Phys. **22**, 1649 (1996).

[52] P. L. Jain *et al.*, Phys. Rev. Lett. **59**, 2531 (1987).

[53] M. I. Adamovich *et al.*, Eur. Phys. J. A **1**, 77 (1998).

[54] A. Abdelsalam, JINR report (Dubna) E1–81–623 (1981).

[55] H. H. Heckman *et al.*, Phys. Rev. C **17**, 1651 (1978).

[56] A. Abdelsalam *et al.*, Czech. J. Phys. B **34**, 1196 (1984).

[57] M. El–Nadi *et al.*, Eur. Phys. J. A **10**, 177 (2001).

[58] M. A. Jilany, Phys. Rev. C **70**, 14901 (2004).

[59] M. A. Jilany *et al.*, Int. J. Mod. Phys. E **4(4)**, 815 (1995).

[60] N. N. Abd-Allah *et al.*, Int. J. Mod. Phys. E **10(1)**, 55 (2001).

[61] R. R. Joseph *et al.*, J. Phys. G: Nucl. Part. Phys. **18**, 1817 (1992).

[62] B. Bhattacharjee *et al.*, Ind. J. Phys. **82(6)**, 735 (2008).

[63] M. I. Adamovich *et al.*, Preprint JINR E1-92-569 (1992).

[64] A. Abd El-Daiem, American J. of Applied Sciences **6(4)**, 608 (2009).

Chapter III

Scaling Behavior of Kr Projectile Fragmentation

3.1. Introduction

It is well known that studies on global observables like multiplicity, transverse energy etc. provide valuable informations on high-energy nucleus-nucleus collisions. Multiplicity of charged particles varies on a number of factors such as – centrality of collision, energy of incident beam, size of the fragmenting system etc.

Besides defining the collision geometry, studies on multiplicity provide important information on particle production mechanism as well as the nuclear fragmentation process and the correlation between the two processes [1]. It was also reported that the total charged fragment multiplicity is proportional to the temperature of the colliding system [2]. Studies on charged particle multiplicity also help us to check the reliability of many models suggested to describe high-energy nuclear collisions [3].

At the early stage of nuclear interactions, prompt nucleons (i.e., protons directly participating in the collision) are emitted from the colliding systems that carry out a large amount of available kinetic energy. They result from quasielastic and inelastic collisions of projectile and target nucleons. Immediately after the collision, the remnant of the projectile nucleus is in an excited state with temperature T_i. The excited remnant then expands and cools evolving into a neighborhood of the critical point on the temperature-density plane [2]. Then it breaks up into many intermediate mass fragments and freezes out at temperature T_f. Such breaking of nuclei into a numbers of fragments having a range of masses is called multifragmentation (MF). Nuclear multifragmentation is a violent reaction associated with a comparatively small impact parameter [4]. In this process excited nuclei break up into several pieces of smaller masses, each more massive then an alpha particle. The fragments produced in such reactions are

believed to carry information about the decay process and hence the collision dynamics. Although MF has been known since the early days of cosmic ray physics [5], it has only become a subject of intense investigation since it was found to occur in high yield in high-energy proton and intermediate-energy heavy ion reactions [6]. Theoretical interest in MF followed upon the discovery that the yields of fragments with mass A_f produced in proton-xenon and proton-krypton collisions obeyed a power law $Y(A_f) \propto A_f^{-\tau}$, with $\tau \sim 2.5$ [7], as expected for a system undergoing a liquid-gas type of phase transition in the vicinity of its critical point. This result raised the possibility that MF could provide information about the equation of state of nuclear matter [2, 8-11]. The question of equilibration in the multi-fragment decay of excited spectator systems is of highest interest. Multifragmentation has been considered a manifestation of the liquid-gas phase transition in finite systems [12].

In the study of high-energy nuclear collisions, it has already been realized that a reasonable comparison of fragmentation of different systems is possible only when the corresponding multiplicity is scaled. It is generally done to test a hypothesis. Data for a wide range of system masses and incident energies collapse on to an approximately universal scaling function. The data collapsing behavior is a fundamental property of homogeneous functions. Homogeneity rules play a central role in the theory of critical phenomena [13]. Near the critical point of a physical system, the thermodynamic functions exhibit homogeneous form which implies the existence of a law of corresponding states: using a suitably chosen scaling transformation it is possible to bring different states of the same system to coincidence and thus to compress many experimental or theoretical results into a compact form [14]. Thus in the study of fragmentation

one can scale the data in two regimes namely with respect to energy of the beam and with respect to system size. In this endeavor, in connection with the study of multiplicity of produced particle in h-h collisions, Koba, Nielson and Olesen in 1972 put forwarded a hypothesis [15] with which one can conveniently compare the multiplicity distributions of produced particles for various systems at different beam energies. On the other hand, different workers have also studied the fragmentation mechanism with respect to mass of the fragmenting system.

In the chapter II a brief idea about the general characteristics of produced particle as well as target associated slow and fast particles were given. In this chapter only the projectile fragments are considered. An attempt has been made to map out the forms of the scaling functions in the energy domain in the light of KNO scaling as well as scaling behavior with respect to system size (mass).

To study the scaling behavior, the analysis of the experimental data of the present investigation has been started with KNO scaling. The results on the scaling behavior of the intermediate mass fragments with the size of the fragmenting system have been furnished at the later part of this chapter.

3.2. Results and Discussion

Charge distribution of various projectile fragments with $Z_{PF} \geq 1$ emitted from ^{84}Kr-H, CNO, Em and Ag/Br interactions are plotted in Fig. 3.1. From this figure it can be readily seen that, irrespective of target mass, the emission of light projectile fragments are most abundant. In case of heavier target, the remnant part of the projectile nucleus splits into lighter fragments more preferably thereby leaving few heavy fragments as is readily evident from Fig. 3.1. On the other hand, heavy PFs are emitted more frequently from the lower target mass system. This is possibly due to the fact that with the increase of target size, a larger

portion of the incident projectile may actually participate in the reaction leaving a relatively smaller portion of the same as the spectator. These results are in good agreement with the results reported by Cherry et al. [16]. From the graph it is also seen that irrespective of target mass the fragments with charges approximately half of the beam charge are the rarest. This may be a hint of rare presence of fission type fragmentation in such collisions. Similar distribution fitted with a power law have also been reported in nuclear fragmentation of ^{238}U at 0.96A GeV, ^{84}Kr at 1.25A GeV and ^{131}Xe at 1.22A GeV in nuclear emulsion [4, 17-19].

3.2.1. KNO Scaling

The experimental data of various projectile fragments of the present investigation are categorized into three different groups –

(i) non interacting protons emitting from projectile spectator having charge $Z_{PF} = 1$

(ii) alpha particles with charge $Z_{PF} = 2$

and (iii) heavy fragments having charge $Z_{PF} \geq 3$.

The study of multiplicity distribution of emitted fragments helps to understand the underlying emission mechanism of the fragments from the spectator region of the collisions. In Figs. 3.2(a)-(c), the variation of normalized multiplicity P(n), defined as f_n/N_{ev} [20], are plotted against the multiplicity n of an event for $Z_{PF} = 1$, $Z_{PF} = 2$ and $Z_{PF} \geq 3$ emitted from the interactions of Kr projectile with Em target at 0.95A GeV. Here f_n is the frequency of events with multiplicity n and N_{ev} is the total number of studied events.

The mean multiplicity of $Z_{PF} = 1$, $Z_{PF} = 2$ and $Z_{PF} \geq 3$ for Kr-Em interactions, as obtained from present investigation, are listed in table 3.1 and the

values are compared with the results obtained by other workers for various systems at few GeV/A energy [21-23]. As obvious, the mean multiplicities of different projectile fragments are found to increase with the increase of projectile mass.

In the recent past, the KNO scaling hypothesis has become a powerful framework for multiplicity studies. This hypothesis was originally derived assuming Feynman scaling of the inclusive particle production cross section. According to this hypothesis, at very high energies s the probability distributions $P_n(s)$ of producing n particles in a certain collision process should exhibit the scaling relation [14]

$$P_n(s) = \frac{1}{< n(s) >} \psi\left(\frac{n}{< n(s) >}\right) \tag{3.1}$$

where <n(s)> is the average multiplicity of a particular secondary charged particles. This scaling is an effect of nuclear geometry, which is energy independent [27]. One can assure the validity of KNO scaling at the concerned energy only when the rescaled P(n) data via stretching (shrinking) the vertical (horizontal) axes by <n> become simple rescaled copies of the universal function $\psi(z)$ depending only on the scaled multiplicity z = n/<n>. The scaling relation Eq. (3.1) can hold only approximately since multiplicity n is a discrete random variable whose stretching or shrinking by a scale factor leaves the probabilities P_n unaltered. The proper meaning of Eq. (3.1) is that with increasing collision energy s the discrete multiplicity distributions P_n can be approximated with increasing accuracy by a continuous probability density function f(x) via $P_n \approx f(x = n)$ (KNO prescription) or by $P_n \approx \int_{x=n}^{x=n+1} f(x)dx$ (called KNO-G "scaling") where,

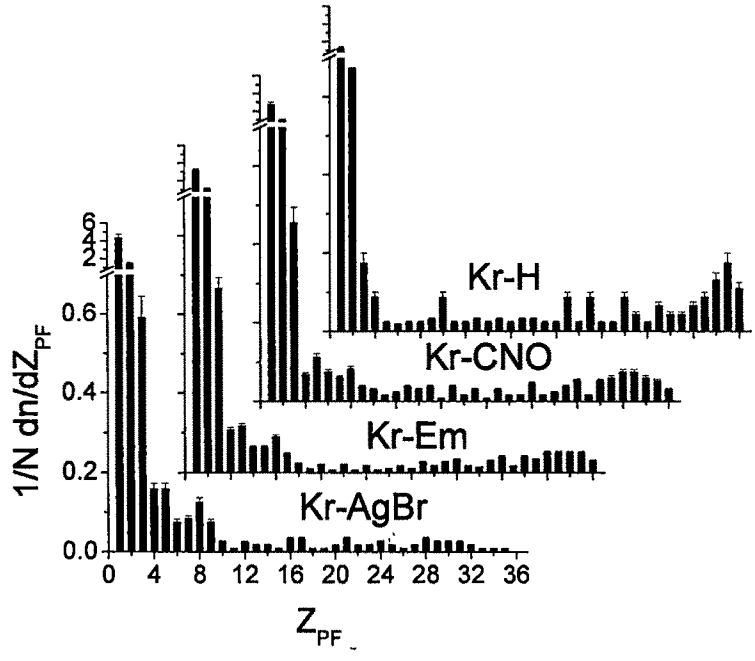

Fig. 3.1: Frequency distribution of different charged projectile fragments with $Z_{PF} \geq 1$ for the collisions of krypton beam with different targets of nuclear emulsion at 0.95 GeV/A. The distributions for various targets are plotted on the same X and Y scales.

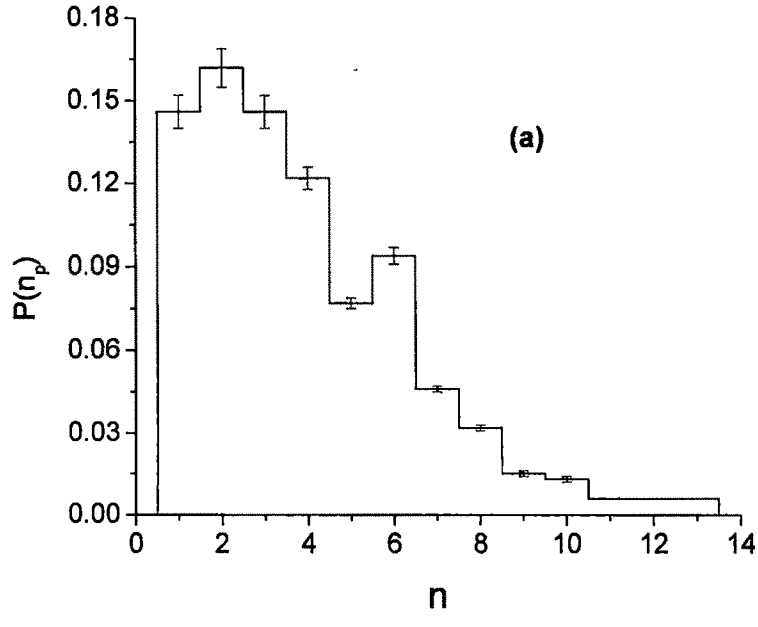

(Fig. 3.2: Cont...)

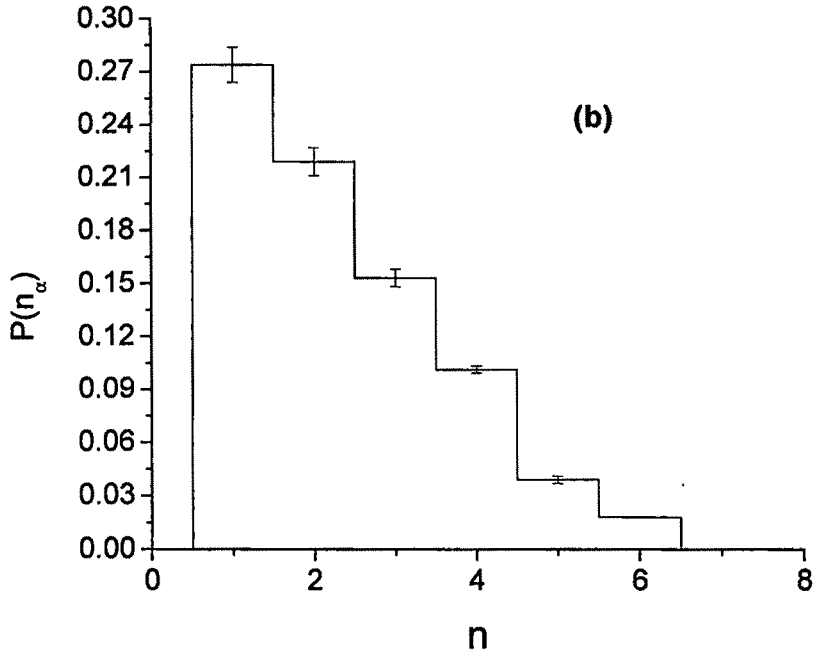

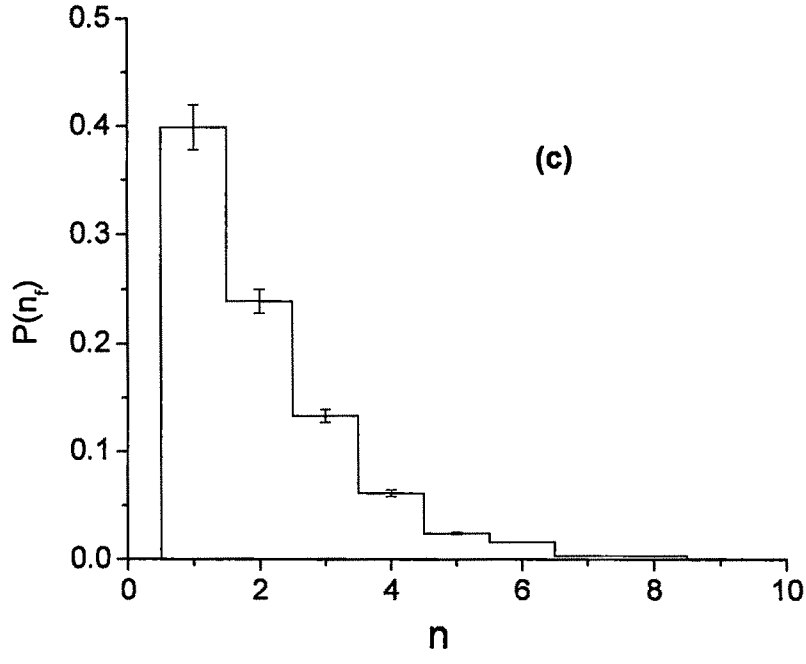

Fig. 3.2: Normalized multiplicity distribution of (a) protons, (b) alpha particles and (c) heavy fragments emitted from Kr-Em interactions.

Table 3.1: The average multiplicities for various PFs emitted from different systems at Dubna and SIS energy

Projectile	Energy (GeV/A)	$Z_{PF}=1$	$Z_{PF}=2$	$Z_{PF}\geq 3$	Ref.
^{16}O	3.7	1.36±0.03	0.75±0.02	0.29±0.01	24
^{22}Ne	4.1	1.36±0.02	0.82±0.02	0.48±0.01	21
^{24}Mg	3.7	1.61±0.04	0.86±0.03	0.49±0.03	22
^{28}Si	3.7	1.53±0.05	1.06±0.03	0.49±0.02	23
^{84}Kr	0.95	3.77±0.09	2.2±0.09	1.90±0.07	P. W.
^{197}Au	10.6	-	4.34±0.09	1.91±0.04	16
^{197}Au	10.6	-	4.63±0.13	2.01±0.06	25
^{197}Au	10.6	-	4.51±0.08	2.37±0.03	26

in the most popular modification of the original scaling rule, f(x) has the generic Czyzewski-Rybicki form [28, 29]

$$f(x)=\frac{1}{\lambda}\psi\left(\frac{x-c}{\lambda}\right) \tag{3.2}$$

with scale parameter $\lambda > 0$ and location parameter c. Data collapsing behavior is observed if the only s-dependent parameters of the approximate shape function f(x) are c and λ, i.e. if f(x) depends on collision energy only through a change of location and scale in x. The variation of λ with increasing s reflects the growth of average multiplicity, whereas the s-dependence of c is usually associated with leading particle effects (so-called AKNO or KNO-α scaling) [14].

The experimental formula used by different workers [30-41] for fast helium and all other PFs are of the form,

$$\psi(z) = az\exp(-bz) \tag{3.3}$$

with z = n/<n_Z> and $\psi(z)$ = <n_Z>P(n_Z). Here n, <n_Z> and P(n_Z) are the multiplicity, mean multiplicity and normalized multiplicity of projectile fragments respectively. a and b are constants.

To check the scaling behavior of proton, alpha and heavy particles coming out of spectator region of projectile, in Fig. 3.3(a)-(c), <n_Z>P(n_Z) distribution is plotted as a function of the scaled variable n/<n_Z> for different PFs emitted in Kr-Em interactions and compared with the universal KNO scaling.. The solid line represents the universal function [35]

$$\psi(z) = 4z\exp(-2z) \tag{3.4}$$

and the dashed line represents the best fit for the experimental data points. When the multiplicities of different PFs of the present work are studied with respect to universal function (Eq. (3.4)), the present set of data is found to be in good agreement. The error bars are estimated considering them to be independent statistical errors only. From the best fit of the experimental data points of different PFs, the values of coefficients a and b are determined and listed in table 3.2 along with χ^2/dof values, where dof stands for degree of freedom. The values of a and b are in good agreement with the values reported by other workers. It is readily evident from these plots that the projectile fragments with charge $Z_{PF} = 1$, $Z_{PF} = 2$ and $Z_{PF} \geq 3$ emitted from Kr-Em interactions obey the universal KNO scaling at SIS energy.

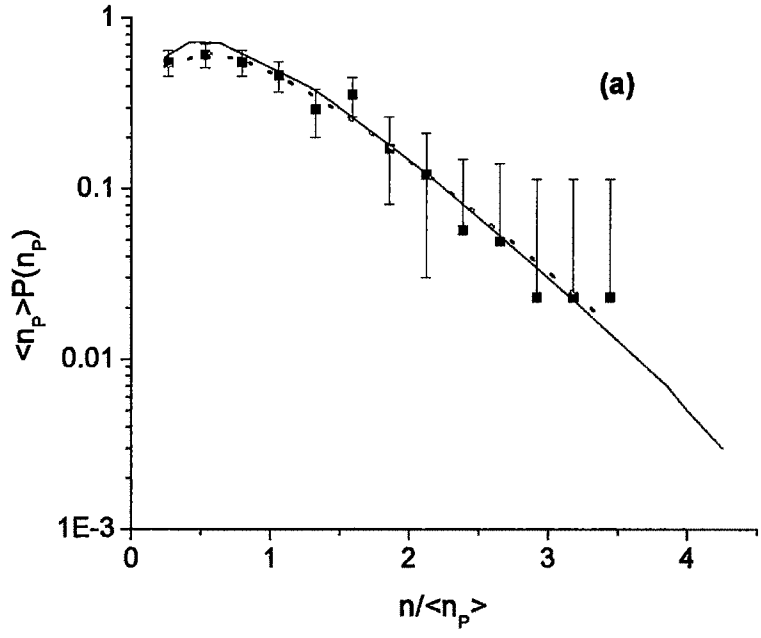

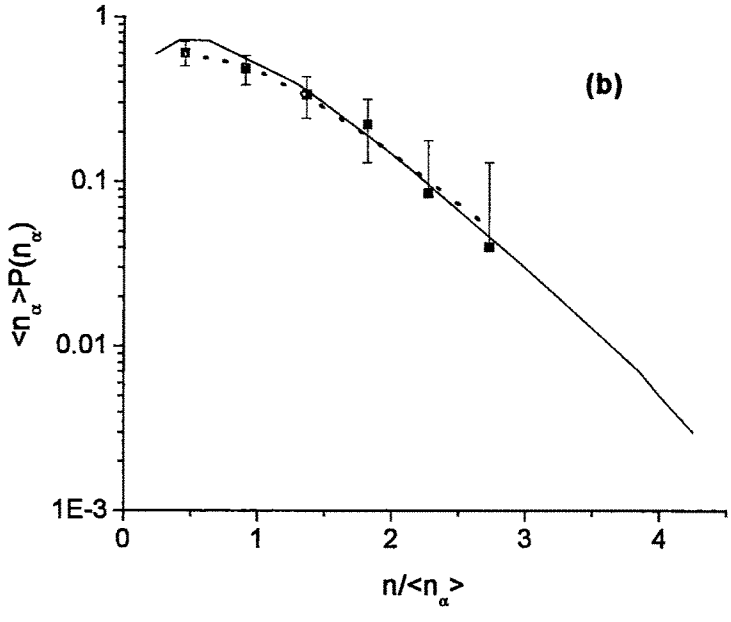

(Fig. 3.3: Cont...)

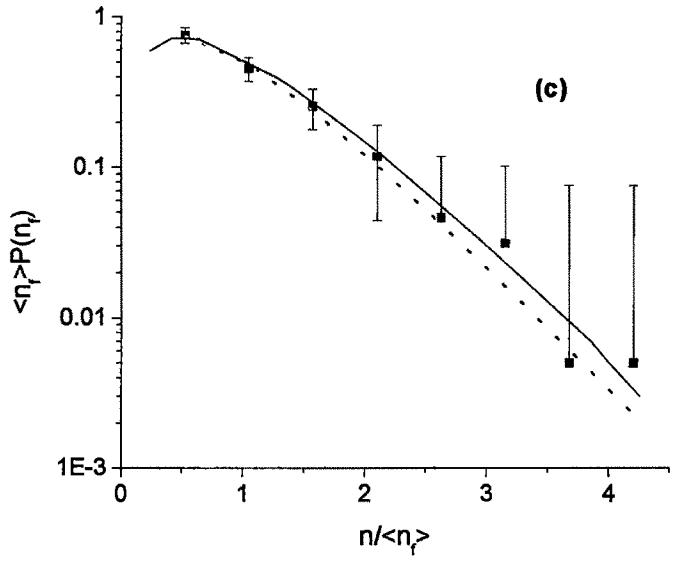

Fig. 3.3: $\langle n_Z \rangle P(n_Z)$ vs. $n/\langle n_Z \rangle$ plot for (a) proton, (b) helium and (c) heavy fragments. Here $\langle n_p \rangle$, $\langle n_\alpha \rangle$ and $\langle n_f \rangle$ stand for mean multiplicity of $Z_{PF} = 1$, $Z_{PF} = 2$ and $Z_{PF} \geq 3$ PFs. The solid and dashed lines represent the universal function (Eq. (3.4)) and the best fit for the experimental data points respectively.

An alternative statement of KNO scaling can be given by considering the multiplicity moments $<n^q>$ [43] where

$$< n^q >= \sum_{n=1}^{\infty} \frac{n^q \sigma_n}{\sigma_m} =< n >^q \sum_{n=1}^{\infty} \left(\frac{n}{< n >} \right)^q \psi \left(\frac{n}{< n >} \right), \tag{3.5}$$

q is a positive integer.

Here σ_n is the topological cross section for the production of n particles and σ_{in} the total inelastic cross section. If $<n>$ is large one can replace the discrete sum in Eq. (3.5) by an integral over the variable $z = n/<n>$:

$$C_q \equiv \frac{< n^q >}{< n >^q} = \int_{1/<n>}^{\infty} dz z^q \psi(z) \cong \int_0^{\infty} dz z^q \psi(z) \tag{3.6a}$$

If one considers charged particle production then the sum in Eq. (3.5) runs only through even values of n, therefore Eq. (3.6a) is changed to

$$C_q = \frac{1}{2} \int_0^{\infty} dz z^q \psi(z). \tag{3.6b}$$

The experimental situation for the C_q has been reported by Slattery [44] who finds that they indeed seem to be remarkably energy independent, as asserted by the right hand side of Eqs. (3.6a) and (3.6b).

The estimated values of C_2, C_3 and C_4 for the PFs with charge $Z_{PF} = 1$, $Z_{PF} = 2$ and $Z_{PF} \geq 3$ are listed in table 3.3. The values of C_q for $Z_{PF} = 2$ PFs for various other systems at different beam energies are also listed in this table for comparison. The various C_q moments calculated from present data points are in good agreement with the results reported by other workers.

Table 3.2: The values of coefficients a and b for different beams in emulsion along with χ^2/dof for the best fitted curve of the experimental data points.

Beam	Energy (GeV/A)	Z_{PF}	a	b	χ^2/dof	Ref.
Kr	0.95	1	3.25±0.21	1.90±0.07	0.0015	P. W.
Kr	0.95	2	3.02±0.18	1.85±0.06	0.0006	P. W.
Kr	0.95	≥3	4.38±0.19	2.14±0.05	0.0003	P. W.
Si, Fe	3.7, 1.88	2	5.01±0.08	2.11±0.04	0.44	42
Mg	3.7	2	5.10±0.11	2.23±0.07	-	27 & Ref. therein
O	4.5	2	3.30±0.27	2.56±0.06	0.28	20
Si, S	14.5, 200	2	4.65±0.09	2.10±0.04	0.003	30
Ne, Si	0.3	2	5.39±0.36	2.18±0.08	1.15	39
Fe, Ar	1.9	2	4.47±0.15	2.02±0.04	0.45	39
Fe, Kr	0.9	2	4.21±0.28	1.99±0.08	1.04	39
Fe	0.9, 1.9	2	4.27±0.14	1.99±0.04	0.44	39
Kr	0.9, 1.5	2	4.19±0.26	2.00±0.07	1.13	39

Table 3.3: The C_q moments for projectile fragments emitted from different A+A collisions at few GeV/A energies.

System	Energy (GeV/A)	Z_{PF}	C_2	C_3	C_4	Ref.
Kr-Em	0.95	1	2.5±0.05	4.61±0.10	10.02±0.2	P. W.
Kr-Em	0.95	2	1.31±0.06	2.21±0.10	4.22±0.19	P. W.
Kr-Em	0.95	≥3	1.32±0.04	2.57±0.09	6.09±0.19	P. W.
Kr-Em	1.5	2	1.38±0.05	2.37±0.09	-	39
Kr-Em	1.5	2	1.39±0.04	2.40±0.07	4.87±0.14	32
Kr-Em	0.9	2	1.38±0.07	2.37±0.09	-	39
Fe-Em	1.9	2	1.35±0.06	2.25±0.10	-	39
Fe-Em	0.9	2	1.35±0.07	2.28±0.09	-	39
Fe-Em	1.9	2	1.34±0.05	2.21±0.08	4.31±0.16	32
Ar-Em	1.9	2	1.34±0.06	2.19±0.10	-	39
Si-Em	0.4	2	1.32±0.06	2.21±0.09	-	39
Ne-Em	0.3	2	1.30±0.06	2.11±0.09	-	39
C-Em	3.7	2	1.20±0.10	1.71±0.15	2.72±0.23	36
Ne-Em	3.7	2	1.29±0.03	2.09±0.05	3.99±0.09	36
Mg-CNO	3.7	2	1.27±0.04	2.04±0.07	3.97±0.13	27
Mg-AgBr	3.7	2	1.33±0.05	2.26±0.09	4.58±0.18	27
Mg-Em	3.7	2	1.32±0.03	2.24±0.06	4.50±0.11	27
Mg-Em	3.7	2	1.3±0.1	2.1±0.1	3.9±0.2	37
Si-Em	3.7	2	1.31±0.03	2.15±0.05	4.20±0.09	45
Si-Em	3.7	2	1.31±0.06	2.17±0.09	4.19±0.18	42

(Cont...)

Si-Em	3.7	2	1.3±0.1	2.2±0.1	4.4±0.2	36
O-Em	3.7	2	1.23±0.07	1.81±0.16	2.99±0.35	20
Au-Em	10.6	2	1.35±0.07	2.21±0.11	4.13±0.21	26
Si-Em	14.5	2	1.30±0.06	2.11±0.09	3.96±0.17	30
O-Em	14.6	2	1.2±0.1	1.7±0.1	2.6±0.2	46
Si-Em	14.6	2	1.34±0.04	2.31±0.07	4.71±0.14	45
Si-Em	14.6	2	1.30±0.10	2.30±0.10	4.60±0.20	38
O-Em	60	2	1.23±0.01	1.77±0.11	2.85±0.17	32
O-Em	60	2	1.2±0.1	1.7±0.1	2.8±0.1	46
O-Em	60	2	1.21±.01	1.74±.01	2.82±.01	47
Pb-Em	160	2	1.37±0.08	2.22±0.13	4.13±0.24	25
O-Em	200	2	1.22±0.11	1.74±0.16	2.76±0.26	32
O-Em	200	2	1.2±0.1	1.7±0.1	2.6±0.1	46
S-Em	200	2	1.35±0.05	2.35±0.08	4.95±0.17	45
S-Em	200	2	1.33±0.05	2.27±0.09	4.66±0.18	32

3.2.2. Scaling Behavior of Projectile Fragments on the Mass of the Fragmenting System

In the study of projectile multifragmentation, the bound charge Z_b, which is the sum of all projectile fragments with charge $Z_{PF} \geq 2$, is considered to be one of the important observables to study the multifragmentation mechanism. For a given collision system, Z_b is related to the size of the excited projectile spectator and gives the measure of the mass of the fragmenting system [48]. Therefore, it should reflect the centrality of the collision and can be used as a measure of the impact parameter; larger Z_b values should correspond to larger impact parameters

and to more peripheral collisions. The size of the projectile spectator remnant is a measure of the geometry of the collision, and therefore, for a given collision system, it should be independent of the beam energy. Different projectile energies lead to different excitations of the spectator remnant, and thus, influence its decay, but not the size. It also gives an idea about the energy-momentum transferred to the participant part of the colliding nuclei [12, 48-57].

Correlation between mean number of intermediate mass fragments (IMFs) and Z_b is one of the most interesting aspects of studying projectile multifragmentation which is studied by different workers for various systems at different energies. It is already established that this correlation follows a target invariance pattern ranging from carbon to lead [48, 52, 55]. Jain et al., [56] have reported similar results with various emulsion targets.

The variation of $\langle N_{IMF} \rangle$ on the mass of the fragmenting system for the present work is shown in Fig. 3.4 and compared with the results reported by ALADIN and KLMM groups [12, 50]. From the figure it is clear that at an intermediate value of the impact parameter, emission of multifragmentation is a dominant decay channel of the projectile nucleus. As expected mean multiplicity of IMFs increases with the increase of projectile mass. According to ALADIN group, when both the variables (i.e., $\langle N_{IMF} \rangle$ and Z_b) are normalized with the charge of projectile Z_p, the variation again follows a universal pattern losing its dependency on projectile mass. Thus an important feature of the multifragmentation decay of the excited spectator nuclei is, therefore, believed to be the apparent absence of dynamical dependencies. To check whether the normalized data follow the universal curve, we plot the variation of normalized $\langle N_{IMF} \rangle$ against normalized Z_b in Fig. 3.5 along with ALADIN and KLMM results. Though the data points of the present investigation exhibit the same

general pattern of the universal curve of ALADIN group, the maximum value of $<N_{IMF}>$ of the present investigation is found to be about 1.3 times larger than that of the universal curve. It may be noted here that in our earlier published result [58] with relatively less number of data this difference was found to be 1.7 times. However, with the increase of studied data size the difference in the peak value of $<N_{IMF}>$ has been reduced to 1.3 times. Considering the large error bar of the data point of the present investigation, it is very difficult to conclude without any ambiguity that the normalized $<N_{IMF}>$ values of the present investigation deviate from the universal pattern of the ALADIN group.

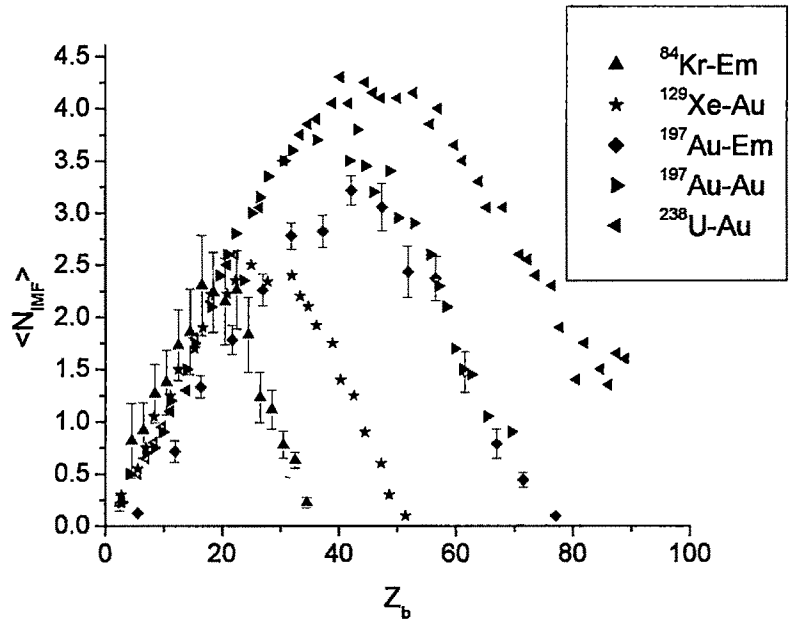

Fig. 3.4: Variation of <N_{IMF}> on the mass of the fragmenting system.

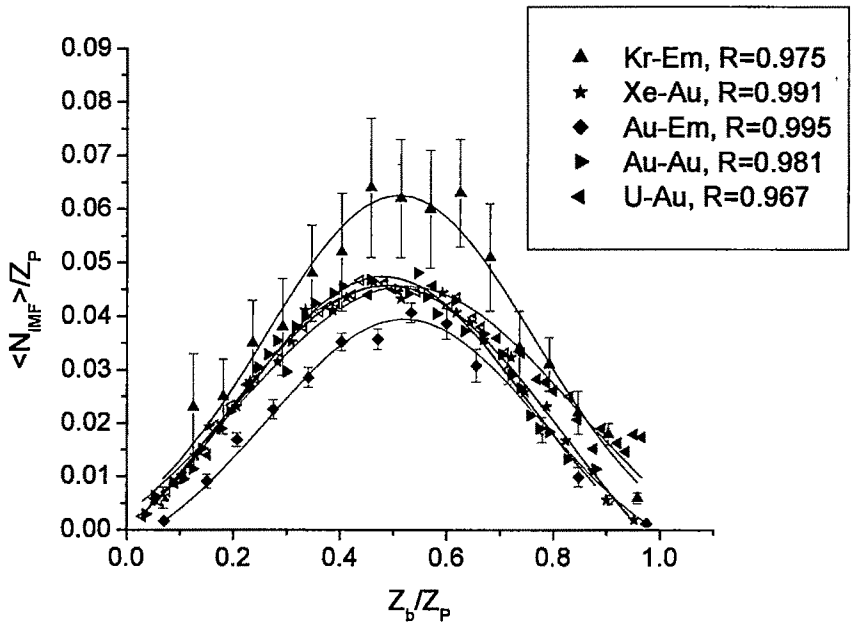

Fig. 3.5: Variation of normalized mean multiplicity with the normalized values of the mass of the fragmenting system.

References

[1] B. Bhattacharjee *et al.*, Ind. J. Phys. **82(6)**, 735 (2008).

[2] J. A. Hauger *et al.*, Phys. Rev. C **57(2)**, 764 (1998).

[3] T. Ahmed and M. Irfan, IL Nuovo Cimento A **106(2)**, 173 (1993).

[4] P. L. Jain and G. Singh, Phys. Rev. C **46(1)**, R10 (1992).

[5] C. F. Powell and G. P. S. Occhialini, Nature (London) **159**, 93 (1947).

[6] L. G. Moretto and G. J. Wozniak, Annu. Rev. Nucl. Part. Sci. **43**, 379 (1993).

[7] J. E. Finn *et al.*, Phys. Rev. Lett. **49**, 1321 (1982).

[8] P. J. Siemens, Nature (London) **305**, 410 (1983).

[9] T. J. Schlagel and V. R. Pandharipande, Phys. Rev. C **36**, 162 (1987).

[10] H. Muller and B. D. Serot, Phys. Rev. C **52**, 2072 (1995).

[11] K. C. Chase and Z. Mekjian, Phys. Rev. Lett. **75**, 4732 (1995).

[12] A. Schuttauf *et al.*, Nucl. Phys. A **607**, 457 (1996).

[13] H. E. Stanley, *Introduction to Phase Transitions and Critical Phenomena* (Clarendon Press, 1971).

[14] S. Hegyi, arXiv:hep-ph/0011301 v1 24 Nov (2000).

[15] Z. Koba *et al.*, Nucl. Phys. B **40**, 317 (1972).

[16] M. L. Cherry *et al.*, Eur. Phys. J. C **5**, 641 (1998).

[17] P. L. Jain *et al.*, Phys. Rev. Lett. **68**, 1656 (1992).

[18] P. L. Jain *et al.*, Phys. Rev. Lett. **52**, 2213 (1984).

[19] G. Singh *et al.*, Mod. Phys. Lett. A **7**, 1113 (1992).

[20] D. H. Zhang *et al.*, Chinese Phys. **13(8)**, 1239 (2004).

[21] N. P. Andreeva *et al.*, Sov. J. Nucl. Phys. **47**, 102 (1988).

[22] M. A. Jilany, Phys. Rev. C **70**, 014901 (2004).

[23] B. K. Singh and S. K. Tuli, Nuovo Cimento Soc. Ital. Fis. A **112**, 1093 (1999).

[24] C. R. Meng and D. H. Zhang, Chinese J. Phys. **44(1)**, 1 (2006).

[25] G. Singh and P.L. Jain, Phys. Rev. C **54(6)**, 3185 (1996).

[26] M. I. Adamovich *et al.*, Eur. Phys. J. A **5**, 429 (1999).

[27] M. A. Jilany, Eur. Phys. J. A **22**, 471 (2004).

[28] O. Czyzewski and K. Rybicki, Nucl. Phys. B **47**, 633 (1972).

[29] M. Blazek, Z. Phys. C **32**, 309 (1986).

[30] G. Singh *et al.*, Phys. Rev. C **43(5)**, 2417 (1991).

[31] G. Singh *et al.*, Phys. Rev. C **42**, 1757 (1990).

[32] K. Sengupta *et al.*, Phys. Lett. B **222**, 301 (1989).

[33] S. Kamel, Nuovo Cimento A **112**, 733 (1999).

[34] F. H. Liu and Y. A. Panebratsev, Nuovo Cimento A **111**, 1219 (1998).

[35] F. H. Liu, Phys. Rev. C **62**, 024613 (2000).

[36] M. El-Nadi *et al.*, Int. J. Mod. Phys. E **2**, 381 (1993).

[37] M. El-Nadi *et al.*, Nuovo Cimento A **108**, 809 (1995) and references therein.

[38] M. El-Nadi *et al.*, J. Phys. G **28**, 1251 (2002).

[39] P. L. Jain and M. M. Aggarwal, Phys. Rev. C **33(5)**, 1790 (1986).

[40] L. S. Liu and T. C. Meng, Phys. Rev. D **27**, 2640 (1983).

[41] B. Bhattacharjee, B. Debnath, Proceedings of the *DAE-BRNS Symposium on Nuclear Physics, Badodara, December 11-15, 2006, eds. S. Kailas, S. Kumar and S. Santra*, Vol. **51**, p. 480 (India, 2006).

[42] B. K. Singh and S. K. Tuli, Int. J. Mod. Phys. E **7(3)**, 341 (1998).

[43] H. Moreno, SLAC-PUB-1190 (T-E) March (1973).

[44] P. SIattery, University of Rochester Report UR-345 (1972) and Phys. Rev. Lett. **29**, 1624 (1972).

[45] B. K. Singh *et al.*, Nucl. Phys. A **570**, 819 (1994).

[46] M. I. Adamovich *et al.* (EMU-01 Collaboration), Phys. Rev. C **40**, 66 (1989).

[47] D. H. Zhang, High Energy Phys. Nucl. Phys. **26**, 40 (2002).

[48] J. Hubele *et al.*, Z. Phys. A **340**, 263 (1991).

[49] A. Dabrowska *et al.*, Acta Physica Polonica B **31(3)**, 725 (2000).

[50] M. L. Cherry *et al.*, Phys. Rev. C **52(5)**, 2652 (1995).

[51] P. L. Jain *et al.*, Phys. Rev. Lett. **74**, 1534 (1995).

[52] C. A. Ogilvie *et al.*, Phys. Rev. Lett. **67**, 1214 (1991).

[53] K. Hagel *et al.*, Phys. Rev. Lett. **68**, 2141 (1992).

[54] J. Hubele *et al.*, Phys. Rev. C **46**, R1577 (1992).

[55] P. Kreutz *et al.*, Nucl. Phys. A **556**, 672 (1993).

[56] P. L. Jain *et al.*, Phys. Rev. C **50**, 1085 (1994).

[57] G. Singh and P. L. Jain, Phys. Rev. C **49**, 3320 (1994).

[58] B. Bhattacharjee and B. Debnath, J. Phys.: Conf. Ser. **110**, 122003 (2008).

Chapter IV

Evidence of Phase Transition in the Break up of Kr-projectile

4.1. Introduction

It is believed that in the complex scheme of high energy reactions, nuclear fragmentation is relatively a well isolated phenomenon. Nuclear fragmentation in which excited nuclei break up into several pieces of smaller masses, each more massive than an alpha particle, is termed as nuclear multifragmentation. Multifragmentation has remained a subject of great interest in nucleus–nucleus collisions at intermediate energies. In normal state, nuclear matter shows the properties of a liquid, but the power law behavior followed by mass (charge) yield distribution of the fragments produced from the remnant parts of the colliding nuclei gives the exponent value which lies within the range expected for a system near its critical point. Such observations led different groups [1-10] to suggest that multifragmentation might be resulted from a continuous phase transition of nuclear matter associated with a critical point. On the other hand, it has been proposed that a back bending in the caloric curve that leads to a negative specific heat can be signed through the occurrence of abnormally large kinetic energy fluctuations. This signature of 1^{st} order phase transition has been applied to a number of multifragmentation data and a liquid–gas phase transition has been tentatively identified, particularly at few hundred MeV/A [12-17]. Also, considering the size of the heaviest fragment produced in each collision event as order parameter, a number of other groups [18-24] have studied the distribution of this order parameter for various systems at few to few hundred MeV/A. From the observation of a characteristic bimodal behavior, a first order type of phase transition is associated with the studied nuclear multifragmentation processes. In the last two decades, intense theoretical and experimental investigations have been carried out on relativistic heavy ion collisions to gather information about

liquid gas phase transition of low density nuclear matter in hot nuclei and hence the fragmentation mechanism [25–30].

To describe nuclear multifragmentation mechanism, a number of theoretical models have been proposed. Whereas some of these describe the evolution dynamics of the system resulting from collisions between nuclei via molecular dynamics [31-37], others adopt stochastic mean field approaches [38-46]. Remaining are related to statistical descriptions based on multi-body phase space calculations [47-55]. The first approach completely describes the time evolution of the collision and thus helps in learning about nuclear matter, its phase diagram, finite size effects and the dynamics of the phase transition. The second, assuming statistical equilibrium has more to do with the thermodynamical description of the phase transition for finite nuclear systems [56]. Of these the statistical model has been extensively used in describing the critical nature of nuclear multifragmentation. It is known that, in statistical physics, systems consisting of mutually interacting units, in general, cannot be evaluated in exact terms, whereas most systems without interaction are easy to characterize. Thus, an often-used approximation is the cluster approximation that tries to transform the problem of interacting units into the approximation of non-interacting clusters. Stauffer [7] has pointed out that percolation, besides being perhaps the simplest statistical tool to study phase transition, also serves as an introduction to cluster approximation of collective phenomena. Percolation problem on a large lattice displays the features of a system undergoing a second-order phase transition [57].

A continuous phase transition in nuclear matter, that might have taken place in the final stage of fragmentation of heavy ion collisions, is generally characterized by the presence of some characteristic features. Certain

experimentally observable quantities might undergo fluctuations or diverge or may even tend to vanish near some critical value of the control parameter giving the signatures of continuous phase transition. This critical value of the control parameter corresponds to the critical point in the phase diagram. In cluster distribution technique of studying phase transition, these experimental observables are described by a finite number of critical exponents namely, σ, β, τ, γ etc. These exponents are universal and depend neither on the structural details of the lattice nor on the type of percolation, but only on the dimension of the lattice. The main characteristic of these exponents is that they obey the scaling relation and all of them can be evaluated from the knowledge of just two.

In an attempt to get the signatures of critical behavior in the case of break up of nuclei, several workers have analyzed their experimental data on various systems at different energies [28-30, 58-67]. The experimentally evaluated values of σ, β, τ and γ are then compared with the values obtained for different three-dimensional known systems exhibiting critical behavior. A striking agreement in the values of these exponents indicates the possibility of existence of criticality in the experimental system under consideration.

However, though there is a broad agreement between the values of different exponents as estimated by various groups [60, 65], in a number of cases, a careful cross check reveals that the cited values of the exponents suffer from internal inconsistencies and do not follow the corresponding scaling relation [63, 64]. There are also reports that the value obtained for an exponent is sensitive to the range of values chosen for the control parameter and to the system under investigation [63, 65]. It may therefore be inferred that the values of the critical exponents, considered as the representative of critical phenomenon, as cited by various groups are not unambiguous.

Moreover, Elliott et al. (EOS Collaboration) [61] have shown that out of several techniques adopted by different workers in estimating percolation exponents, only a few of these may serve as true sensitive tools to study the criticality. From a study of 1A GeV Au–C data and its comparison with two theoretical models, such as one that undergoes phase transition and the other that does not, they categorized the traditional signals of critical behavior into a number of insensitive and sensitive tools. Further, EOS and KLMM Collaborations [60, 63] have studied Au multifragmentation at two different energies, namely at 1.0A GeV and 10.6A GeV respectively. Remembering the results of ALADIN Collaboration on the target mass independence nature of projectile multifragmentation [68], a comparison of EOS and KLMM Collaborations' results suggests that the exponent values calculated at two different energies for the same system differ significantly. KLMM Collaboration on the basis of their analysis concluded that percolation theory becomes a less satisfactory representation of the break-up of the excited nuclei at high-energy interactions then it is at lower energies. However, EMU01 Collaboration from the study of Au–Em interactions at KLMM energy has reported a clear evidence of the critical behavior of the fragmentation process with universal features of second order phase transition. Clearly, the findings of one group differ significantly from that of the other indicating that the studies on break up of the nuclei in high energy A + A collisions are far from complete. At the same time, many different measurements of the nuclear caloric curve [69] performed on various systems to realize 1^{st} order type of liquid–gas phase transition also show quite diverse behavior [12]. The EOS Collaboration has studied three systems of different masses, namely, Au, La and Kr interactions on C at 1A GeV. They considered thermal excitation energy E_{th}^{*} of the remnants as the control

parameter and performed analyses on fragment properties and critical exponents. Looking at the differences in the results of these preliminary analyses it is claimed that while Au and La indicate towards a 2^{nd} order phase transition, the Kr fragmentation is possibly governed by 1^{st} order type of phase transition. But the observed results are not insulated from the surface effect, as is seen in three-dimensional (3d) percolation studies and therefore the observed differences in the results cannot exclusively be attributed to the differences in the order of phase transition. Their cited results reveal that various properties of the fragments and values of the exponents τ, β, γ and β/γ vary systematically with mass or otherwise size of the fragmenting nuclei. Moreover, the authors themselves have pointed out that their results on the analysis of heat capacity [21, 22] for all the three systems are inconclusive in identifying the exact order of phase transition. Nevertheless, a back bending in the caloric curve in Kr data is taken as a signature of first order phase transition in that system. But the observed back bending is found to be very much sensitive to the particular mass cut for the studied systems of Au and Kr and therefore may not be unambiguously considered as a sensitive tool to realize order of phase transition involved in nuclear multifragmentation process.

The problem of identification and characterization of nuclear liquid–gas phase transition therefore still remains to be solved. Though some progresses have already been made in understanding the nuclear multifragmentation process, there are still a few more queries that need to be addressed for a better understanding of the process. A few of these are identified as: can those systems that contain critical behavior be readily distinguished from those that do not? Which exactly are insensitive and sensitive tools for studying criticality? Is the list put forwarded by EOS Collaboration final and complete? What is the nature

of production of clusters: is it a sequential or simultaneous decay? It is opined that a single existing theoretical model cannot satisfactorily describe all the characteristics of nuclear multifragmentation and demands more results on such process for several other systems at different energies.

In this work a 'toy model' of nuclear multifragmentation has been developed and using cluster approximation technique, the effect of mass conservation constraint on the traditional signals of critical behavior has been examined. Possible signatures of phase transitions have also been investigated by using Campi's technique of finding critical exponents. The estimated values of the critical exponents τ, β and γ of the present investigation are then compared with the values reported for various other systems. A higher order moment M_3, related to skewness [20, 70], is also evaluated using the experimental data and the corresponding exponent δ is calculated. An attempt has been made to establish the scaling relationship between these experimentally evaluated exponents τ, β, γ and δ.

4.2. Methodology

Considering that the temperature T of the system is linearly dependent on the total multiplicity m, in a number of nuclear experiments [64, 71-73], multiplicity is taken as the control parameter. This control parameter could not be finely tuned explicitly in order to convert the system into the critical state. However, in a number of events, a favorable situation is spontaneously developed where the system itself evolves to a critical one. The total charged projectile fragment multiplicity m is defined as [8, 9, 64]

$$m = N_f + N_\alpha + N_{prot} \tag{4.1}$$

where N_f, N_α and N_{prot} denote the number of heavy PFs with charge $Z_{PF} \geq 3$, alpha particles with $Z_{PF} = 2$ and the number of emitted protons with $Z_{PF} = 1$ respectively. Here N_{prot} is determined using charge balance of the PFs. The distance ε of a given event with multiplicity m from the critical point m_c is defined as [60, 64]

$$\varepsilon = m_c - m \tag{4.2}$$

For a single event, Campi [8] defined the k^{th} moment of charge distribution as

$$M_k = \sum_{Z_{PF}} n_{Z_{PF}}(\varepsilon) {Z_{PF}}^k \tag{4.3}$$

and for a collection of data, $<M_k(\varepsilon)>$ in the small bins of multiplicity m as

$$< M_k(\varepsilon) >= \frac{1}{N}\sum M_k^i(\varepsilon) = \frac{1}{N}\sum_i \left(\sum_{Z_{PF}} n_{Z_{PF}}(\varepsilon) {Z_{PF}}^k \right). \tag{4.4}$$

Here $n_{Z_{PF}}$ is the normalized charge distribution and is defined as $n_{Z_{PF}} = N_{Z_{PF}}/Q_{PF}$, Q_{PF} is the sum of charges of all the projectile spectator protons, fast alpha particles and heavy projectile fragments with charges $Z_{PF} \geq 3$. N denotes the total number of events in a given small range of ε, and M_k^i is the k^{th} order charge distribution moment for i^{th} event. Being motivated by Fisher model, in the calculation of various charge moments in the gas phase, the contribution of prompt protons and in liquid phase, the contributions of fragments with largest charge Z_{max} as well as the prompt protons are excluded.

A variable γ_2, related to variance of charge σ^2, is defined as [9]

$$\gamma_2 = \frac{M_2 M_0}{{M_1}^2} = 1 + \frac{\sigma^2}{< Z_{PF} >^2}. \tag{4.5}$$

Here M_0, M_1 and M_2 are the zeroth, first and second order moments of charge distribution respectively. While M_0 and M_1 correspond to mean number and

mean size of the clusters, M_2 is a quantity that is related to the fluctuation in the size of the fragments.

It is believed that in nuclear fragmentation process the system is at coexistence in the neighborhood of the critical point and cluster distribution follows a pure power law with Z_{PF} as

$$n_{Z_{PF}}(\varepsilon) \sim Z_{PF}^{-\tau} \quad \text{at } \varepsilon=0 \tag{4.6}$$

and near the critical point, $M_2(\varepsilon)$ and Z_{max} are related with ε as

$$M_2(\varepsilon) \sim |\varepsilon|^{-\gamma} \quad \text{for } \varepsilon \to 0, \tag{4.7}$$

$$Z_{max}(\varepsilon) \sim \varepsilon^{\beta} \quad \text{for } \varepsilon > 0. \tag{4.8}$$

Here τ, γ and β are critical exponents. $Z_{max}(\varepsilon)$ is the average charge of the largest fragment for a given distance from the critical m. Far away from the critical point, the behavior of the system is dominated by the mean field regime and these relations are not followed [64].

In scaling theory, k^{th} moment of the cluster number density is related with the values of critical exponents as

$$M_k(\varepsilon) \propto |\varepsilon|^{-(1+k-\tau)/\sigma} \quad \text{for } \varepsilon \to 0. \tag{4.9}$$

with the restriction $1 + k - \tau > 0$ for dimension $d > 1$ and $k \geq 0$ for $d = 1$ [74]. Here σ is a critical exponent related to the characteristic cluster size. Using relation (4.9) one can easily find out the scaling relation among any three critical exponents and for β, γ and τ, it can be given as

$$3\beta + 2\gamma = \tau(\gamma + \beta). \tag{4.10}$$

Next, an attempt has been made to estimate the critical exponent τ. In estimating τ it is to be remembered that the assumptions of FDM are not valid for the charges less than 6 and in present case most of the PF's charge lies within 1–

6. Therefore for the calculation of critical exponent τ, rather than Eq. (4.6), the following relation [4, 60, 61] is used

$$\mu = \frac{\Delta \ln M_3}{\Delta \ln M_2} = \frac{\tau - 4}{\tau - 3}. \tag{4.11}$$

In an attempt to get a better set of exponents with present experimental data, another critical exponent δ related to the third order moment, M_3 as

$$M_3(\varepsilon) \sim |\varepsilon|^{-\delta} \tag{4.12}$$

is evaluated, where δ bears a scaling relation with γ and τ as

$$3\delta - 4\gamma = \tau(\delta - \gamma). \tag{4.13}$$

Having a set of three experimental exponents that obey the scaling relationship, the β value is re-evaluate considering τ and δ as the other two parameters from the corresponding scaling relation

$$4\beta + 2\delta = \tau(\beta + \delta). \tag{4.14}$$

4.3. Formulation of Toy Model

Analysis is being started by formulating a 'toy model' of nuclear multifragmentation that is different from the EOS Collaboration [61] and is based on the following algorithm: first the total charge Q_{PF} of a fragmenting system is determined randomly from 36 total system constituents which is the charge of the projectile for present investigation. The number of prompt protons emitted from a particular event is then considered as $N_{prompt} = 36 - Q_{PF}$. Each Q_{PF} is then allowed to disintegrate randomly to give the total number n of PFs in an event from a uniform distribution on (1, Q_{PF}). The assignment of maximum charge Z_{max_i} of a cluster which may be emitted from an event having n number of PFs is guided by two factors, namely, Q_{PF} and *n*. Following Elliott, the first cluster is

then randomly chosen with maximum charge Z_{max_1} from uniform distribution on (1, Z_{max}), where $Z_{max} = Q_{PF} - (n - 1)$. Obviously, the subsequent (n − 1) clusters are then to be generated from the remaining ($Q_{PF} - Z_{max_1}$) constituents. Thus, Z_{max_2}, the maximum charge of the second cluster is then chosen from random partitioning of Z'_{max} on (1, Z'_{max}), where $Z'_{max} = [(Q_{PF} - Z_{max_1}) - (n-2)]$. For each event this process is repeated until total Q_{PF} is disintegrated into respective (n − 1) number of PFs and ends with $Z_{max_n} = (Q_{PF} - Z_{max_k})$, where k = 1, 2,..., (n-1). Present algorithm of random partitioning differs from that of the EOS one [61] in the sense that here the charge of the remnant part of the projectile nucleus is considered as the charge of the fragmenting system, not the total charge of the projectile. This technique rests on the random selection of total charge of the fragmenting system from a uniform distribution of (1, Z_{proj}), while EOS's technique relies on the random selection on (1, Z_{proj}) of multiplicity in which the incident projectile will disintegrate. Thus the major difference between the two toy models is that while in current algorithm the mass conservation is violated, as it should be due to pre-equilibrium emission, the EOS model ignores this aspect. In order to introduce the two toy models, their physical meaning and their differences more sensibly, in Figs. 4.1(a) and (b) the distributions of pre-equilibrium particles and cluster multiplicity are being plotted respectively.

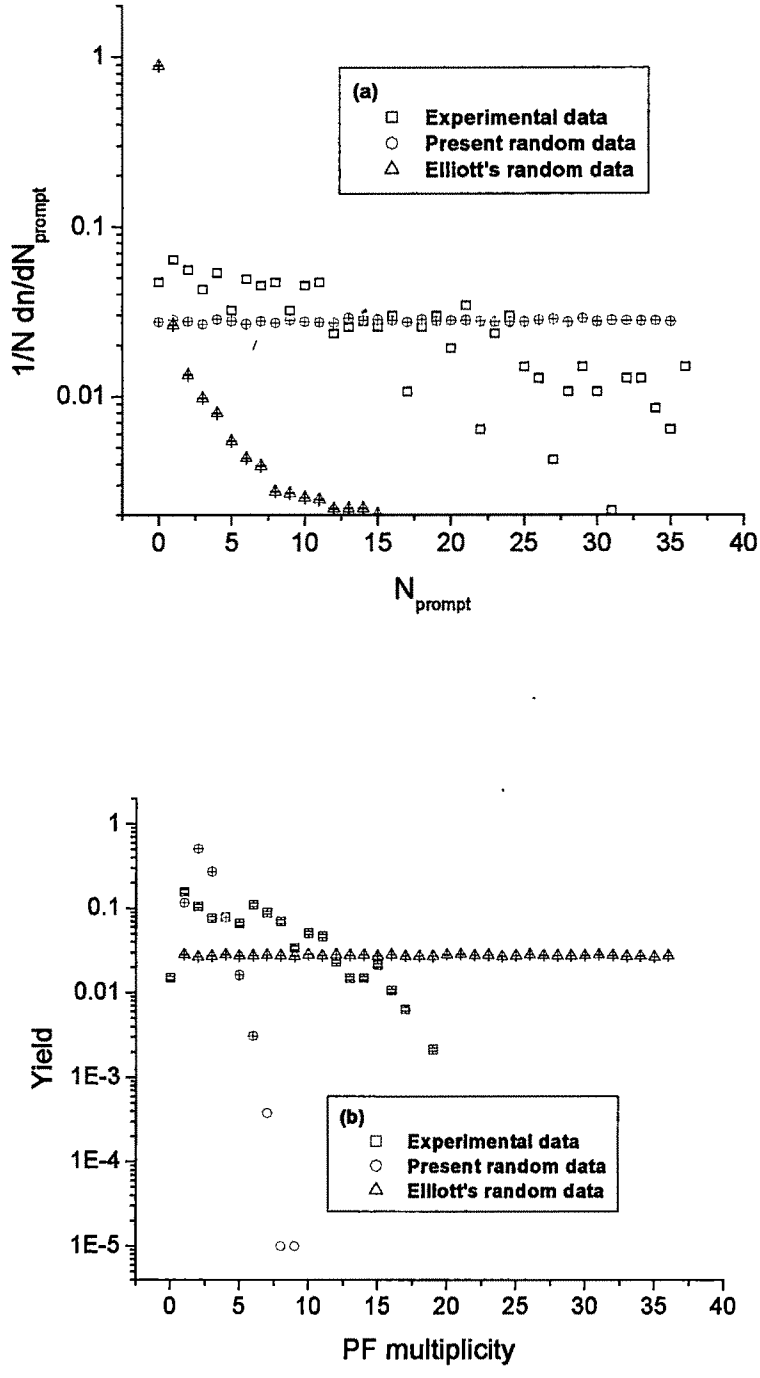

Fig. 4.1: (a) Frequency distribution of the prompt particles and (b) multiplicity distribution of projectile fragments for Kr–Em interactions and randomly generated data.

It could be readily seen from these plots that the two toy models assume respectively a flat distribution of pre-equilibrium particles (this work) and a flat distribution of cluster multiplicity (Elliott et al.). For both distributions, the experimental data lay in between and in this sense indeed the two toy models can be considered as two extreme limits to describe data with minimal hypothesis and without any critical behavior or phase transition. It can be seen that, when tested for a total 36 system constituents, both the toy models are found to be capable of producing signals traditionally associated to criticality. The data generated with present toy model may therefore be used as a tool to evaluate the effect of mass conservation constraint on traditional signals of critical behavior.

For the experimental and randomly generated data, considering total number of system constituents as 36 for both the toy models, the yields of the fragments charge distribution, lying between Z_{PF} = 1-10, have been plotted in Fig. 4.2 in log–log scale and a straight line fit to the respective data points gives the values of the exponent τ as 2.12 ± 0.15, 0.66 ± 0.03 (for present) and 2.06 ± 0.21 (for EOS) respectively. The value of Pearson's correlation coefficient R, is found to be not less than 0.981 in any of these cases.

4.4. Result and Discussion

4.4.1. Sensitivity Test of Various Observables

4.4.1.1. Fluctuations in Z_{max}

It is known that a system exhibits significant fluctuations in the neighborhood of the critical point in a small range of the control parameter and appears at increasingly large scale as $\varepsilon \rightarrow 0$. It is also known that the most readily observed fluctuations in the cluster distribution are those in the size of the largest

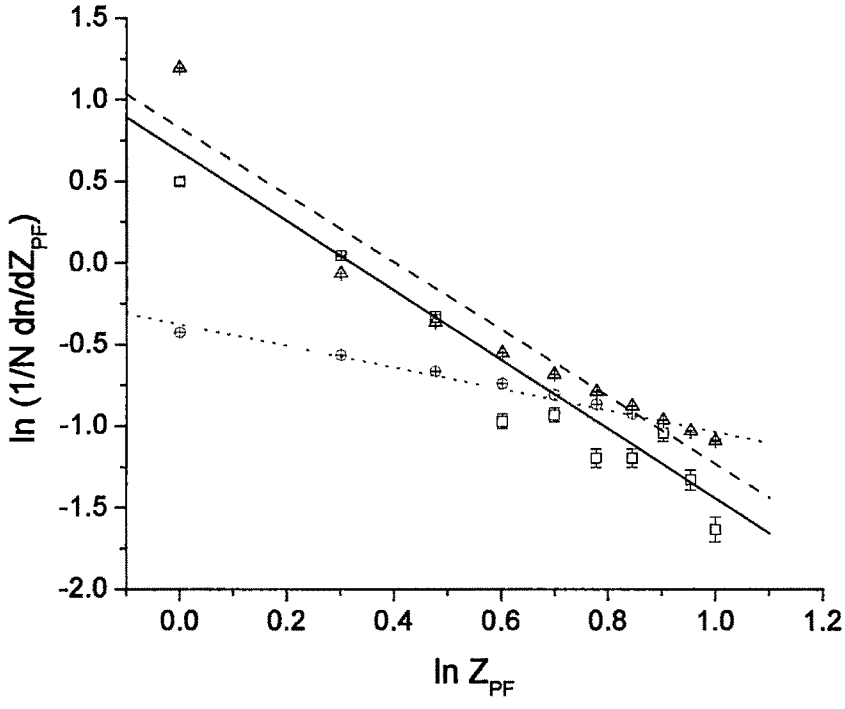

Fig. 4.2: Frequency distribution for experimental as well as randomly generated events in log–log scale upto $Z_{PF} = 10$. Open circles and open triangles are for randomly generated data following present and EOS algorithms respectively for a total 36 system constituents and open squares are for present experimental data. Solid (experimental data), dot (present random events) and dash (EOS's random event) lines are the best fitted lines.

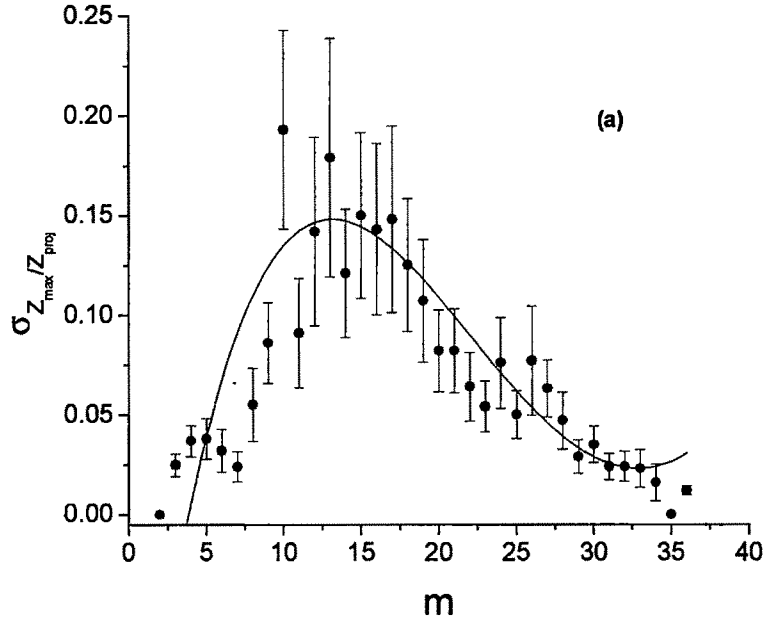

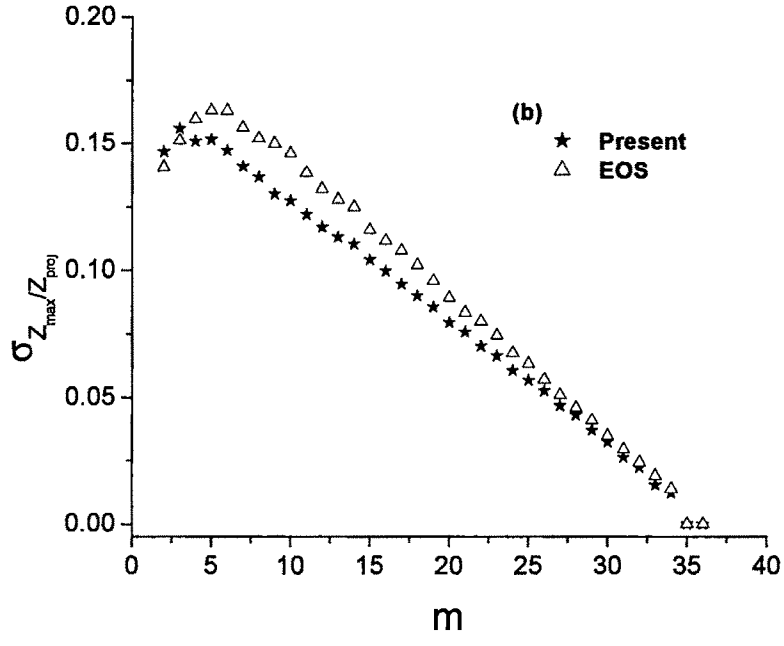

Fig. 4.3: Standard deviation of normalized Z_{max} as a function of multiplicity m for (a) experimental data, (b) randomly generated data.

cluster [61, 70, 75]. In Fig. 4.3(a), the standard deviation of Z_{max} normalized with respect to the charge of the projectile is shown as a function of multiplicity for the present experimental set of data.

Large fluctuations in the multiplicity range within 11-19 are readily seen from this plot. It also indicate a clear peak at m = 13 with error ± 3 as calculated from the polynomial fitting having R = 0.838. As in the case of Ref. [61], peaks have also been observed for both the sets of randomly generated data (plots are not shown here). But at this point one has to remember the fact that the point with $\sigma_{Z_{max}}/Z_{proj} = 0$ and m = 1 corresponds to a single projectile fragment moving with total charge of the projectile itself and therefore is not associated with the fragmentation of the nucleus and hence may be ignored. With this point being excluded, no well defined peak could be observed in $\sigma_{Z_{max}}/Z_{proj}$ vs. m plot [Fig. 4.3(b)], particularly with present set of generated data, and the behavior of this distribution differs significantly from that of the experimental one. However, recently, Gulminelli et al. [75] have pointed out that there exists a major problem in connecting such fluctuation peak to a phase transition or critical behavior in the analysis of nuclear multifragmentation data. A number of effects such as finiteness of the system under investigation, use of different event sorting procedure, etc., smooth the fluctuation effect to such an extent that not only the transition point is loosely defined and shifted, but also the signal is qualitatively the same for a critical point, a first order phase transition or even a continuous change or cross over. Thus the heap like structure that has been observed in Fig. 4.3(a) with experimental data may not carry as much information as one would expect for cluster approximation of critical behavior analysis for an infinite system.

4.4.1.2. Charge Moments and Conditional Moment

It has also been suggested that the conditional moments give more selective information [8, 9]. It is used to describe fluctuations in the average cluster size. In Fig. 4.4(a), $<\gamma_2>$ is plotted as a function of multiplicity m for Kr–Em interactions and compared with the result of EOS Collaboration for Au–C and Kr–C collisions at 1.0A GeV. The error bars show the standard deviation in $<\gamma_2>$. Fig. 4.4(b) represents the same plot for the randomly generated data. A peak in γ_2 is expected from random partitions only if the fragmenting system is of constant size. If this is not the case because of pre-equilibrium (as in the present data-set), no pronounced peak should be expected in the absence of a phase transition or a critical phenomenon. This is exactly what is seen in Fig. 4.4(b), no distinct rise and fall in $<\gamma_2>$ is seen with present set of generated data. However, from Fig. 4.4(a) it is clearly seen for all the three colliding systems that $<\gamma_2>$ increases monotonically with m, attains a maximum and then gradually decreases. Thus the appearance of a crest in $<\gamma_2>$ value might have been resulted from a phase transition occurring at $m = m_c$ which for the present experiment is found to be 21 ± 6. For gold it was reported to be at $m = m_c = 32$. Further, it is interesting to note from this figure that the emulsion data of this work confirms EOS finding that the position and height of the γ_2 peak is essentially determined by the source size [28, 30].

To have further insight into current sample of data, the mean values of 2nd moment of charge distribution, $<M_2>$, is plotted against m in Fig. 4.5(a) and compared with the result of EOS Collaboration. Fig. 4.5(b) represents the same plot for randomly generated events. A similar rise and fall of second order charge moment is clearly evident in Fig. 4.5(a) for both Kr and Au projectiles. Strong

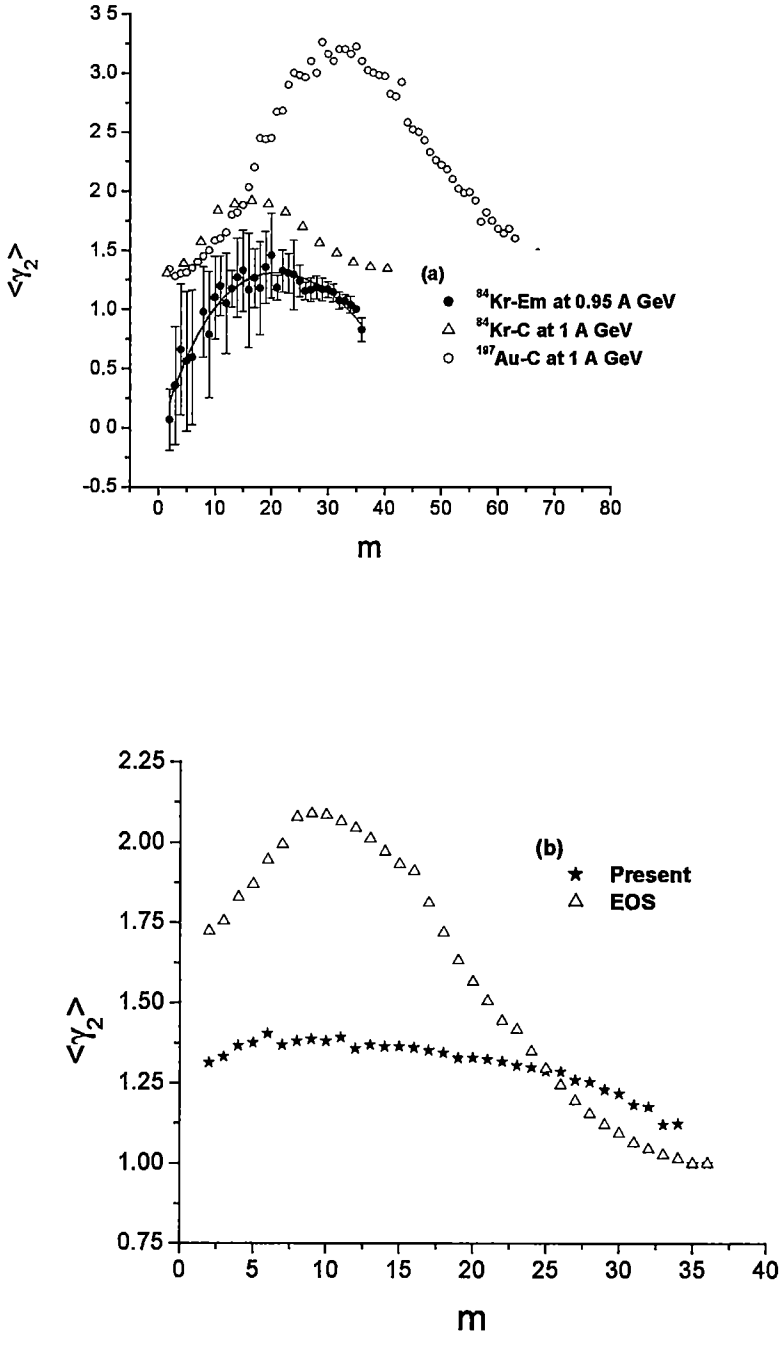

Fig. 4.4: Variation of $<\gamma_2>$ with total charged fragment multiplicity m for (a) experimental data of ^{84}Kr–Em (this work) and ^{84}Kr–C and ^{197}Au–C (EOS Collaboration); (b) randomly generated data.

fluctuations in $<M_2>$ values are found for m = 8 - 24 for Kr–Em interactions. Here again it is seen that the distribution of 2nd charge moments for experimental set of data points differs significantly from current generated data. Once again, a rise and fall in $<M_2>$ values with non-critical EOS generated data suggests that $<M_2>$ can be considered as an observable of critical behavior if the experimental values differ with the values obtained from both the sets of simulated data, differing from only one of the two may not be sufficient. The EMU-01 Collaboration, from their studies on 10.6A GeV Au–Em interactions [65], has pointed out that the distributions of different moments as well as conditional moment are not influenced by the target masses. The differences in conditional moment of Fig. 4.4(a) and 2nd charge moment of Fig. 4.5(a) may therefore be attributed to the difference in the projectile masses of various systems (Au–C and Kr–Em/C).

Figs. 4.6(a) and (b) show the scattered and contour plots of 2nd charge moments M_2' versus multiplicity m for individual events of Kr–Em interactions of the present investigation. From the experimental plot it is seen that M_2' values fluctuate strongly for multiplicities $10 \leq m \leq 24$. Clearly, the experimental data points are grouped in two distinct categories: one consists of events with multiplicity less than 19 with $M_2' < 0.9$ and the other with multiplicity m > 13 and largest M_2 values for a given m. While small multiplicity and small M_2' values of former group are believed to be characteristic features of liquid phase, large multiplicities and large M_2' values of the later group of events are expected features of gas phase. No such grouping of the data points could be seen [Figs. 4.6(c) and (d)] with both the sets of random numbers and therefore strongly support liquid gas type of phase transition in Kr multifragmentation.

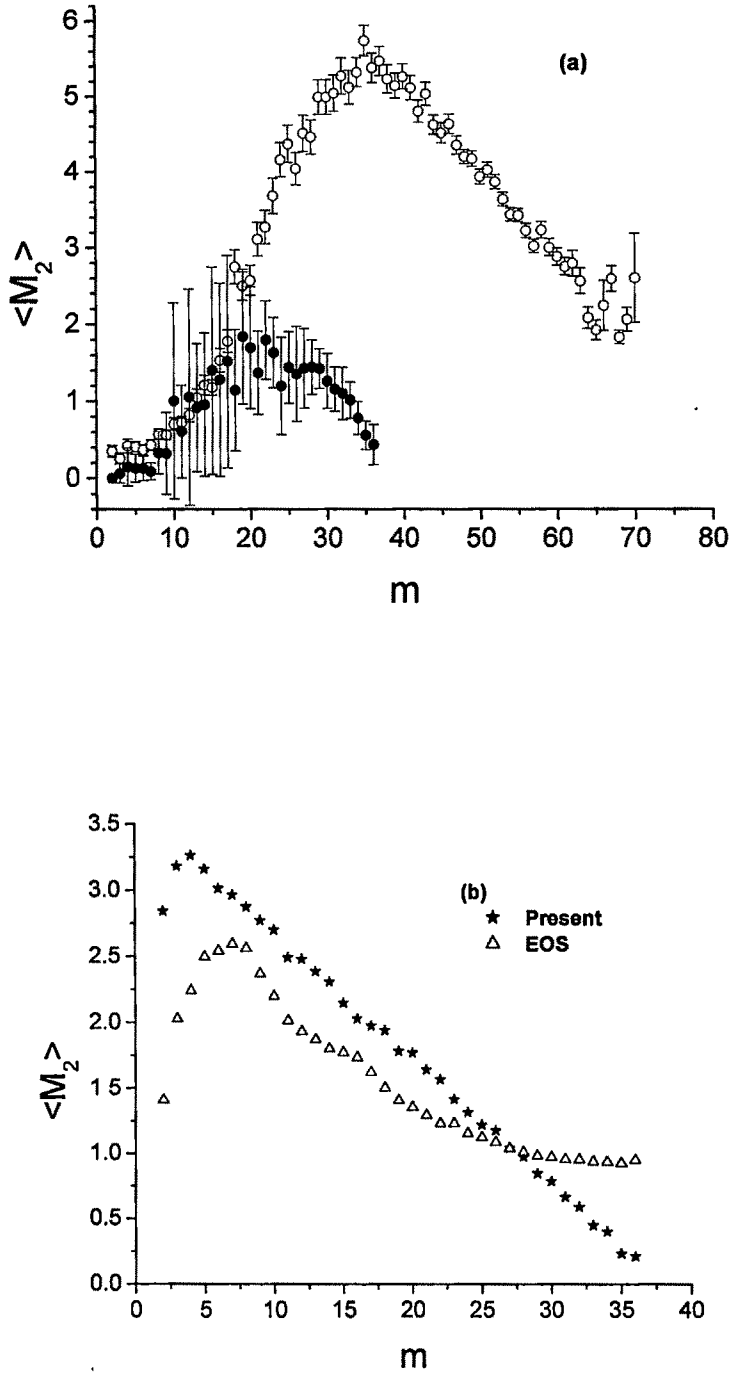

Fig. 4.5: Average of second charge moments as a function of multiplicity m for (a) ^{84}Kr–Em (solid circles) and ^{197}Au–C (open circles) data and (b) generated data.

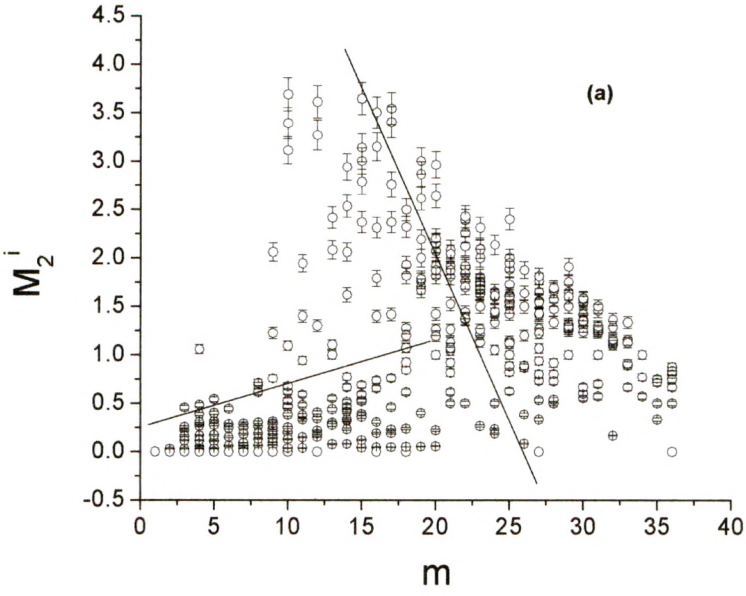

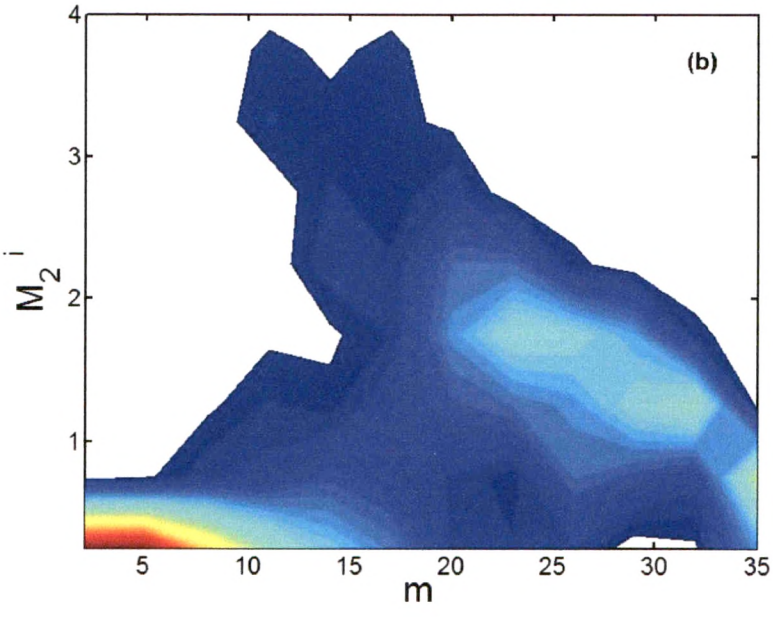

(Fig. 4.6: Cont…)

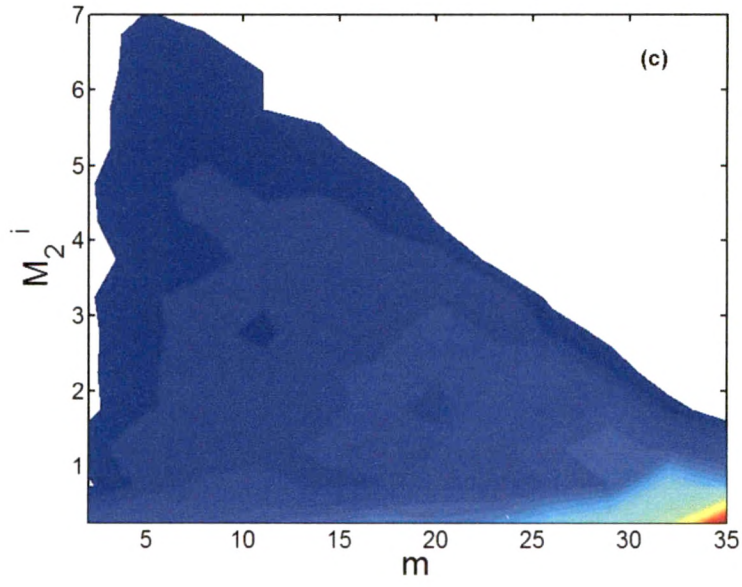

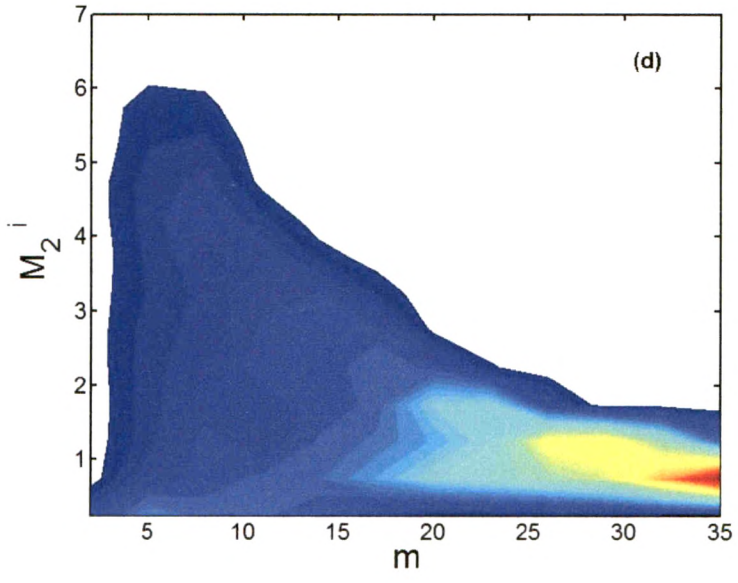

Fig. 4.6: Plots of second charge moments for individual events as a function of m. (a) Scattered plot for present experimental data, (b) contour plot of same, (c) contour plot for randomly generated events following present algorithm and (d) following EOS algorithm.

4.4.1.3. Multiplicity Distribution of Intermediate Mass Fragments

Another predicted consequence of the liquid–gas phase transition is the abundant emission of intermediate mass fragments. Therefore, in Fig. 4.7 the average number of intermediate mass fragments whose charges lie within 3–14 (in present case) against the multiplicity m for experimental and generated set of data is plotted. All these plots look similar and may not serve as a sensitive signature of phase transition study.

4.4.1.4. Variation of Mean Fragment Size

Fig. 4.8(a) shows the variation of $<M_1>$ with the maximum charge of the fragments for $m < m_c$ and as expected, it monotonically decreases with the increase of Z_{max} value. However, a similar result with randomly generated events [Fig. 4.8(b)] suggests that such variation of $<M_1>$ with Z_{max} cannot be taken as a genuine signature of percolation type of phase transition in the system under consideration.

From the above results one therefore gets enough indications that the system under present investigation shows some definite evidences of critical behavior suggesting the relevance of further analysis of the data to estimate the various exponents. However, one at the same time cannot deny the fact that these evidences, particularly the scattered plot of 2nd charge moments M_2' and the fluctuations in the size of the largest cluster, are compatible with first order phase transition as well thereby suggesting the relevance of studying bimodality signals [76, 77] with the present set of experimental data.

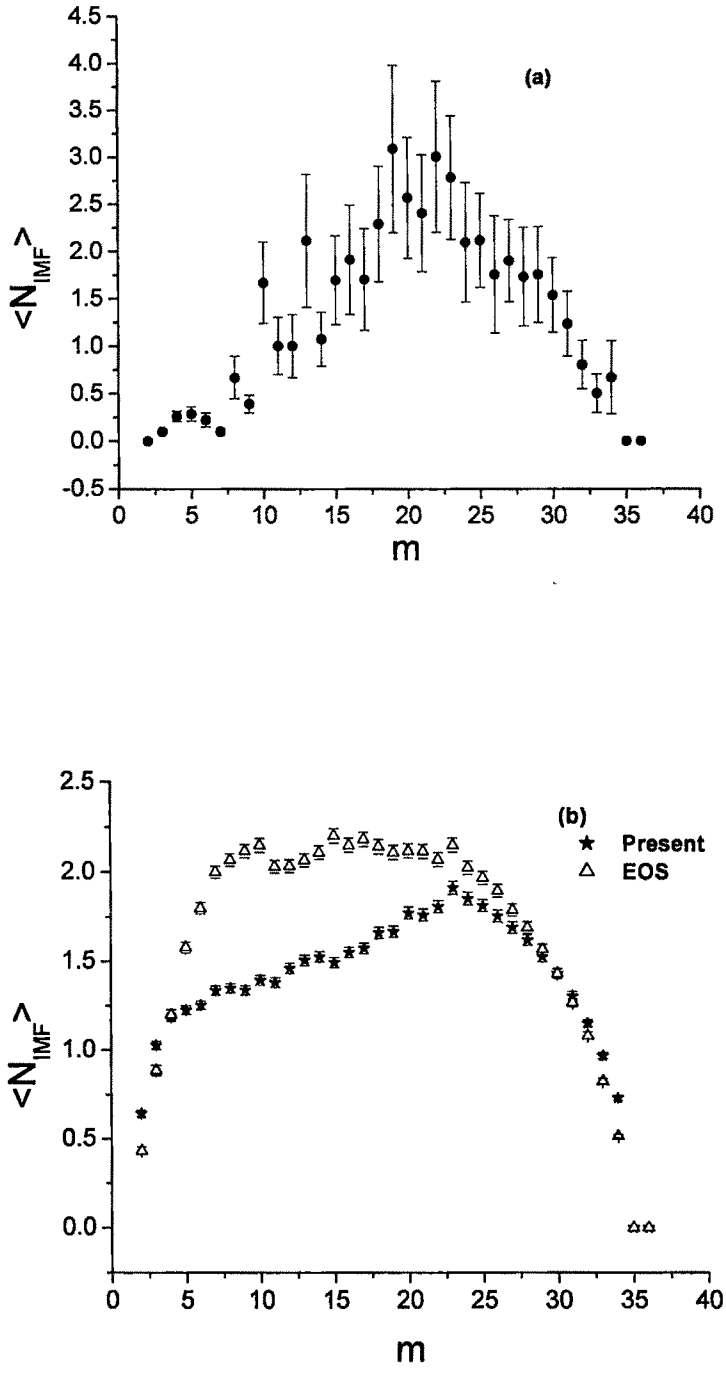

Fig. 4.7: Distribution of average number of IMFs as a function of multiplicity for (a) experimental events and (b) randomly generated events.

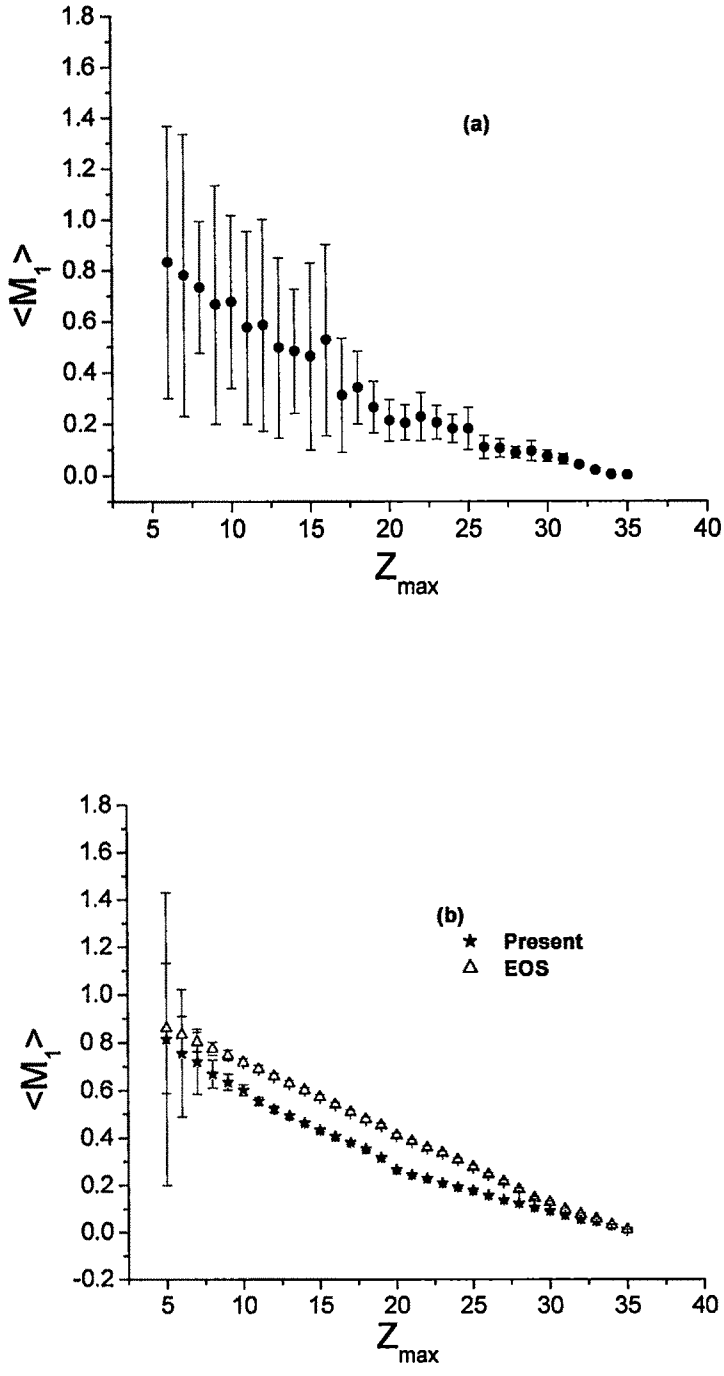

Fig. 4.8: Variation of mean size with Z_{max}; (a) for experimental events and (b) for randomly generated events.

4.4.2. Critical Exponents and Testing of Scaling Laws

The observation of a power law behavior for the size distribution of the fragments has triggered a number of studies that have looked for evidence of critical behavior [60, 63, 78-80]. These analyses consider nuclear multifragmentation as one example of a critical phenomenon and attempts are made to extract from the data the related critical exponents [65].

4.4.2.1. Estimation of Critical Exponents

To find out the different critical exponents, on the basis of Fig. 4.6(a), the selected data is considered instead of the whole data set. To estimate the critical exponent γ and the critical multiplicity m_c, the "γ-matching" [4, 61, 64] technique is adopted. According to this technique a trial value of the critical multiplicity m_c is chosen. For a particular m_c, a distribution of mean values of the moment $\langle M_2(\varepsilon)\rangle$ is determined as a function of distance from the critical point $\varepsilon = m\text{-}m_c$. Then the ranges in ε are chosen to fit the power law (4.7) to the experimental data, separately for the gas and liquid phases. With fitting boundaries determined, the linear fit to the $\ln\langle M_2(\varepsilon)\rangle$ versus $\ln|\varepsilon|$ is made to extract values of the slope γ separately for gas and liquid phases [64]. Figs. 4.9(a)-(p) show the variation of $\langle M_2\rangle$ against ε in log–log scale for liquid and gas phases. Due to mean field and finite size effects, far away from the critical point, cluster distributions do not follow the above power laws. It is therefore reasonable to ignore the extreme points of Figs. 4.9(a)-(p) and do the straight line fitting with the remaining data points. Also following the suggestion of Fisher Drop Model (FDM), a model that relates various moments to relevant thermodynamical quantities, γ-value in gas

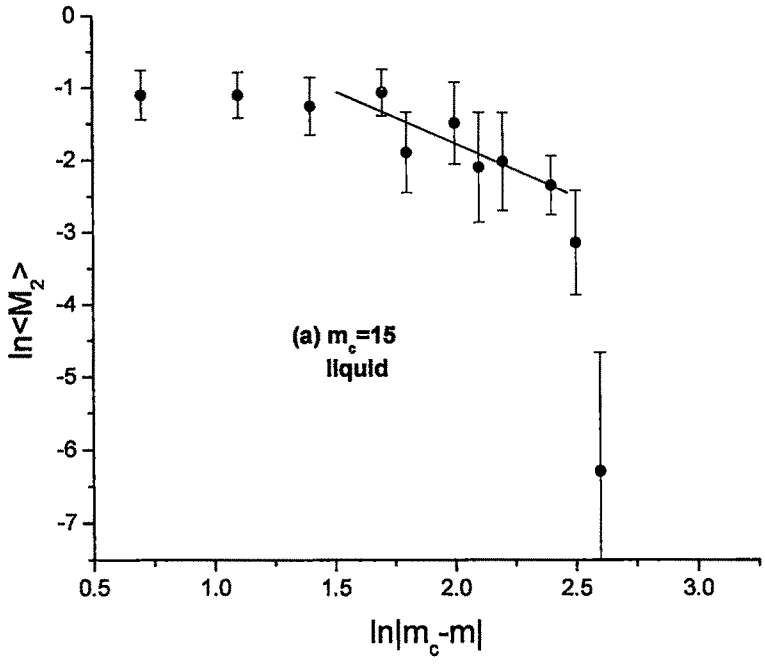
0
-1
-2
-3
-4
-5
-6
-7
ln<M2>
(a) mc=15
liquid
0.5
1.0
1.5
2.0
2.5
3.0
ln|mc-m|

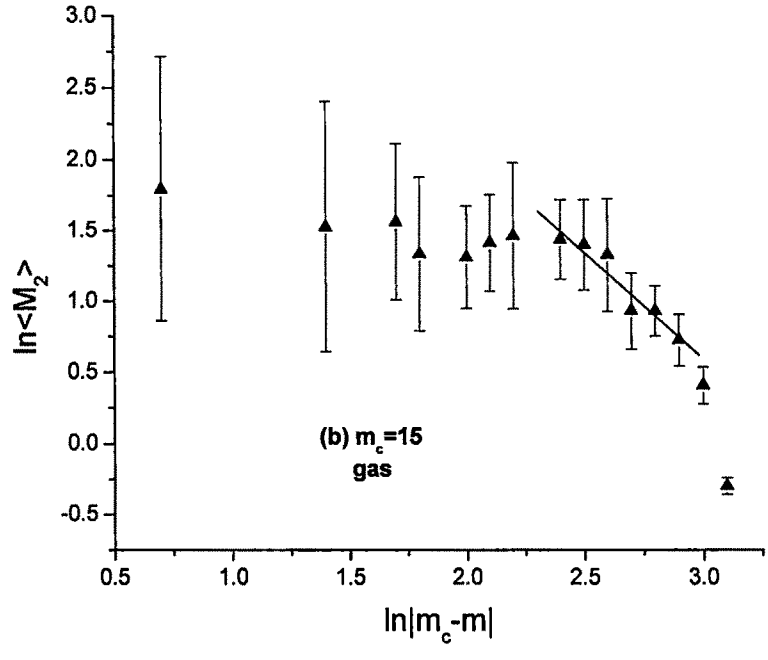
3.0
2.5
2.0
1.5
1.0
0.5
0.0
-0.5
ln<M2>
(b) mc=15
gas
0.5
1.0
1.5
2.0
2.5
3.0
ln|mc-m|

(Fig. 4.9: Cont...)

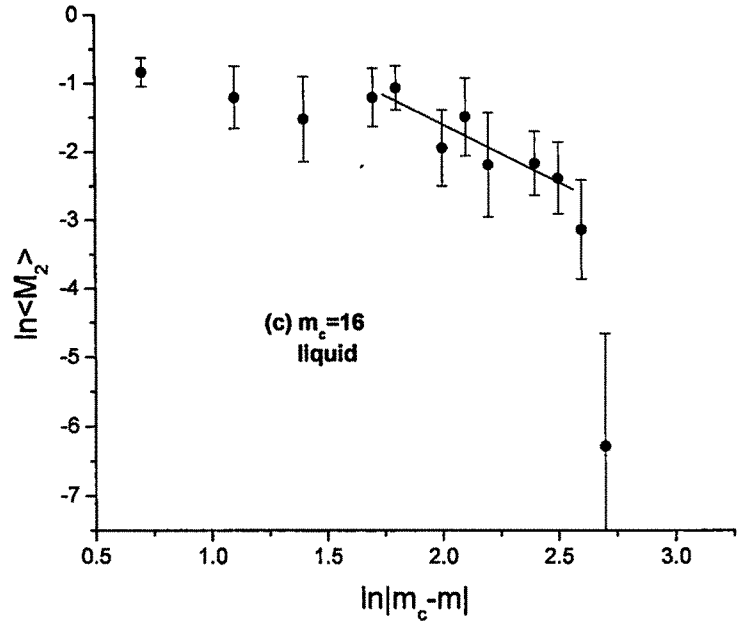
0
-1
-2
-3
-4
-5
-6
-7
0.5
1.0
1.5
2.0
2.5
3.0
ln<M2>
ln|mc-m|
(c) mc=16
liquid

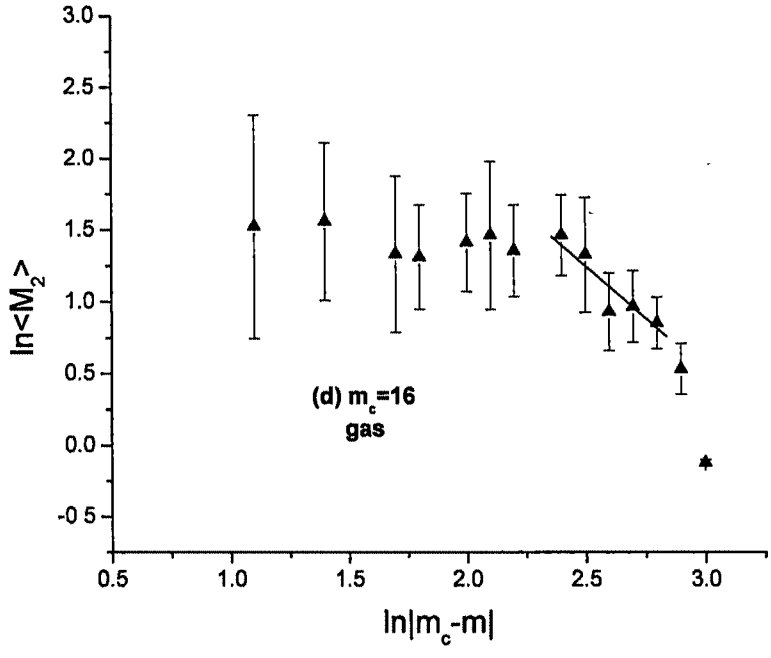
3.0
2.5
2.0
1.5
1.0
0.5
0.0
-0 5
0.5
1.0
1.5
2.0
2.5
3.0
ln<M2>
ln|mc-m|
(d) mc=16
gas

(Fig. 4.9: Cont...)

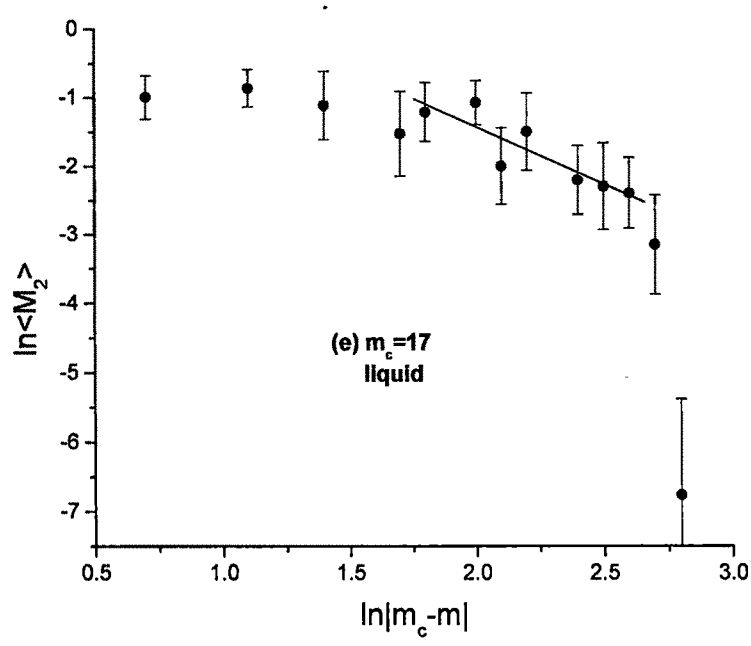
0
-1
-2
-3
-4
-5
-6
-7
ln<M2>
(e) mc=17
liquid
0.5
1.0
1.5
2.0
2.5
3.0
ln|mc-m|

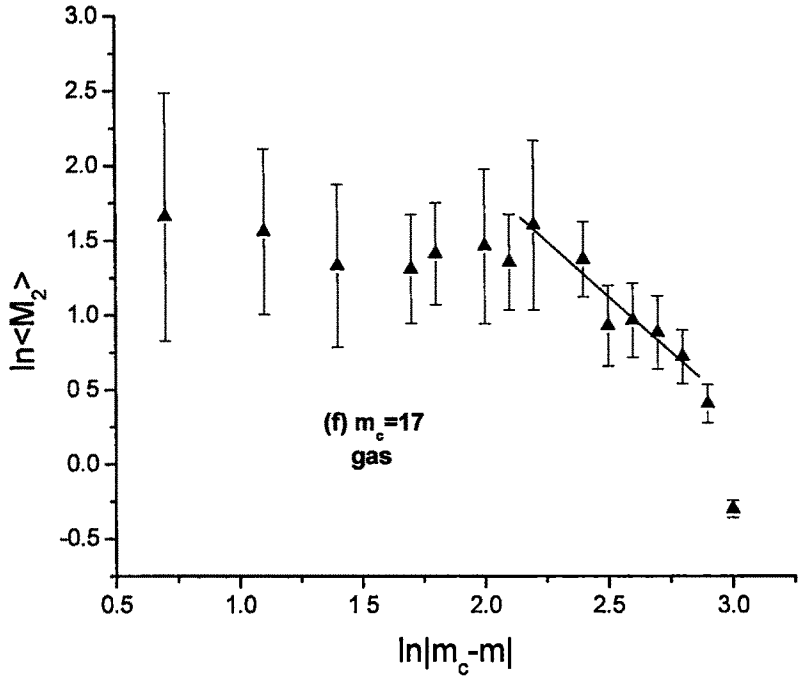
3.0
2.5
2.0
1.5
1.0
0.5
0.0
-0.5
ln<M2>
(f) mc=17
gas
0.5
1.0
1.5
2.0
2.5
3.0
ln|mc-m|

(Fig. 4.9: Cont...)

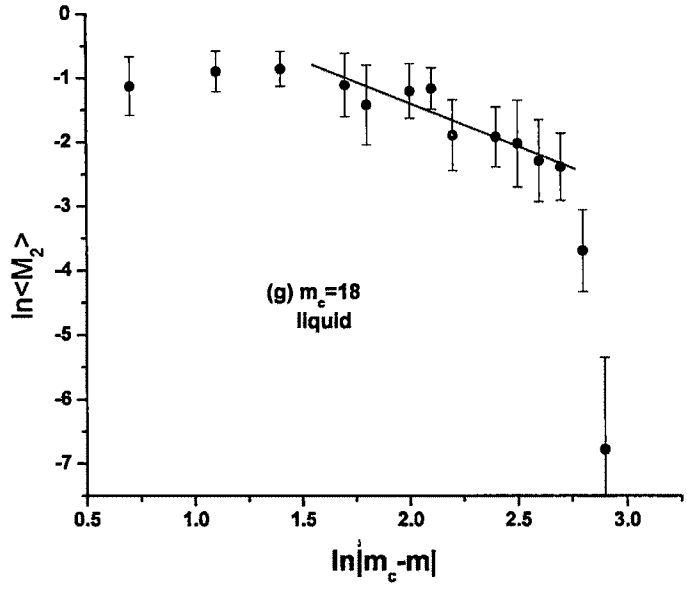
0
-1
-2
-3
-4
-5
-6
-7
ln<M2>
(g) mc=18
liquid
0.5
1.0
1.5
2.0
2.5
3.0
ln|mc-m|

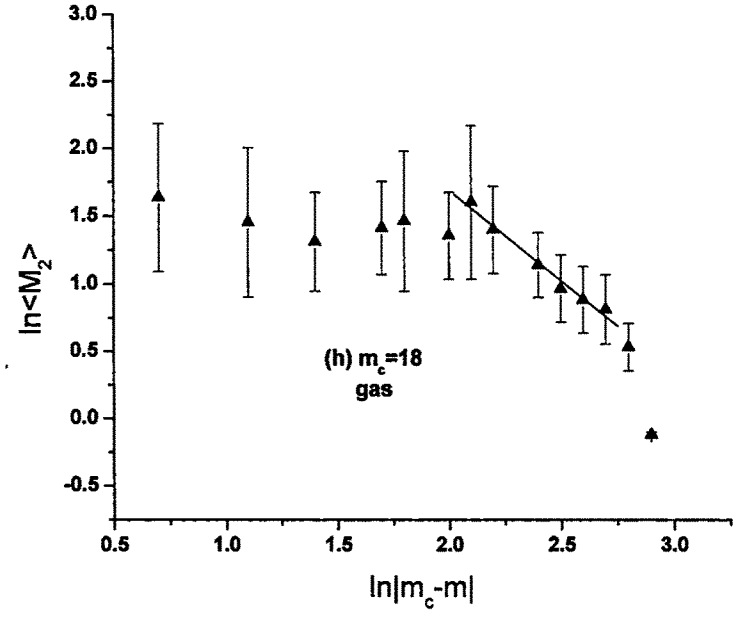
3.0
2.5
2.0
1.5
1.0
0.5
0.0
-0.5
ln<M2>
(h) mc=18
gas
0.5
1.0
1.5
2.0
2.5
3.0
ln|mc-m|

(Fig. 4.9: Cont...)

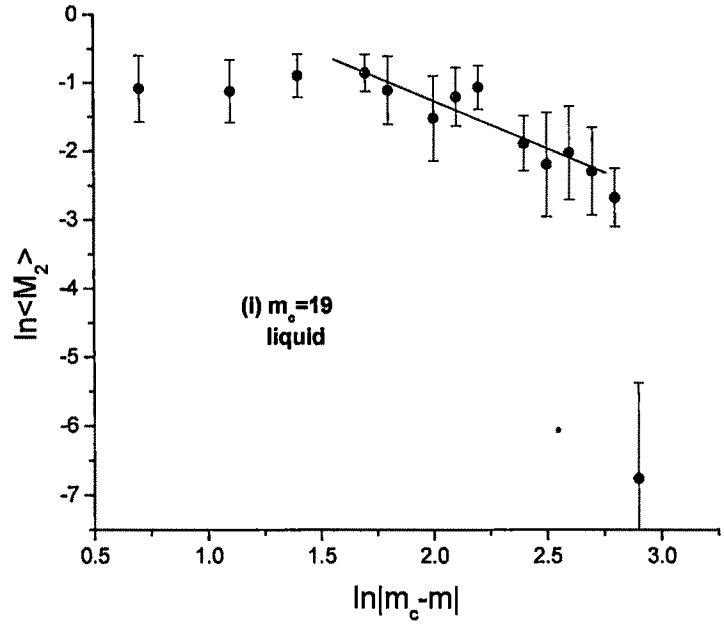
0
-1
-2
-3
-4
-5
-6
-7
ln<M2>
(i) mc=19
liquid
0.5
1.0
1.5
2.0
2.5
3.0
ln|mc-m|

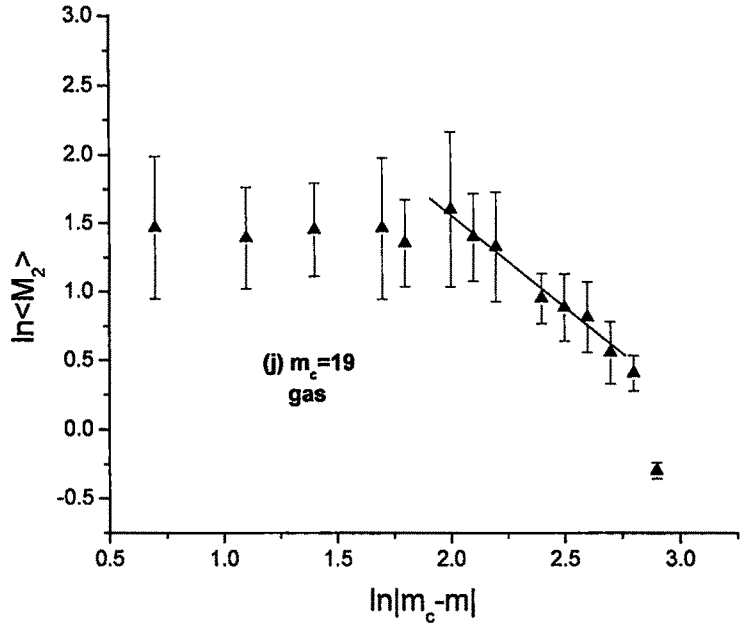
3.0
2.5
2.0
1.5
1.0
0.5
0.0
-0.5
ln<M2>
(j) mc=19
gas
0.5
1.0
1.5
2.0
2.5
3.0
ln|mc-m|

(Fig. 4.9: Cont...)

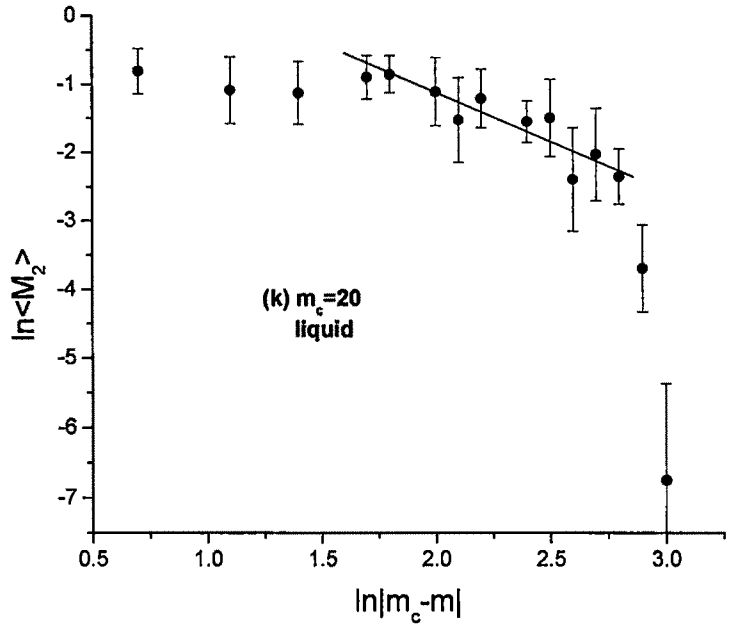
0
-1
-2
-3
-4
-5
-6
-7
0.5
1.0
1.5
2.0
2.5
3.0
ln<M2>
ln|mc-m|
(k) mc=20
liquid

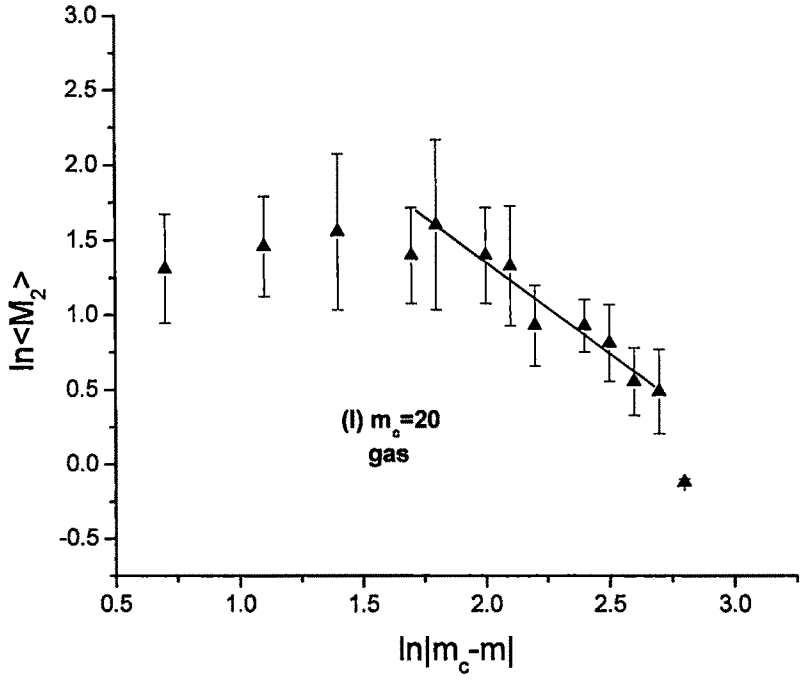
3.0
2.5
2.0
1.5
1.0
0.5
0.0
-0.5
0.5
1.0
1.5
2.0
2.5
3.0
ln<M2>
ln|mc-m|
(l) mc=20
gas

(Fig. 4.9: Cont...)

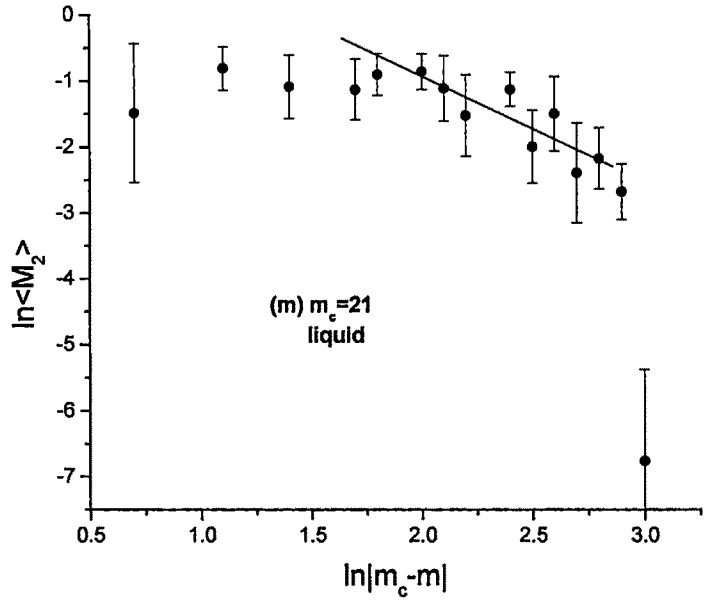
0
-1
-2
-3
-4
-5
-6
-7
ln<M2>
(m) mc=21
liquid
0.5
1.0
1.5
2.0
2.5
3.0
ln|mc-m|

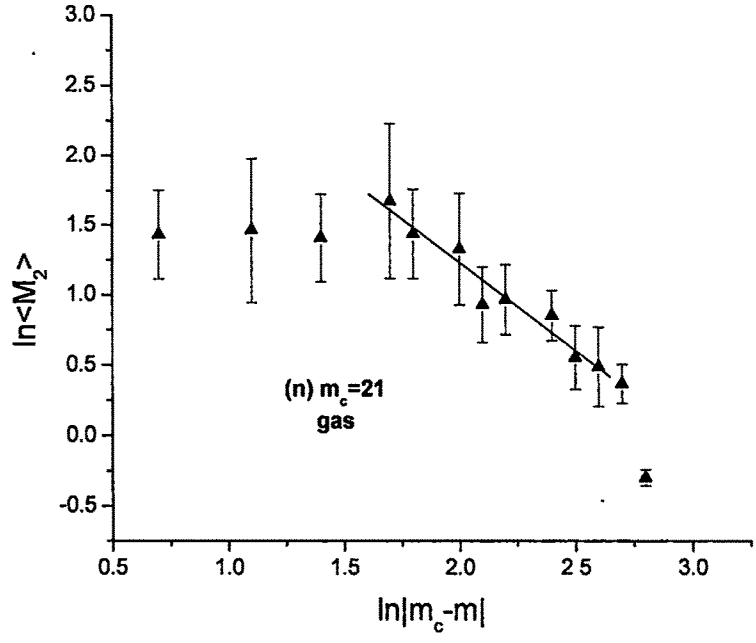
3.0
2.5
2.0
1.5
1.0
0.5
0.0
-0.5
ln<M2>
(n) mc=21
gas
0.5
1.0
1.5
2.0
2 5
3.0
ln|mc-m|

(Fig. 4.9: Cont...)

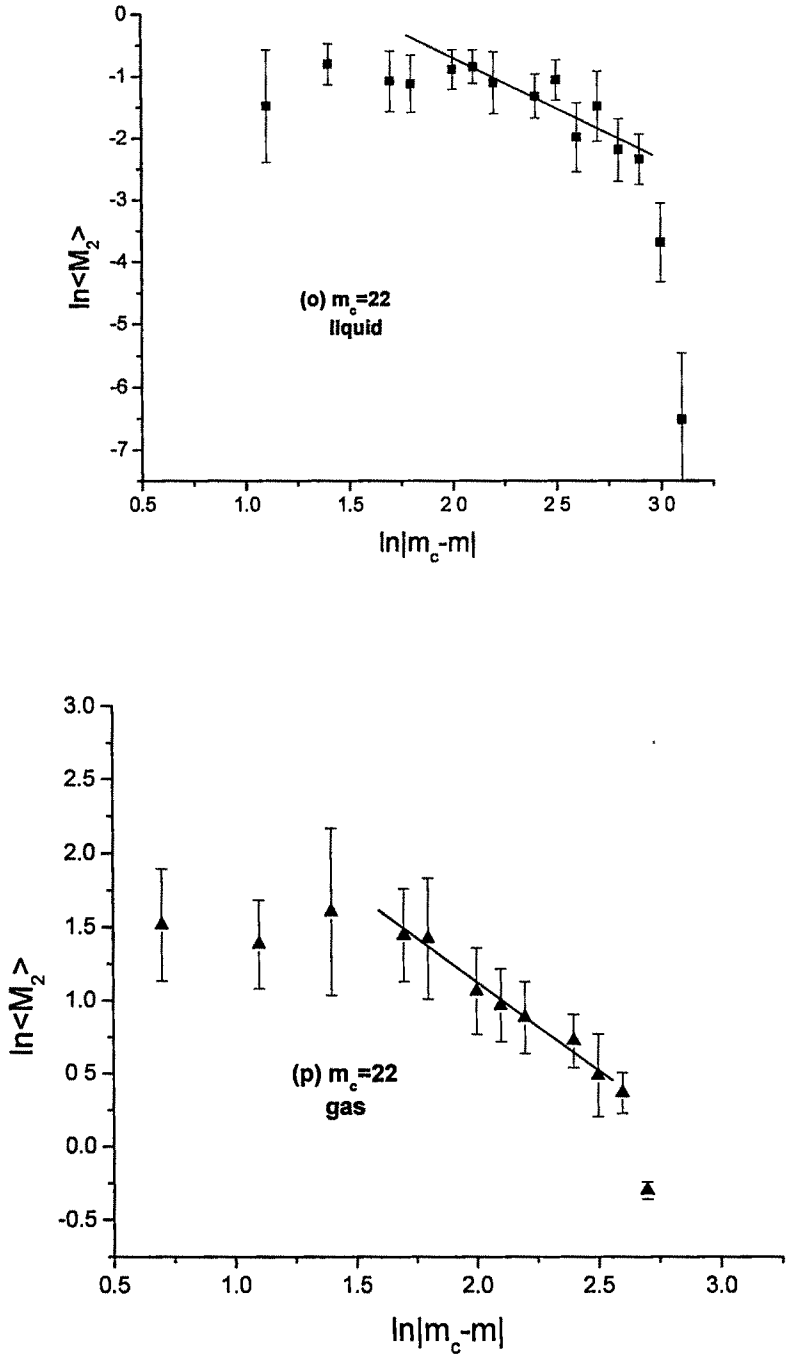

Fig. 4.9: Mean values of second charge moments $<M_2>$ for liquid and gas phases as a function of ε at different trial values of critical multiplicity.

phase has been calculated including Z_{max}. Different ranges were selected for liquid and gas phase events and γs were estimated for several trial values of the critical point m_c. The different values of γ for liquid and gas phases are tabulated in table 4.1.

Table 4.1: Critical exponent γ for gas and liquid phases for different trial values of m_c.

Sl. No.	m_c	γ_{liquid}	R	γ_{gas}	R
1	15	1.96 ± 0.24	0.936	1.54 ± 0.12	0.978
2	16	1.69 ± 0.24	0.932	1.44 ± 0.15	0.963
3	17	1.68 ± 0.20	0.940	1.47 ± 0.12	0.975
4	18	1.34 ± 0.14	0.944	1.33 ± 0.05	0.995
5	19	1.39 ± 0.12	0.952	1.35 ± 0.05	0.994
6	20	1.44 ± 0.13	0.950	1.22 ± 0.10	0.972
7	21	1.61 ± 0.21	0.918	1.25 ± 0.05	0.990
8	22	1.61 ± 0.16	0.944	1.20 ± 0.05	0.992

It is expected that at $m = m_c$, $|\gamma_{liquid}-\gamma_{gas}|$ attains a minimum value and γ_{gas}, within the statistical error, should agree with the value of γ_{liquid}. A plot of $|\gamma_{liquid}-\gamma_{gas}|$ against various hypothetical m_c values (Fig. 4.10) clearly shows a minimum in $|\gamma_{liquid}-\gamma_{gas}|$ value at $m_c = 18 \pm 1$ indicating that critical multiplicity for Kr–Em interactions at 0.95A GeV, as determined by the γ-matching procedure, is 18 ± 1 and the critical exponent $\gamma = 1.34 \pm 0.19$, the average of γ_{liquid} and γ_{gas} for which $|\gamma_{liquid} - \gamma_{gas}|$ is minimum.

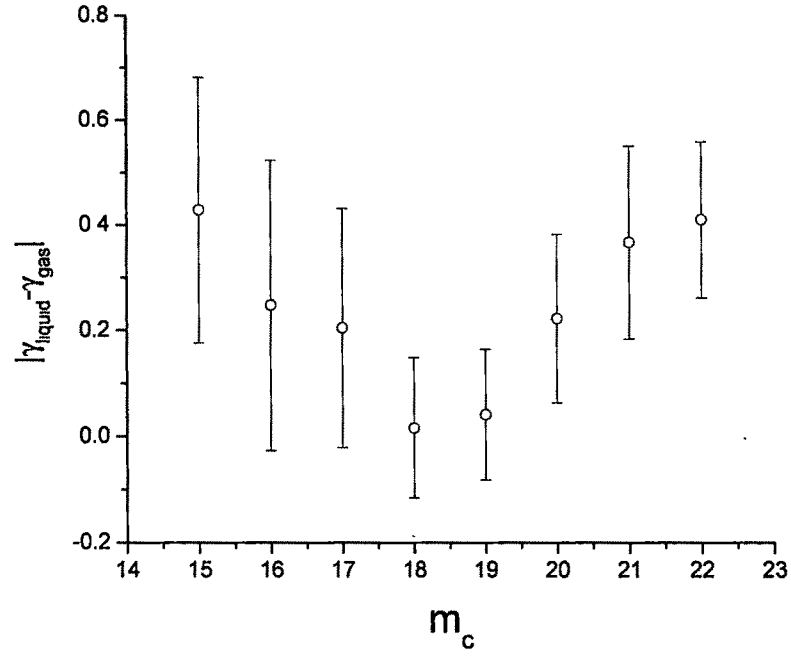

Fig. 4.10: $|\gamma_{liquid} - \gamma_{gas}|$ as a function of m_c.

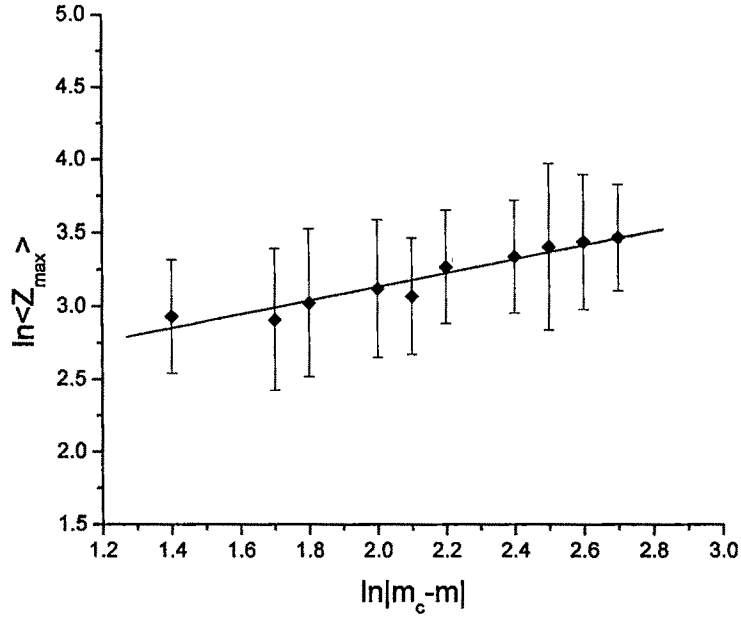

Fig. 4.11: Variation of $\ln\langle Z_{max}\rangle$ with $\ln|m_c - m|$.

The critical exponent β is calculated using Eq. (4.8). The value of $\ln\langle Z_{max}\rangle$ is plotted as a function of $\ln |m_c - m|$ in Fig. 4.11. From the linear fit carried out within the fitting boundaries, determined during the γ-matching procedure, β is estimated to be 0.47 ± 0.05 with $R = 0.980$.

Now to calculate τ, though Eq. (4.11) is valid on both sides of critical point, the gas phase is only used as the finite and small size effect of the system become much more prominent in liquid phase [81]. It should be noted that to calculate M_2 in the liquid phase Z_{max} is excluded and thus there are only very few fragments left in the calculation, resulting in altering the calculated value of the exponent. The variations of $\ln M_3$ as a function of $\ln M_2$ for each event and $\ln\langle M_3\rangle$ against $\ln\langle M_2\rangle$ are shown in Figs. 4.12(a) and (b) respectively. The straight line drawn is the best fitted line for the experimental data points and from the slope of this line the value of τ is found to be 2.31 ± 0.06, which, within statistical error, agrees with the value obtained from the charge distribution of this work.

Experimental values of γ, β and τ for different systems, including this work, are listed in table 4.2. β values estimated using the scaling relation (4.10) for these systems are also listed in this table. From table 4.2, it is seen that, for all but Ref. [65], the experimental β values differ significantly from that estimated using scaling relation (4.10) involving τ and γ as other two parameters, thereby raising doubt about the correctness of the values of different exponents.

4.4.2.2. Testing of Scaling Laws

In Fig. 4.13, variation of $\ln\langle M_3(\varepsilon)\rangle$ with $\ln |m_c - m|$ is plotted at critical multiplicity $m_c = 18$ to get the value of δ. A linear fit of the data points for $\ln |m_c - m|$ lying between $2.10 - 2.70$ gives the value of critical exponent δ as 2.95 ± 0.14

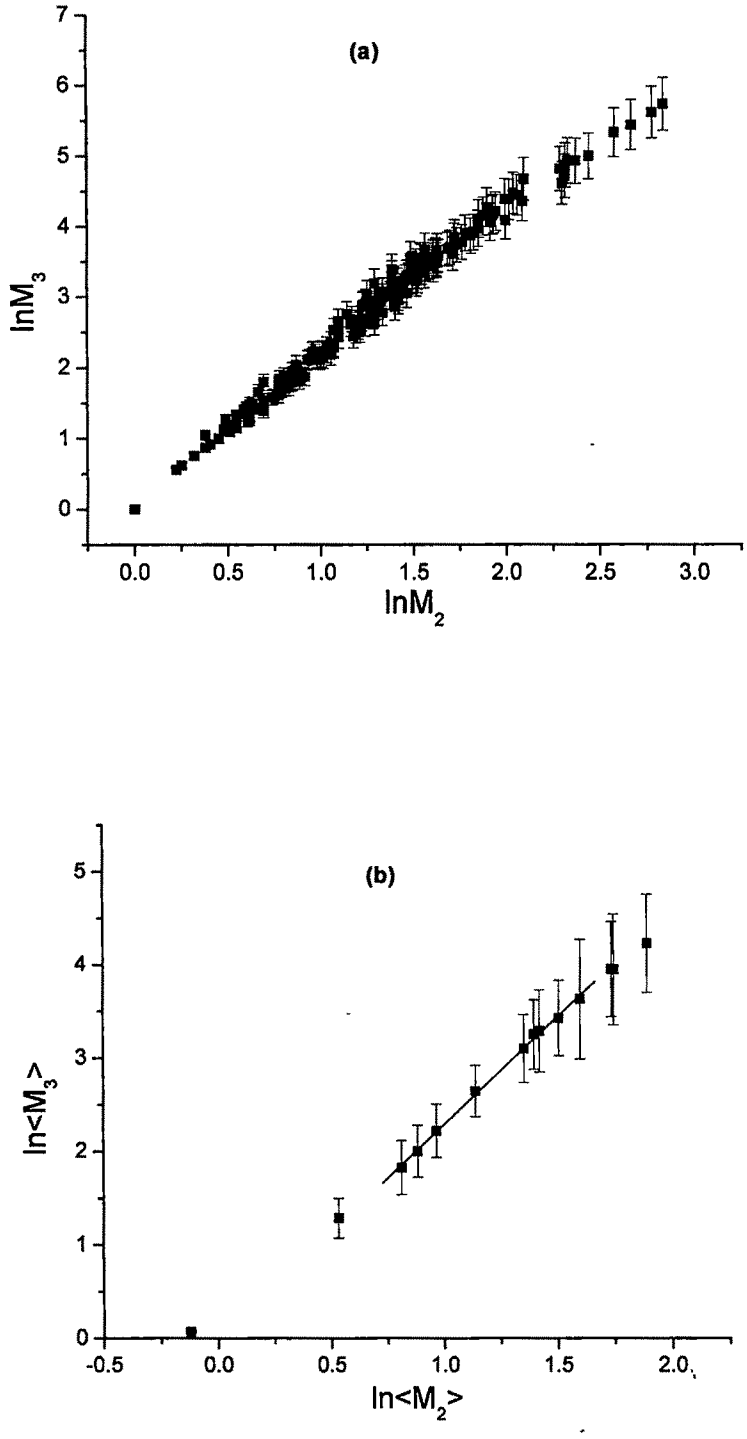

Fig. 4.12: (a) Event-by-event distribution of $\ln M_3$ vs. $\ln M_2$ and (b) variation of $\ln\langle M_3\rangle$ with $\ln\langle M_2\rangle$.

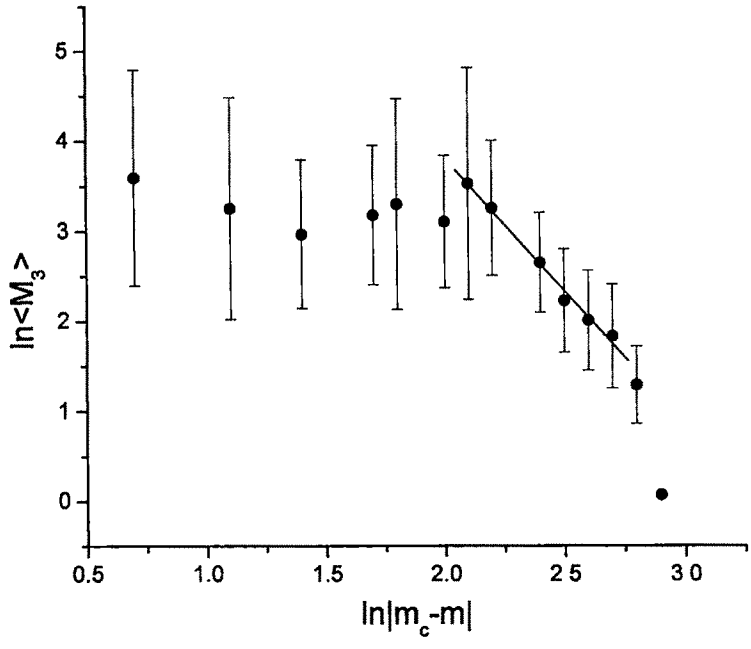

Fig. 4.13: Variation of ln$\langle M_3 \rangle$ as a function of ln $|m_c - m|$ for gas phase.

with R value 0.997. The relation (4.12) is valid for both the phases but here only the gas phase is considered again due to the finite size effect. Using this value of δ in scaling relation (4.13), exponent γ is found to be 1.20 ± 0.17, which, within the statistical errors, lies close to the graphically obtained value. Thus the experimental values of the set of three exponents δ, γ and τ obey the scaling relation (4.13).

The value of β calculated using relation (4.14) is found to be 0.54 ± 0.15 which is in good agreement with the value reported by Srivastva et al. [28] and also nearer to the value obtained from relation (4.10) using present experimental values of τ and γ . Taking β as 0.54 ± 0.15 the successive estimations of τ and γ from the scaling relation (4.10) give their values respectively as 2.29 and 1.20. It is readily seen that these values are in good agreement with present experimental values. Thus, finally for Kr–Em interactions at 0.95A GeV, a set of values of γ , β and τ is obtained that obey the scaling relationship as 1.34 ± 0.19, 0.54 ± 0.15 and 2.31 ± 0.06 respectively.

Table 4.2: Different values of γ , τ and β for various systems.

Exp.	Energy (A GeV)	γ	τ	β	β (calculated)	Ref.
Kr-Em (norm)	0.95	1.34 ± 0.19	2.31 ± 0.06	0.47 ± 0.05	0.60 ± 0.25	P. W.
Kr-C	1	-	1.88 ± 0.08	0.53 ± 0.05	-	28
La-C	1	-	2.10 ± 0.06	0.34 ± 0.02	-	28
Au-Em	1	-	2.16 ± 0.08	0.32 ± 0.02	-	28
Au-Em (norm)	4	1.15 ± 0.09	2.12 ± 0.04	0.34 ± 0.01	0.16 ± 0.07	64
Au-Em (norm)	10.6	1.17 ± 0.09	2.11 ± 0.05	0.33 ± 0.01	0.14 ± 0.08	64
Au–Em	4	1.23 ± 0.09	2.15 ± 0.04	0.36 ± 0.02	0.22 ± 0.09	64
Au–Em	10.6	1.11 ± 0.09	2.16 ± 0.05	0.33 ± 0.02	0.21 ± 0.10	64
Au–C	1	1.40 ± 0.10	2.14 ± 0.06	0.29 ± 0.02	0.23 ± 0.13	60
Au–Em	10.6	0.86 ± 0.05	2.23 ± 0.05	0.25 ± 0.02	0.26 ± 0.09	65
Au–Em	10.6	–	1.88 ± 0.06	0.19 ± 0.02	–	63
d = 3 Ising (liquid–gas)	–	1.23	2.21	0.33	0.33	
d = 3 percolation	–	1.80	2.18	0.41	0.40	

References

[1] A. S. Hirsch *et al.*, Phys. Rev. C **29**, 508 (1984).

[2] J. E. Finn *et al.*, Phys. Rev. Lett. **49**, 1321 (1982).

[3] R. W. Minich *et al.*, Phys. Lett. B **118**, 458 (1982).

[4] W. Bauer, Phys. Rev. C **38**, 1297 (1988).

[5] W. Bauer *et al.*, Annu. Rev. Nucl. Sci. **42**, 77 (1992).

[6] J. D. Desbois, Nucl. Phys. A **466**, 724 (1987).

[7] D. Stauffer, Phys. Rep. **54**, 1 (1979).

[8] X. Campi, J. Phys. A **19**, 917 (1986).

[9] X. Campi, Phys. Lett. B **208**, 351 (1988).

[10] X. Campi and H. Krivine, Z. Phys. A **344**, 81 (1992).

[11] T. Sil *et al.*, Phys. Rev. C **63**, 054604 (2001).

[12] Ph. Chomaz *et al.*, Phys. Rev. Lett. **85**, 3587 (2000).

[13] J. Pochodzalla *et al.*, Phys. Rev. Lett. **75**, 1040 (1995).

[14] H. Xi *et al.*, Z. Phys. A **359**, 397 (1997).

[15] J. Pochodzalla (Aladin Collaboration), *Proceedings of the 1st Catania Relativistic Ion Studies, Acicastello, May 27–31, 1996, eds. S. Costa, S. Albergo, A. Insolia, C. Tuve*, p. 1 (Italy, 1996).

[16] G. Imme (Aladin Collaboration), *Proceedings of the 1st Catania Relativistic Ion Studies, Acicastello, May 27–31, 1996, eds. S. Costa, S. Albergo, A. Insolia, C. Tuve*, p. 143 (Italy, 1996).

[17] C. Schwartz (Aladin Collaboration), *XXXV Int. Winter Meeting on Nuclear Physics, Bormio, February 3–7, 1997, eds. I. Iori*, p. 456 (Italy, 1997).

[18] M. Pichon *et al.*, Nucl. Phys. A **779**, 267 (2006).

[19] N. Le Neindre *et al.*, Nucl. Phys. A **795**, 47 (2007).

[20] E. Bonnet *et al.*, arXiv:0812.1871v2 [nucl-ex].

[21] M. D'Agostino *et al.*, Phys. Lett. B **473**, 219 (2000).

[22] M. D'Agostino *et al*, Nucl. Phys. A **699**, 795 (2002).

[23] M. Bruno *et al.*, Nucl. Phys. A **807**, 48 (2008).

[24] Y. G. Ma *et al.*, Phys. Rev. C **71**, 054606 (2005).

[25] J. Hufner, Phys. Rep. **125**, 129 (1985).

[26] M. A. Jilany, J. Phys. G: Nucl. Part. Phys. **29**, 2263 (2003).

[27] M. A. Jilany, Phys. Rev. C **70**, 014901 (2004).

[28] B. K. Srivastava *et al.*, Phys. Rev. C **65**, 054617 (2002).

[29] B. K. Srivastava *et al.*, Phys. Rev. C **64**, R041605 (2001).

[30] B. K. Srivastava (EOS Collaboration), Pramana J. Phys. **57**, 301 (2001).

[31] G. Peilert *et al.*, Phys. Rev. C **39**, 1402 (1989).

[32] H. Feldmeier, Nucl. Phys. A **515**, 147 (1990).

[33] A. Ono *et al.*, Phys. Rev. C **47**, 2652 (1993).

[34] S. Pratt *et al.*, Phys. Lett. B **349**, 261 (1995).

[35] A. Ono and H. Horiuchi, Phys. Rev. C **53**, 2598 (1996).

[36] Y. Sugawa and H. Horiuchi, Phys. Rev. C **60**, 064607 (1999).

[37] R. Nebauer and J. Aichelin (INDRA Collaboration), Nucl. Phys. A **658**, 67 (1999).

[38] S. Ayik and C. Gregoire, Phys. Lett. B **212**, 269 (1988).

[39] S. Ayik and C. Gregoire, Nucl. Phys. A **513**, 187 (1990).

[40] J. Randrup and B. Remaud Nucl. Phys. A **514**, 339 (1990).

[41] Ph. Chomaz *et al.*, Phys. Lett. B **254**, 340 (1991).

[42] Ph. Chomaz *et al.*, Phys. Rev. Lett. **73**, 3512 (1994).

[43] A. Guarnera *et al.*, Phys. Lett. B **373**, 267 (1996).

[44] A. Guarnera *et al.*, Phys. Lett. B **403**, 191 (1997).

[45] Ph. Chomaz, Ann. Phys. Paris **21**, 669 (1996).

[46] F. Matera and A. Dellafiore, Phys. Rev. C **62**, 044611 (2000).

[47] A. Z. Mekjian, Phys. Rev. C **17**, 1051 (1978).

[48] D. Gross, Rep. Prog. Phys. **53**, 605 (1990).

[49] S. J. Lee and A. Z. Mekjian, Phys. Rev. C **45** 1284 (1992).

[50] D. Hahn and H. Stocker, Phys. Rev. C **37**, 1048 (1988).

[51] D. Hahn and H. Stocker, Nucl. Phys. A **476**, 718 (1988).

[52] J. Konopka *et al.*, Phys. Rev. C **50**, 2085 (1994).

[53] J. Bondorf *et al.*, Phys. Rep. **257**, 133 (1995).

[54] F. Gulminelli and D. Durand, Nucl. Phys. A **615**, 117 (1997).

[55] A. H. Raduta and A. R. Raduta, Phys. Rev. C **55**, 1344 (1997).

[56] B. Borderie, J. Phys. G: Nucl. Part. Phys. **28**, R217 (2002).

[57] H. E. Stanley, *Introduction to Phase Transitions and Critical Phenomena*, (Oxford University Press, Oxford, 1971).

[58] M. Kleine Berkenbusch *et al.*, Phys. Rev. Lett. **88**, 022701 (2002).

[59] S. S. Abdel-Aziz *et al.*, *Proceedings of the 26th Int. Cosmic Ray Conference, Salt Lake City, Utah, August 17–25, 1999*, p. 33 (USA, 1999).

[60] M. L. Gilkes *et al.*, Phys. Rev. Lett. **73**, 1590 (1994).

[61] J. B. Elliott *et al.*, Phys. Rev. C **62**, 064603 (2000).

[62] J. B. Elliott *et al.*, Phys. Rev. Lett. **88**, 042701 (2002).

[63] M. L. Cherry *et al.*, Phys. Rev. C **52**, 2652 (1995).

[64] D. Kudzia *et al.*, Phys. Rev. C **68**, 054903 (2003).

[65] M. I. Adamovich *et al.*, Eur. Phys. J. A **5**, 429 (1999).

[66] J. D. Frankland *et al.*, Phys. Rev. C **71**, 034607 (2005).

[67] M. D'Agostino *et al.*, Nucl. Phys. A **724**, 455 (2003).

[68] A. Schuttauf *et al.*, Nucl. Phys. A **607**, 457 (1996).

[69] J. B. Natowitz *et al.*, Phys. Rev. C **65**, 034618 (2002).

[70] F. Gulminelli and Ph. Chomaz, Phys. Rev. C **71**, 054607 (2005).

[71] W. Bauer and A. Botvina, Phys. Rev. C **52(4)**, R1760 (1995).

[72] W. Bauer and W. A. Friedman, Phys. Rev. Lett. **75(4)**, 767 (1995).

[73] J. A. Hauger *et al.*, Phys. Rev. Lett. **77(2)**, 235 (1996).

[74] K. Christensen and N. R. Moloney, *Complexity and Criticality* (Imperial College Press, London, 2005).

[75] F. Gulminelli and M. D'Agostino, Eur. Phys. J. A **30**, 253 (2006).

[76] O. Lopez and M. F. Rivet, Eur. Phys. J. A **30**, 263 (2006).

[77] F. Gulminelli, Nucl. Phys. A **791**, 165 (2007).

[78] M. I. Adamovich *et al.* (EMU01 Collaboration), Eur. Phys. J. A **1**, 77 (1998).

[79] G. Singh and L.P. Jain, Phys. Rev. C **54**, 3185 (1996).

[80] N. T. Porile (for EOS Collaboration), *Proc. of the 7 th Int. Conf. on Nuclear Reaction Mechanisms, eds. E. Gadioli, Varena, June 6-11, 1994*, p555 (Varena, 1994).

[81] J. B. Elliott *et al.*, Phys. Rev. C **49(6)**, 3185 (1994).

Chapter V

Intermittency & Fractality in Projectile Fragmentation

5.1. Introduction

In an attempt to get the signatures of critical behavior in breaking up of nuclei, several workers have analyzed their experimental data on various systems at different energies using different mathematical tools [1-8]. In chapter IV, the data of this work on Kr-Em interaction at 0.95A GeV is analyzed using cluster approximation technique and clear evidences of liquid gas phase transition in fragmentation of projectile nucleus [9] could be observed. As mentioned earlier, cluster approximation acts as a theme of percolation [10] that is a simple example of geometrical phase transition. Moreover Bauer [11, 12], Desbois [13] and Campi [14] showed that fragments size distribution exhibits similar features to those known in percolation models. Campi's studies [2, 14] on conditional moments of projectile fragments size distribution revealed that atomic nuclei break up as in finite size percolation model.

Stanley [15] first pointed out that the structure of percolation clusters can be well described by the fractal concept [16]. As in multifragmentation, nuclei break up like percolation clusters, there might be some possibility of fractality in projectile fragments mass distribution also. It is known that fractal geometry allows one to mathematically describe systems that are intrinsically irregular at all scale. The fact that a fractal structure has the property of self-similarity, that is, similar at all scales means that if one magnifies a small portion of it, this shows the same complexity as the entire system. The concept of fractal geometry of the object, in turn, is connected with the intermittency, a term borrowed from hydrodynamics of turbulent fluid flow [17-19] to mean random deviations from smooth or regular behavior [20].

Ploszajczak and Tucholski [21, 22] for the first time look for intermittency in the nuclear multifragmentation and percolation model. For that they had used the technique of scaled factorial moments (SFM), first introduced by Bialas and Peschanski [23, 24] to study the dynamical fluctuation in density distribution of particles produced in high-energy collisions. Ploszajczak and Tucholski [21, 22] had done similar analysis to look for intermittency in the mass and charge distribution of the fragments due to existence of non-statistical fluctuation in fragments size in heavy ion collision. Subsequently, different workers used this technique and intermittent behavior is found to follow by charge distribution in case of breakup of ^{238}U at 0.96A GeV [25-27], ^{131}Xe at 1.22A GeV [25], ^{84}Kr at 1.52A GeV [25] and ^{197}Au at 10.6A GeV [28]. In Ref. [21, 22, 25-27] no clear evidence of critical behavior could be observed due to absence of a minimum in λ_q at $q = q_c$, λ_q is a parameter related to intermittency indices. Cherry et al., [28] from the dependence of anomalous fractal dimension on the order of the moments opined that multifragmentation of gold follow a sequential decay rather than prompt decay mechanism. On the other hand there are other experimental evidences that indicate that multifragmentation of Au is manifestation of a continuous phase transition [3, 5, 29, 30]. Clearly the results obtained from various experiments contradict one another.

In this paper an attempt has been made to describe inclusive charge (mass) yield data obtained from ^{84}Kr-Em interactions at 0.95A GeV in the light of intermittency. An attempt has also been made to study the data in terms of generalized fractal moments G_q and generalized fractal dimension D_q to get information about fractality, if any.

5.2. Mathematical Formulism

5.2.1. Scaled Factorial Moment Analysis

The average scaled factorial moments of order q, for a physical system can be expressed as [26, 31-33]

$$< F >_q = \frac{1}{< n >^q} < \frac{1}{M} \sum_{m=1}^{M} n_m (n_m - 1)...(n_m - q + 1) > \tag{5.1}$$

Where

$$n = \frac{1}{M} \sum_{m=1}^{M} n_m \tag{5.2}$$

and

$$< n >= \frac{1}{N_{ev}} \sum_{i=1}^{N_{ev}} n \tag{5.3}$$

Here N_{ev} is the total number of events in the data sample; n_m is the number of fragments in the m^{th} bin in the i^{th} event. M is the total number of bins in which the fragment charge interval Δs is divided into bins of equal width $\delta s = \Delta s / M$. n is the fragment multiplicity in the interval Δs. For non-flat fragment multiplicity distribution varying within a finite bin of width Δs introduces an extra M-dependent correction factor R_q which can be given by

$$R_q = \frac{1}{M} \sum_{m=1}^{M} \frac{M^q < n_m >^q}{< n >^q} \tag{5.4}$$

Thus, $<F_q>/R_q = <F_q>_c$ measures the contribution of dynamical fluctuations. In doing so, one must be careful in selecting the smallest bin, which must not be smaller than the resolution of the detector [34]. If self-similar fluctuations exist at all scales δs, the corrected factorial moment of the order q is given by $< F_q >_c = (\Delta s / \delta s)^{\phi_q}$. The exponent ϕ_q is the slope characterizing a linear rise of $\ln<F_q>_c$ with $-\ln \delta s$ for all bins of width δs. ϕ_q increases with increasing

order q of the moment; however, for a random uncorrelated particle production, $\ln\langle F_q\rangle_c$ should be flat for all values of q when plotted against $-\ln \delta s$ giving $\phi_q = 0$ [26].

It has been reported by A. Bialas and K. Zalewski [35, 36] that the intermittent behavior in the final state of multiparticle production in the heavy-ion collision may be a projection of non-thermal phase transition believed to occur during the evolution of the collision that in turn would be responsible for the occurrence of anomalous events. If a non-thermal phase transition really occurs, then

$$\lambda_q = \frac{(\phi_q + 1)}{q} \tag{5.5}$$

is predicted to have a minimum value at some value of $q = q_c$, where q_c need not necessarily be an integer. The region satisfying the condition $q < q_c$ is dominated by many small fluctuations whereas the region $q > q_c$ contains rarely occurring large fluctuations.

In the calculation of SFM, if the width of the bin is of the order of unit charge, then the division of the fragment charge interval Δs with this resolution may results in some empty bins. These empty bins act as the holes in the charge distribution and constitute with the set of non-empty bins one of the fractal sets of the fractal structure of the distribution spectrum. It was Lipa and Bushbeck [37] who have correlated the scaling behavior of the factorial moments to the physics of fractal and multifractal objects through the relation

$$d_q = \frac{\phi_q}{(q-1)}. \tag{5.6}$$

d_q is called the anomalous dimension and is used for the description of the fractal objects. The order independence of d_q indicates monofractal behavior,

whereas an increase of d_q with q indicates the multifractal behavior of emission spectrum [32, 33].

5.2.2. Generalized Moment Analysis

According to Bialas and Peschanski [23], the power law behavior of the factorial moments F_q with decreasing phase space interval size signals the onset of intermittent behavior. Such a power law is characteristics of scale invariant dynamics. It was speculated that the intermittent type of nonstatistical self-similar fluctuation of produced particles at all scales might be a manifestation of quark-gluon plasma phase transition [38-42]. There were other published experimental data also which tried to explain this power law behavior as the self-similar random cascading mechanism [43], formation of jets and minijets [44], Bose-Einstein interference [45], conventional short-range correlation [46], etc., but none of them are accepted universally. Different data sets prefer different explanation. The theoretical interpretation was not clear [47]. Hwa [48] then found that F_q are not the optimal moments to investigate and then proposed an alternative set of moments G_q, which are far more direct in exhibiting an order in the seemingly random fluctuations in the rapidity distributions. The generalized moments G_q for produced particle in high-energy collisions are defined as [48, 49]

$$G_q = \sum_{m=1}^{M} \left(\frac{n_m}{n} \right)^q \tag{5.7}$$

and

$$\langle G_q \rangle = \frac{1}{N_{ev}} \sum_{1}^{N} G_q \tag{5.8}$$

where n is the total number of particles in the event. Here, unlike SFM, q can have any positive or negative integral or nonintegral values.

However for low multiplicity event G_q moments are found to be dominated by the statistical fluctuation. Later on to filter out the dynamical fluctuation in low multiplicity event, Hwa and Pan [50] proposed a modified G_q moment in terms of step function for q = 1, 2, ..., which can be defined as

$$G_q = \sum_{m=1}^{M} \left(\frac{n_m}{n} \right)^q \theta(n_m - q) \tag{5.9}$$

where $\theta(n_m - q)$ is a step function defined as

$\theta(n_m - q) = 1$, for $n_m \geq q$

0, for $n_m < q$

Thus for $n_m > q$, modified G_q moment is nothing but the generalized moment G_q. The step function minimizes the statistical noise by excluding the empty bins for low multiplicity events. Now if one applies the same concept in charge distribution of projectile fragments also, then according to the theory, if the charge distributions have fractal structure, the G_q moment should follow a power law i.e.

$$< G_q > \propto (\delta s)^{\tau_q} \tag{5.10}$$

where τ_q is fractal index or mass exponent. From the linear dependence of $\ln<G_q>$ on $\ln \delta s$, τ_q can be calculated as

$$\tau_q = \lim_{\delta s \to 0} \frac{\Delta \ln \langle G_q \rangle}{\Delta \ln(\delta s)}. \tag{5.11}$$

Since G_q of Eq. (5.9) contains contribution from both statistical as well as dynamical components, it is therefore necessary to extract the dynamical information from the mixture of the two. To calculate the statistical contribution to $<G_q>$, equal numbers of events are generated by random number generator

lying within 1 to 36 as the charge of PFs [32]. $<G_q^{stat}>$ is then calculated for uncorrelated projectile fragments in randomly generated events. The dynamical part of $<G_q>$ can be determined from [51]

$$< G_q >^{dyn} = \frac{< G_q >}{< G_q >^{stat}} (\delta s)^{q-1} \tag{5.12}$$

If all the G_q factor follow the power law behavior with δs then their respective exponent can be related as

$$\tau_q^{dyn} = \tau_q - \tau_q^{stat} + q - 1 \tag{5.13}$$

Clearly any deviation of τ_q^{dyn} from q - 1 is the deviation of τ_q from τ_q^{stat} giving the dynamical contribution to τ_q.

Information about multifractality can also be obtained from the study of spectral function $f(\alpha_q)$. It can be calculated using multifractal theory [52-54] from fractal index by Legendre transformation as follows:

$$f(\alpha_q) = q\alpha_q - \tau_q,\ \alpha_q = d\tau_q/dq \tag{5.14}$$

α_q is known as Lipschitz-Holder exponents [55].

The spectral function is a smooth function, concave downwards with its maximum at $\alpha_{q=0}$ for multifractal structure. $f(\alpha_q)$ gives a quantitative description of the fluctuation of density in both the dense and sparse regions in rapidity space corresponding to the $\alpha_q < \alpha_0$ and $\alpha_q > \alpha_0$ regions of the plot of the function [49].

The width of the distribution determines inhomogeneity of the distribution. The non-existence of a sharp peak in $f(\alpha_q)$ versus α_q plot at α_q corresponding to q = 0 reveals non-smooth nature of the distribution [48, 56].

One of the most basic properties of the fractals, which describe the scaling behavior, is the generalized dimensions D_q, introduced by Hentschel and Procaccia [57]. τ_q is related to the generalized dimension D_q through the relation

$$D_q^{dyn} = \frac{\tau_q^{dyn}}{q-1} \tag{5.15}$$

Here, D_0 is the fractal dimension, D_1 is the information dimension and D_2 is the correlation dimension [48, 52, 58]. If D_q decreases with increase of q, the emission pattern is said to be multifractal. On the other hand, if D_q remains constant, then the emission pattern is referred to as monofractal [57, 59].

5.3. Results and Discussion

5.3.1. Intermittency

Variations of $\ln\langle F_q\rangle_c$ against -ln δs for different orders of moments are shown in Fig. 5.1. It can be readily seen from this plot that the moments for the fragment multiplicity distribution increase according to power law with decreasing bin width δs, thereby indicating that the PF charge (mass) distribution follow an intermittent pattern with the size of the projectile fragments emitted from Kr-Em interactions. The errors shown in this plot are standard deviations and the straight lines drawn are the best fitted lines for the respective set of data points. The different values of intermittency indices ϕ_q along with the correlation coefficient R for the present work and the values reported by earlier workers are listed in table 5.1.

Thus the increasing values of $\ln\langle F_q\rangle$ with –ln δs suggest an intermittent behavior followed by the PF charge (mass) distribution. Earlier Cherry et al. [28] reported that intermittency is stronger for lower energy. From the above table it could be readily seen that the values of intermittency indices that characterizes the strength of intermittency effect, show a strong dependence on projectile mass also and this variation of ϕ_q with q is shown in Fig. 5.2. From this plot it is

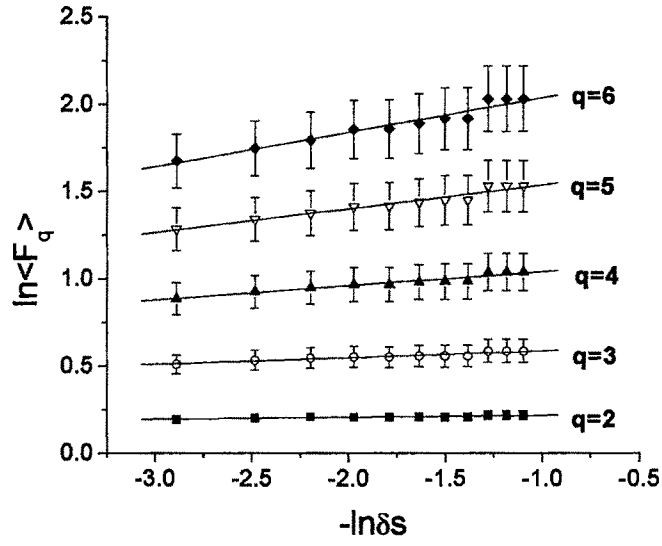

Fig. 5.1: Variations of $\ln\langle F_q\rangle_c$ with -ln δs for different orders of moment q. Solid lines are the best fitted lines.

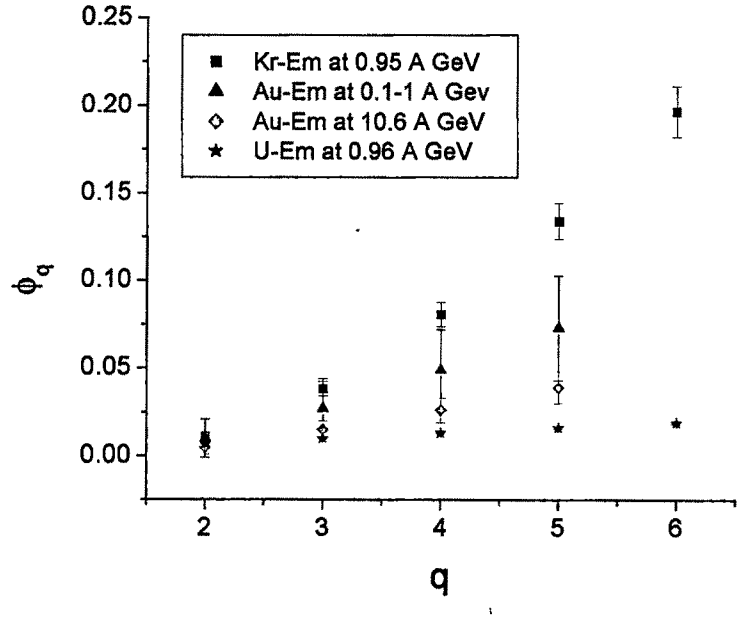

Fig. 5.2: Variation of ϕ_q with q.

observed that intermittency become stronger with the decrease of the projectile mass.

Table 5.1: Values of ϕ_q along with R for LFT for different orders of moment.

System	Energy A GeV	ϕ_2 (R)	ϕ_3 (R)	ϕ_4 (R)	ϕ_5 (R)	ϕ_6 (R)	Ref
Kr-Em	0.95	0.011 ± 0.002 (0.892)	0.038 ± 0.004 (0.949)	0.081 ± 0.007 (0.968)	0.134 ± 0.010 (0.974)	0.196 ± 0.014 (0.976)	P. W.
Au + Em	0.1-1	0.010 ± 0.011	0.027 ± 0.017	0.049 ± 0.023	0.073 ± 0.030	--	28
Au + Em	10.6	0.005 ± 0.004	0.015 ± 0.005	0.026 ± 0.007	0.039 ± 0.009	--	28
U + Em (0.29<m< 0.87)	0.96	0.0068 ± 0.0002	0.0102 ± 0.0003	0.0133 ± 0.0004	0.0163 ± 0.0006	0.0191 ± 0.0006	26

Fig. 5.3 shows the variation of λ_q against the various order of moment q for the present study along with the results obtained from Au [28] and U [26] projectiles. From the figure it is seen that for all the three beams, λ_q decreases exponentially without any minimum value contradicting the prediction for non-thermal phase transition in fragmentation of the beams.

In Fig. 5.4, the variations of anomalous dimension d_q with the order of the moment q are shown for the charge distribution of projectile fragments and compared with the results calculated from the reported result of other workers

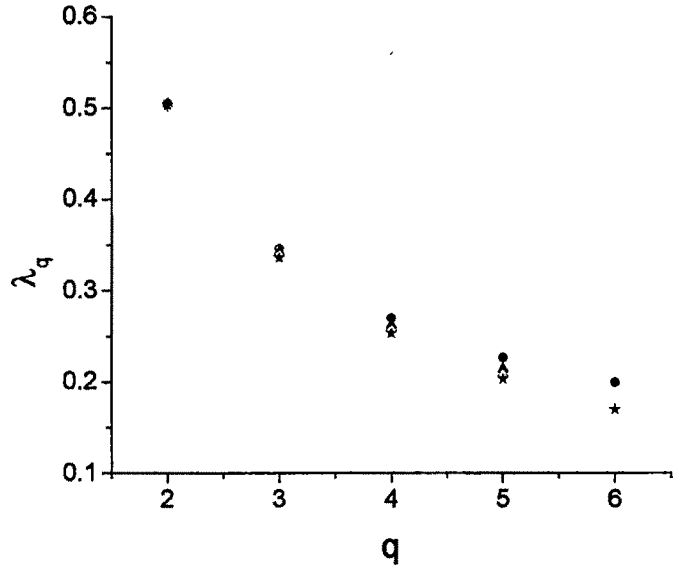

Fig. 5.3: Variation of λ_q with q. Different symbols are for Kr-Em at 0.95A GeV (magenta), Au-Em at 0.1-1A GeV (red), Au-Em at 10.6A GeV (green) and U-Em at 0.96A GeV (blue) respectively.

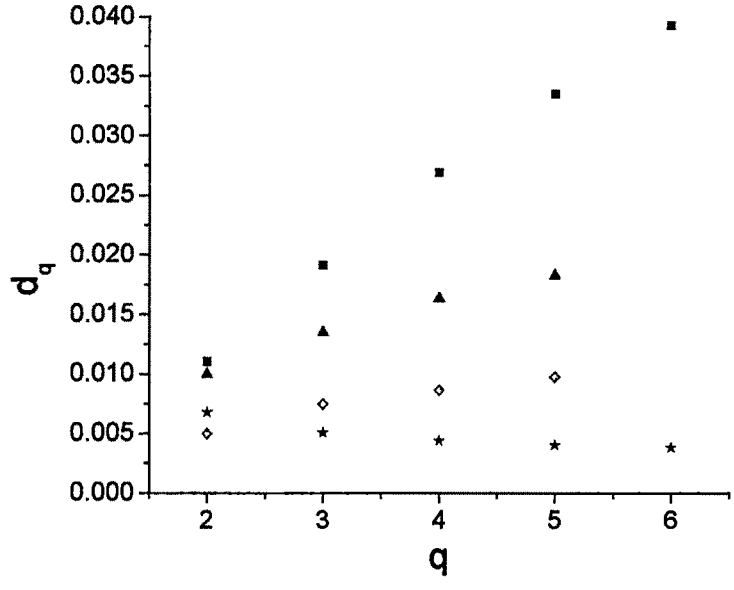

Fig. 5.4: Variation of anomalous dimension d_q with the order of the moments q. Different symbols represent the same set of data as mentioned in the caption of Fig. 5.3.

[26, 28]. The order dependence of anomalous dimension for Kr and Au beam can readily be seen from Fig. 5.4 thereby indicating the multifractal nature of the PF size distribution. For U-Em at 0.96A GeV data, a slight decrease in d_q values could be observed with the increase of order of moment q. The dependence is stronger in case of lighter projectile. From the figure the effect of energy is also clearly visible. For Au beam with the decrease of energy from 10.6A GeV to 0.1-1A GeV, dependence of d_q becomes stronger.

5.3.2. Fractality

It has now been realized from the above study that projectile fragmentation exhibits self-similarity & intermittency. Study of anomalous dimension gives a hint of multifractality. To study multifractality and self-similarity in more details in multiparticle production, Hwa [48] for the first time gave the idea of estimation of multifractal moments, G_q.

Now to inspect the dependence of $\langle G_q \rangle$ on δs for the experimental set of data, in Fig. 5.5, $\ln\langle G_q \rangle$ is plotted against $-\ln \delta s$ for the order of the moments q having integral values only. By definition, in both the methods, $G_1 = 1$. Therefore, to calculate G_q moments for $q \geq 2$, Eq. (5.9) is used.

The variation of $\ln\langle G_q^{stat} \rangle$ caculated for uncorrelated projectile fragments in randomly generated events is also shown in Fig. 5.5. From this figure, for a particular order of moment q, a significant difference could easily be seen between the experimental and random sets of data. The slopes of the straight line fit of the respective data points from -2.9 to -1.8, both for experimental and generated events, give the fractal indices τ_q and τ_q^{st}. In Fig. 5.6 the variations of these mass exponents namely with q are shown. It is clearly seen that τ_q^{dyn} varies

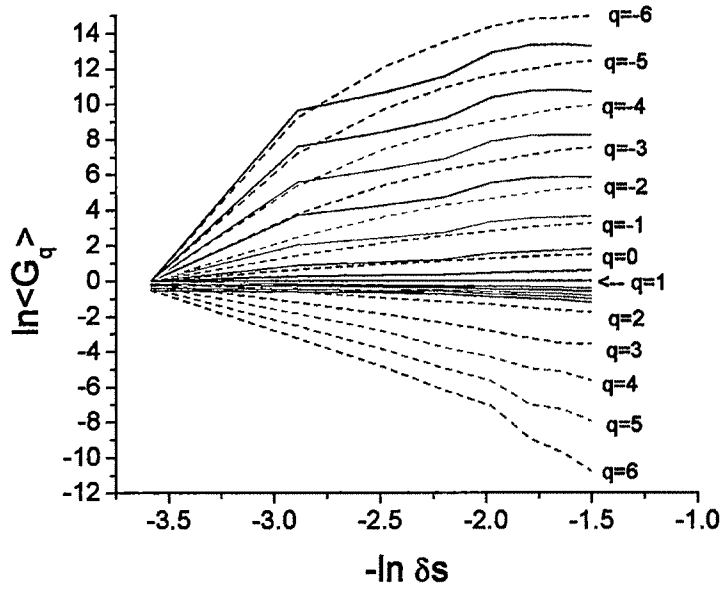

Fig. 5.5: Variation of ln<G_q> with –ln δs for Kr beam. For the same order of moment experimental (solid lines) and random (dash lines) values are represent by the same colour.

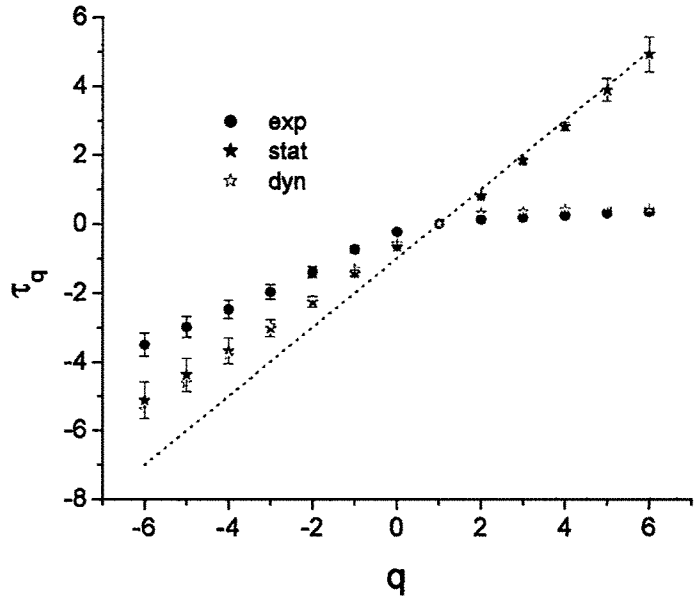

Fig. 5.6: Variation of τ_q with different moments. Dotted line is for (q - 1).

significantly from q - 1 indicating the presence of dynamical fluctuation. It is also clear from the figure that τ_q and τ_q^{dyn} almost saturated for positive values of q.

In Fig. 5.7, the variation of the spectral function $f(\alpha_q)$ as a function of the Lipschitz–Holder exponent, α_q is shown. From the figure it is readily evident that the spectra is concave downwards centered on α_q corresponding to q = 0. However, non exhibition of a pronounced peak by $f(\alpha_q)$ indicate a non-smooth nature of the charge (mass) distribution of the PFs emitted in the interactions of the present investigation.

The values of generalized dimensions D_q for various values of q have been estimated using Eq. (5.15) and their variations with different order of moments q equal to -6 to +6 are shown in Fig. 5.8. It is observed from the figure that D_q^{dyn} gradually decreases with the increase of q indicating the presence of multifractality. For Kr projectile, it is found that the values of generalized dimension are always less than 1. Jain et al. [60] have observed similar pattern of variation of D_q in η and φ phase spaces for Kr-Em interactions at 1.52A GeV, along with U-Em and Fe-Em interactions at 0.96A GeV and 2.1A GeV respectively.

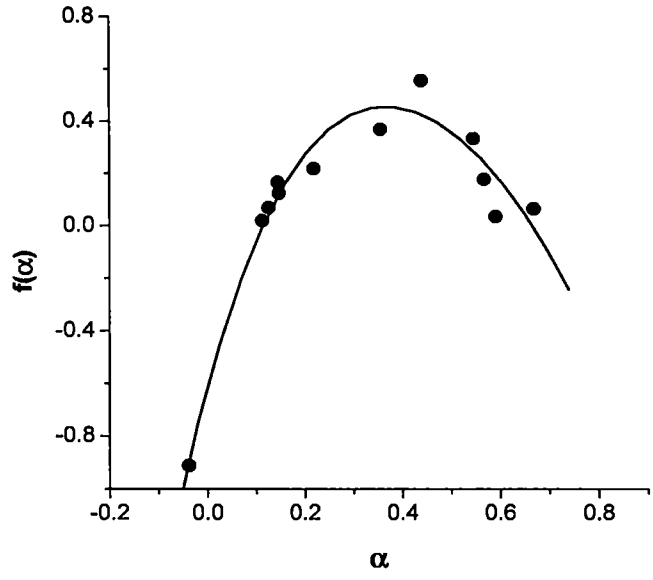

Fig. 5.7: Variation of f(α_q) with α_q.

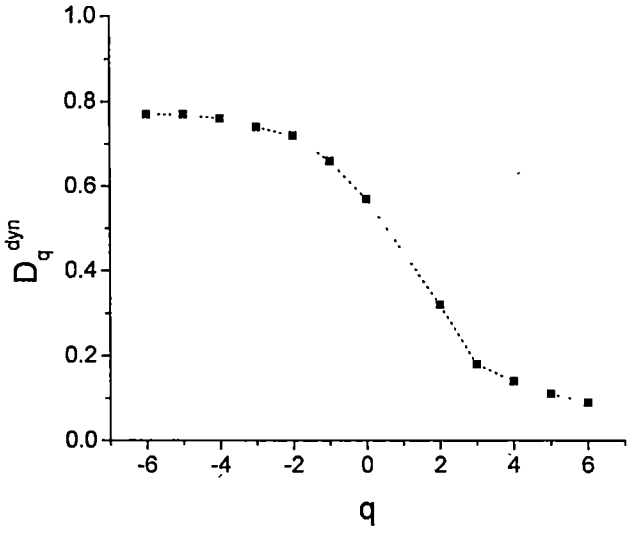

Fig. 5.8: Variation of D_q^{dyn} with q.

References

[1] W. Bauer, Phys. Rev. C **38**, 1297 (1988).

[2] X. Campi, Phys. Lett. B **208**, 351 (1988).

[3] B. K. Srivastava *et al.*, Phys. Rev. C **65**, 054617 (2002).

[4] M. L. Gilkes *et al.*, Phys. Rev. Lett. **73**, 1590 (1994).

[5] J. B. Elliott *et al.*, Phys. Rev. C **62**, 064603 (2000).

[6] J. B. Elliott *et al.*, Phys. Rev. Lett. **88**, 042701 (2002).

[7] M. L. Cherry *et al.*, Phys. Rev. C **52**, 2652 (1995).

[8] D. Kudzia *et al.*, Phys. Rev. C **68**, 054903 (2003).

[9] B. Bhattacharjee and B. Debnath, Nucl. Phys. A **829**, 210 (2009).

[10] D. Stauffer, Phys. Rep. **54**, 1 (1979).

[11] W. Baur *et al.*, Nucl. Phys. A **452**, 699 (1896).

[12] W. Baur *et al.*, Phys. Rev. Lett. **58**, 863 (1987).

[13] J. Desbois, Nucl. Phys. A **466**, 724 (1987).

[14] X. Campi, J. Phys. A **19**, 917 (1986).

[15] H. E. Stanley, J. Phys. A **10**, L211 (1977).

[16] B. Mandelbrot, *Fractals: Form, Chance and Dimension* (Freeman, San Francisco 1977).

[17] B. Mandelbrot, J. Fluid Mech., **62**, 331 (1974).

[18] U. Frisch *et al.*, J. Fluid. Mech., **87**, 719 (1978).

[19] S. Lovejoy and D. Schertzer, *Proc. Conf. on Turbulent Shear Flows, eds. L. J. S. Bradbury et al.,* Vol. **4** (Springer, Berlin 1984).

[20] H. Satz, CERN-TH 5312/89, March (1989).

[21] M. Płoszajczak and A. Tucholski, Phys. Rev. Lett. **65**, 1539 (1990).

[22] M. Płoszajczak and A. Tucholski, Nucl. Phys. A **523**, 651 (1991).

[23] A. Bialas and R. Peschanski, Nucl. Phys. B **273**, 703 (1986).

[24] A. Bialas and R. Peschanski, Nucl. Phys. B **308**, 857 (1988).

[25] P. L. Jain *et al.*, Phys. Rev. C **47(1)**, 342 (1993).

[26] P. L. Jain *et al.*, Phys. Rev. Lett. **68(11)**, 1656 (1992).

[27] G. Singh *et al.*, Mod. Phys. Lett. A **7**, 1113 (1992).

[28] M. L. Cherry *et al.*, Phys. Rev. C **53(4)**, 1532 (1996).

[29] B. K. Srivastava *et al.*, Phys. Rev. C **64**, R041605 (2001).

[30] B. K. Srivastava (EOS Collaboration), Pramana J. Phys. **57(2 & 3)**, 301 (2001).

[31] B. Bhattacharjee *et al.*, Ind. J. Phys. **81(7)**, 717 (2007).

[32] B. Bhattacharjee and S. Sengupta, Int. J. Mod. Phys. E **14**, 1223 (2005).

[33] B. Bhattacharjee, Nucl. Phys. A **748**, 641 (2005).

[34] P. L. Jain and G. Singh, Phys. Rev. C **44**, 854 (1991) and references therein.

[35] A. Bialas and K. Zalewski, Phys. Lett. B **238**, 413 (1990).

[36] A. Bialas and K. Zalewski, Nucl Phys., B **237**, 65 (1989).

[37] P. Lipa and B. Buschbeck, Phys. Lett. B **223**, 465 (1988).

[38] I. V. Ajinenko *et al.*, Phys. Lett. B **222**, 306 (1989).

[39] R. Holynski *et al.*, Phys. Rev. Lett. **62**, 733 (1989).

[40] K. Sengupta *et al.*, Phys. Lett. B **236**, 219 (1990).

[41] B. Bushbeck *et al.*, Phys. Lett. B **215**, 788 (1988).

[42] W. Braunschweig *et al.*, Phys. Lett. B **231**, 548 (1989).

[43] A. Bialas and R. C. Hwa, Phys. Lett. B **253**, 436 (1991).

[44] W. Ochs and J. Wosiek, Phys. Lett. B **214**, 617 (1988).

[45] P. Carruthers *et al.*, Phys. Lett. B **222**, 487 (1989).

[46] P. Carruthers and I. Sarcevic, Phys. Rev. Lett. **63**, 1562 (1989).

[47] D. Ghosh *et al.*, Phys. Rev. D **51(7)**, 3298 (1995).

[48] R. C. Hwa Phys. Rev. D **41**, 1456 (1990).

[49] C. B. Chiu and R. C. Hwa, Phys. Rev. D **43**, 100 (1991).

[50] R. C. Hwa and J. Pan Phys. Rev. D **45**, 1476 (1992).

[51] C. B. Chiu *et al.*, Mod. Phys. Lett. A **5**, 2651 (1990).

[52] P. Grassberger and I. Procaccia, Physica D **13**, 34 (1984).

[53] L. D. Landau and E. M. Lifshitz, Phys. Sz. Sowjet **6**, 244 (1934).

[54] L. D. Landau and E. M. Lifshitz, *Statistical Physics, Part I* (Pergamon, Oxford, 1980).

[55] E. A. De Wolf *et al.*, Phys. Rep. **270**, 1 (1996).

[56] D. Ghosh *et al.*, Phys Rev., D **46**, 3712 (1992).

[57] H. G. F. Hentschel and I. Procaccia, Physica D **8**, 435 (1983).

[58] G. Paladin and A. Vulpiani, Phys. Rep. **156**, 147 (1987).

[59] N. Prashar, IL Nuovo Cim. A **108**, 489 (1995).

[60] P. L. Jain *et al.*, Nucl. Phys. A **561**, 651 (1993).

Chapter VI

Summary

Present work dealt with the systematic study on projectile fragmentation in ^{84}Kr-Em interactions at 0.95A GeV.

From the current investigation, the mean multiplicities of produced particles as well as the other charged secondaries emitted from the target spectator are found to be $\langle n_s \rangle = 10.73 \pm 0.69$, $\langle n_g \rangle = 8.18 \pm 0.52$ and $\langle n_b \rangle = 4.65 \pm 0.29$. The multiplicity distribution of produced particles shows good agreement with that of FRITIOF generated data. For knocked out proton, except for higher multiplicity region, the experimental values are more or less in agreement with the results predicted by the FRITIOF model. Whereas, multiplicity distribution of target associated slow particles doesn't agree well with the model prediction. Multiplicity distribution of projectile fragments shows that $Z_{PF} = 1 - 3$ contribute about 90% of all PFs.

A positive linear correlation could be observed between the sum total charge Q_{PF} of the various PFs and the average number of produced & heavy ionizing particles that are generally taken as a measure of degree of centrality of the collision. The correlation coefficient in either case is found to be more than 0.9.

Charge distributions of various projectile fragments emitted from different targets of emulsion indicate that light projectile fragments are most copious irrespective of target mass. Heavy PFs are emitted more often from collision of the lower target mass system. Mean multiplicities of protons, alpha particles and heavy fragments emitted from ^{84}Kr-Em interactions are found to be $n_p = 3.77 \pm 0.09$, $n_\alpha = 2.2 \pm 0.09$ and $n_f = 1.9 \pm 0.07$. When the various PFs are studied in the light of KNO scaling, it is found that all the PFs having charge $Z_{PF} = 1, 2 \,\&\, \geq 3$ emitted from Kr-Em interactions pursue the same universal KNO scaling of the

type $\psi(z) = az\exp(-bz)$ with z = n/<n_z> and ψ(z) = <n_z>P(n_z). Here n, <n_z> and P(n_z) are the multiplicity, mean multiplicity and normalized multiplicity of PFs respectively. a and b are constant. C_q moments of different orders are calculated for protons, alpha particles and heavy fragments and for helium it is found to be energy independent. Studies on intermediate mass fragments with respect to mass of the fragmenting system, Z_b reveal the general pattern of the universal 'rise and fall'.

Charge distribution spectrum of projectiles emitted from Kr-Em interactions is found to follow a power law indicating the relevance of analyzing the gathered data in the light of criticality and a possible liquid-gas phase transition. To test the sensitivity of traditionally accepted signature of critical behavior, a 'toy model' of nuclear multifragmentation has been developed following the algorithm as suggested by EOS collaboration. However, the toy model of the present investigation is different from that of EOS one in the sense that in the present investigation the mass conservation has been violated to account for the pre-equilibrium emission. A number of traditionally accepted signatures of critical behavior that have been considered to be insensitive by EOS group are rather found to be sensitive when compared with the result of toy model of this work. From the present investigation on Kr–Em interactions at 0.95A GeV and a comparison of the results with Au–C at about same energy, it is seen that the distribution of 2nd charge moments and conditional moment depend on the sizes of the projectiles. The maximum values of these moments are found to be large for the larger projectile system as is the case for a lattice with larger volume. It is further seen from present and EOS generated data that, depending upon the different algorithm followed in regards to the random partitioning, the total number of system's constituents, a number of charge moments and the

corresponding conditional moments vary differently with the variation of the control parameter. These observed differences in the variation of charge and conditional moments are attributed to the different degree of mass conservation constraint of the two toy models. Fluctuations in the size of the largest cluster and particularly two distinct regions in the scattered plot of 2^{nd} charge moments clearly suggests that the present experimental sample may present the bimodality signal which is a significative observable of (first order) phase transition. Work on bimodality with current set of data will be carried out in separate study. Nevertheless, the present investigation on the fragmentation of Kr-projectile with emulsion nuclei shows clear evidences of critical behavior and liquid gas phase transition. By estimating a higher order moment, which is related to skewness, a complete set of values of exponents γ , β and τ could be found out that follow the respective scaling behavior $3\beta + 2\gamma = \tau(\gamma + \beta)$ with the present set of experimental data. In this work, these values of γ , β and τ are respectively found to be 1.34 ± 0.19, 0.54 ± 0.15 and 2.31 ± 0.06. However, this investigation remains inconclusive in fixing the order of phase transition as the presence of thermodynamically consistent critical exponents is merely a signal of phase transition but does not allow to fix the order of the transition due to the fact that because of finite size effect, critical exponents can be found also within the coexistence region of a first order transition.

The scaled factorial moment (SFM) analysis of projectile fragments exhibits a power law behavior with decreasing bin width for various orders of the moments q = 2 - 6. Exhibition of power law indicates intermittent pattern of emission of PFs from Kr-Em interaction of present investigation. The different

values of the exponent ϕ_q, called intermittency indices are found to increase with the order of moments.

At $q = q_c$, absence of any minimum value in λ_q, a parameter related to intermittency indices, does not support the prediction for non thermal phase transition in the fragmentation of Kr beam.

The anomalous dimension d_q increases linearly with the order of the moments 'q' thereby signifying the multifractal structure of the PF size distribution.

To make a more detailed investigation on the fractal behavior of the charge distribution, the G_q moments have been evaluated for various projectile fragments. Generalized moments, $\langle G_q \rangle$ shows a power law dependence on bin size thus indicating self-similarity in the size of the projectile fragments. The fractal indices τ_q and τ_q^{st} for the experimental data points and generated events respectively are obtained from the slopes of the best fitted lines. A clear deviation of τ_q^{dyn} from q - 1 as obtained for the present experimental data indicates that $\langle G_q \rangle$ contains dynamical information.

Non exhibition of sharp peak by the spectral function, $f(\alpha_q)$ point out the non smooth nature of the charge distribution.

The generalized dimension D_q characterizing the self-similarity of fractal have been estimated for different order of moments and their variations for q = -6 to +6 show that D_q decreases with the increase of q. This is considered to be a signature of the association of multifractality in the size of the projectile fragments emitted in ^{84}Kr-Em interactions at energy of 0.95 GeV/A.

List of Publication

1. List of Publication in Journal

i. B. Bhattacharjee, **B. Debnath,** A. Mukhopadhyay and S. Sengupta, "Erraticity moment of bin multiplicity & rapidity gap of fast TFs from ^{84}Kr-AgBr interaction at 0.95A GeV/c", **Indian J. of Phys. 81(7)**, 1-10, 2007.

ii. **B. Debnath**, R. Talukdar and B. Bhattacharjee, "Emission characteristics of intermediate mass fragments on the residual part of the projectile nucleus", **Indian J. of Phys. 82(5)**, 633, 2008.

iii. B. Bhattacharjee, **B. Debnath** and S. Sengupta, "Effect of collision geometry on the multiplicity of secondary charged particles emitted from ^{84}Kr-AgBr interactions at 950 MeV/A", **Indian J. of Phys. 82(6)**, 734, 2008.

iv. B. Bhattacharjee and **B. Debnath**, "Variation of mean multiplicity of intermediate mass fragments with the bound charge of the fragmenting system-Deviation from the universal behaviour", **IoP, Journal of Physics: CS 110**, 122003, 2008.

v. B. Bhattacharjee and **B. Debnath,** "Evidence of phase transition in the break up of Kr-projectile nuclei at 0.95A GeV", **Nucl. Phys. A 829**, 210, 2009.

2. List of Publication in Proceedings of Conference, Symposia etc.

i. B. Bhattacharjee, G. Patwari and **B. Debnath,** "Erraticity of rapidity gap analysis for fast protons emitted from ^{84}Kr-AgBr interaction at 0.95 GeV/A", **Proceedings of DAE-BRNS symposium on Nuclear Physics** held at BARC, Mumbai during 12-16 Dec., 2005.

ii. B. Bhattacharjee and **B. Debnath,** "Observation of scaling behavior of fast helium fragments emitted at the SIS energy", **Proceedings of DAE-BRNS symposium on Nuclear Physics** held at MSU, Baroda during 11-15 Dec., 2006.

iii. **B. Debnath** and B. Bhattacharjee, "Estimation of critical exponents of lattice percolation model for ^{84}Kr-Em interactions at 0.95 GeV/A", **Proceedings of DAE-BRNS symposium on Nuclear Physics** held at IIT, Roorkee during 22-26 Dec., 2008.

School / Workshop / Conference attended

i. DAE-BRNS symposium on Nuclear Physics held at BARC, Mumbai during 12-16 Dec., 2005.
ii. QGP Meet'06 and IWLSC at VECC Kolkata during 5-10 Feb. 2006.
iii. Workshop on Simulation Techniques in Physics at Aligarh Muslim University during 19-25 March, 2006.
iv. DAE-BRNS symposium on Nuclear Physics held at MSU, Baroda during 11-15 Dec., 2006.
v. VI SERC school on experimental HEP held at Jammu University during 5-25 Feb., 2007.
vi. 5th conference of Physics Academy of the North East held at Gauhati University, Guwahati during 1-2 March, 2007.
vii. Advanced School on QGP held at IIT, Mumbai during 3-13 July, 2007.
viii. QGP Winter School 2008 held at Jaipur during 1-3 Feb., 2008.
ix. 20th International Conference on Ultra-Relativistic Nucleus Nucleus collisions held at Jaipur during 4-10 Feb., 2008.
x. Workshop on High Energy Physics: Particle Physics, Strings and Cosmology held at IIT, Guwahati during 21-23 February 2008.
xi. QGP Meet'08 at VECC Kolkata during 25-27 Nov. 2008.
xii. National workshop on simulation & data analysis techniques for high energy cosmic ray experiments held at Dept. of Physics, Gauhati University, Guwahati during 23-25 March 2009.

Erraticity moment of bin multiplicity and rapidity gap of fast TFs from ^{84}Kr-Ag/Br interaction at 0.95A GeV/c

B Bhattacharjee*, B Debnath, A Mukhopadhyay[1] and S Sengupta

Department of Physics, Gauhati University, Guwahati-781 014, Assam, India
[1]Department of Physics, North Bengal University, Siliguri-734 430, West Bengal, India

E-mail : bb_22@rediffmail.com

Received 19 December 2006, accepted 6 July 2007

Abstract : Here we report the emission characteristics of spatial distribution of target associated fast particles from ^{84}Kr-Ag/Br interaction at 0.95A GeV. The erraticity analysis of bin multiplicity of knocked out protons confirms a power law behavior of the form $C_{p,q} \propto M^{\psi_q(p)}$. The $\psi_q(p)$ are found to have non zero values confirming erratic behavior of spatial pattern. To further characterise the spatial pattern of emitted fast particles, erraticity moments of rapidity gap between the tracks have also been estimated. The entropy like quantity S_q are found to differ significantly from 1 thereby confirming again the erratic behavior of target associated fast particles. Due to low averaged muliplicity, the conclusions drawn from gap analysis are found to be more convincing than those from erraticity analysis of bin multiplicity.

Keywords : Nucleus-nucleus collision, scaled factorial moment, erraticity, rapidity gap.

PACS Nos. : 25.75-q, 25.70.Pq, 13 85.Hd

1. Introduction

Unusually large local fluctuations observed in the density distribution of charged particles produced in a few JACEE events [1] lead Bialas and Peschanski [2] to device a mechanism to filter out the dynamical part of such fluctuations from the corresponding statistical component. For this purpose they introduced a set of multiplicity moments called the scaled factorial moments (SFM), denoted the q-th order of such moments by F_q, and observed that these moments scale with diminishing phase space interval (bin) size obeying a power law. Taking a clue from the turbulence in hydrodynamics, they coined the term 'intermittency' for such a scaling behavior, and since its introduction the phenomenon has been verified in different types of high-energy interactions [3]. It is, however, to be noted that most of these investigations to study

*Corresponding Author

Indian J. Phys. **82** (5), 633-638 (2008)

Emission characteristics of intermediate mass fragments on the residual part of the projectile nucleus

B Debnath, R Talukdar and B Bhattacharjee*

Department of Physics, Gauhati University,
Guwahati-781 014, Assam, India

E-mail . bb_22@rediffmail com

Abstract : In the study of projectile multifragmentation, a number of properties such as multiplicities, energy of fragments etc. of the emitted intermediate mass fragments (IMFs) are found to vary significantly with Z_b, where Z_b is a measure of the mass of the fragmenting system. In this work we report the variation of $<N_{IMF}>$ with Z_b for 950 MeV/A ^{84}Kr interactions with different targets of photonuclear emulsion. The maximum value of $<N_{IMF}>$ has been found to vary systematically with the target mass. Further, from this study it has been observed that $<Z_b>$ is linearly correlated with the number of emitted projectile protons (N_p) for the studied interactions.

Keywords : Nucleus-nucleus collision, multifragmentation, intermediate mass fragments

PACS Nos. : 25.75.-q; 25 70.Pq ; 13 85.Hd

1. Introduction

In projectile multifragmentation process, a projectile spectator, on excitation, splits into several pieces of intermediate mass fragments (IMFs) which span the mass-range between alpha particle and fission fragments. It is believed that studies on the decay of such excited nuclear systems may provide information about the nuclear collision dynamics. The sum of all projectile fragments (PFs) with charge $Z = 2$, which is also known as bound charge Z_b, gives the measure of the mass of the fragmenting system [1]. Correlation between average number of IMFs and the mass of the fragmenting system is one of the most interesting aspects of studying projectile multifragmentation. For a given collision system, the magnitude of Z_b is independent of the beam energy and is also taken as a measure of the degree of centrality of the collision [2,3]. On the other hand, when the variation of $<N_{IMF}>$ is studied with Z_b for a given projectile, in reactions with the lighter targets, the maximum value of the mean multiplicities of IMFs depend on the bombarding

* Corresponding Author

Indian J Phys. 82 (6), 735-740 (2008)

Effect of collision geometry on the multiplicity of secondary charged particles emitted from ^{84}Kr-AgBr interactions at 950 MeV/A

B Bhattacharjee*, B Debnath and S Sengupta

Department of Physics, Gauhati University, Guwahati-781 014, Assam, India

E-mail bb_22@rediffmail com

Abstract . The total charge of the projectile spectator fragments, Q_{PF} is taken as a measure of the degree of centrality of the collision thus defining the collision geometry The mean multiplicities of different charged secondaries emitted in the interactions of ^{84}Kr-AgBr nuclei at 950 MeV/A have been investigated as a function of the total charge Q_{PF} of the projectile spectator fragments. It has been observed that the average number of produced particles decreases exponentially with the increase of Q_{PF}. In case of target associated fast particles, the average number is found to decrease linearly with the increase of Q_{PF}.

Keywords : Nucleus-nucleus collision, Collision geometry, multiplicity

PACS Nos. · 25 75.-q, 25.70.Pq, 13 85.Hd

1. Introduction

The number of particles produced in an interaction, called particle multiplicity is considered to be an important parameter in the studies of high energy hadron-nucleus and nucleus-nucleus interactions, because such studies is expected to yield significant information about the dynamics of such interactions. The studies on multiplicity is also important from the point of view that this parameter can help us to check the predictions of different phenomenological and theoretical models used to describe high energy nuclear collision [1]. Particle multiplicity is often used as an important tool for understanding the multiparticle production mechanism and the nuclear fragmentation process and also for investigating the correlation between the two processes.

According to the participant-spectator model [2-4], the overlapping region of nuclear volumes of two colliding nuclei is called the participant part. The remaining parts of projectile

* Corresponding Author

The 2007 Europhysics Conference on High Energy Physics IOP Publishing
Journal of Physics: Conference Series 110 (2008) 122003 doi:10.1088/1742-6596/110/2/122003

Variation of mean multiplicity of intermediate mass fragments with the bound charge of the fragmenting system-deviation from the universal behaviour

B Bhattacharjee and B Debnath
Department of Physics, Gauhati University, Guwahati-781014, India
E-mail: bb_22@rediffmail.com

Abstract. In this work an attempt has been made to study the variation of normalized mean multiplicity with the normalized Z_b for 0.95A GeV $^{84}Kr - Em$ and $^{84}Kr - AgBr$ interactions. Though the data points of the present investigation exhibit the same pattern of the universal curve of ALADIN group, the maximum value of $< N_{IMF} >$ of the present investigation is found to be about 1.7 times larger than that of the universal curve.

1. Introduction

It is now almost an established fact that a projectile spectator, when excited up to its binding energy or beyond, often breaks up into several parts of intermediate mass fragments (IMF) with their masses lying between alpha particles and fission fragments. The phenomenon is known as multifragmentation. Correlation between mean multiplicity of IMF, $< N_{IMF} >$ and the mass of the fragmenting system, whose measure is so called bound charge Z_b, where $Z_b = \sum Z_{PF_i}$ with $Z_{PF_i} \geq 2$, is an aspect of projectile multifragmentation that has been studied thoroughly by a number of groups [1,2]. ALADIN [1,2] group has reported that the mean multiplicity $< N_{IMF} >$ of PFs were found to be same for all targets ranging from Beryllium to Lead and for all E/A ranging from 400 to 1000 MeV/A. Jain et al. [1] have reported similar results with various emulsion target. However, more $< N_{IMF} >$ were produced for larger projectile system. When both the variables (i.e., $< N_{IMF} >$ and Z_b) were normalized with the charge of projectile Z_p, the variation again follows a universal pattern losing its dependency on projectile mass. Thus an important feature of the multifragmentation decay of the excited projectile spectator nuclei is, therefore, believed to be the apparent absence of dynamical dependencies. ALADIN group, however, with their upgraded spectrometer reported that there might be a weak dependency of nuclear multifragmentation pattern on the bombarding energy [2]. The aim of the present work is to study the effect of mass of the fragmenting system on the fragmentation of the spectator part of the projectile nucleus for 0.95A GeV $^{84}Kr - Em$ and $^{84}Kr - AgBr$ interactions.

2. Experimental technique

NIKFI BR-2 photonuclear emulsion pellicles exposed horizontally at SIS of the GSI, Dramstadt, were used for present investigation. Charge of various PFs, confined at an angle $0.2/p_L$=0.122 radian, were identified by measuring (i) grain/blob density (ii) Hole density (iii) delta rays density (iv) track width measurements etc. [3].

Available online at www.sciencedirect.com

ScienceDirect

Nuclear Physics A 829 (2009) 210–233

NUCLEAR PHYSICS A

www.elsevier.com/locate/nuclphysa

Evidence of phase transition in the break up of Kr-projectile nuclei at 0.95*A* GeV

B. Bhattacharjee *, B. Debnath

Department of Physics, Gauhati University, Guwahati-781014, India

Received 27 January 2009; received in revised form 24 July 2009; accepted 24 July 2009

Available online 22 August 2009

Abstract

Projectile fragmentation mechanism and the possible liquid gas phase transition have been studied by extracting the critical exponents using cluster approximation technique. A 'toy model', schematically accounting for pre-equilibrium, has been developed and various moments as well as conditional moments have been evaluated with the data obtained from the toy model to see the effect of mass conservation constraint. An exponent δ, related to third order moment, has been evaluated to obtain a set of values of γ, β and τ that follow the corresponding scaling relation. The values of γ, β and τ so obtained are found to be 1.34 ± 0.19, 0.54 ± 0.15 and 2.31 ± 0.06 respectively.

PACS: 25.75.-q, 25.70.Pq, 13.85.Hd

Keywords: Nucleus–nucleus collision; Multi-fragmentation; Power law; Phase transition; Charge moment; Critical exponents

1. Introduction

It is believed that in the complex scheme of high energy reactions, nuclear fragmentation is relatively a well isolated phenomenon. Nuclear fragmentation in which excited nuclei break up into several pieces of smaller masses, each more massive than an alpha particle, is termed as nuclear multi-fragmentation. It is opined that one of the most important challenges of heavy ion physics is the identification and characterization of nuclear liquid–gas phase transition believed to be

* Corresponding author Tel: +913612570531; fax: +913612700133
E-mail address: bb_22@rediffmail.com (B. Bhattacharjee)

0375-9474/$ – see front matter
doi:10.1016/j.nuclphysa.2009.07.015